The Amundsen Sea Expedition 2012 (ANA02C)

Chief Scientist: SangHoon Lee

IBRV Araon, 31 January 2012 – 20 March 2012
(Christchurch to Christchurch, NZ)

Prologue

The sea ice was thicker and the snow accumulated on top was deeper. It was somehow foreseen, as the sea-ice retreat pattern in the Amundsen Sea was monitored via SSMIS website since the beginning of the austral summer. Prevailing winds from north east built up a compact band of the sea-ice blocks along the continental slope, which prevented further spreading of the following ice pieces from south to north. The ice conditions seemed ominous, yet we had loads of missions – more than 40 stations to be investigated intensively this season, because Araon will be locked up next year to the construction site of the 2^{nd} Korean station at Terra Nova Bay. In addition, on our shoulder were 9 of British iSTAR moorings (Keith Nicholls, BAS), 3 Swedish moorings (Anna Wahlin, Gotenburg Univ), and a US ASPIRE sediment trap (Hugh Ducklow, MBL). Departure of the cruise was delayed for 9 days because of the rescue operations for 2 fishing boats, which pushed the cruise leg further into the late summer.

As we crossed the ice band into the Amundsen polynya, we had to skip some stations that were in thick ice, in order to save time for priority work, hoping the ice condition would be better on our return voyage. Some stations had to be given up in the end; others were managed to be occupied; 5 of iSTAR moorings that were originally planned to be deployed in front of Abbot ice shelf had to be relocated to plan B area; Araon spent 20 hours to ram though a 30-mile route north of B22a iceberg, returning from Pine Island Bay – it was the day many of us thought about the desperate voyage of Shackleton. Sailing was rough, work load was to the limit, and the lab was on 24/7, but all 43 of us was one for the mission to accomplish. During the 50 days (30 days at the study site) of the Amundsen cruise, we have carried out 52 CTD stations, countless incubations and net sampling, 15 mooring deployments and 7 recoveries (1 failed), 3 weather station maintenance, 2 sea ice mechanical studies, 2 safety lectures, 3 situation briefings, 11 airborne recon, and 29 science seminars.

With this cruise and the previous one, the KOPRI Amundsen project wraps up the 1st stage of its study. The Amundsen project is to investigate the warming trends and mechanisms in the study area, and to assess the chemical, biological, and biogeochemical consequences of the rapid warming. We currently investigate, and continue to do as data become available; physical, chemical, and biological processes under the current trend of climate change; flux of the climate gases in and out of the ploynya and their roles in ecological processes; biological processes and biogeochemical cycles associated with polynya; links between biogeochemical processes and food web structure; key functional biology groups, their roles, and interactions.

This is to report our activities and preliminary results of the 2^{nd} Amundsen cruise. I regret that I have got no chance to present my warm affection and gratitude to my A-Team during the cruise.

2012 Amundsen cruise ANA02C chief scientist, SangHoon Lee

Contents

Chapter 1

Physical Oceanography

요약문

2012년 겨울, 쇄빙연구선 아라온호를 이용하여 남극 아문젠해에서 종합적인 해양조사를 실시하였다. 해양물리분야의 주된 연구는 대륙붕 위의 골 (trough)을 따라 유입되는 남극순환 심층수 (circumpolar deep water)의 공간적 분포와 이동경로를 파악하고, 남극순환 심층수 유입량의 변화에 미치는 주된 요인을 파악하는 것이다. 총 52개의 CTD 정점을 통해 세 종류의 수괴가 수직적으로 뚜렷하게 구분되어 분포하는 것을 밝혀냈다. 골의 하부에는 높은 온도와 높은 염분의 특성을 지닌 남극순환 심층수가 겨울철 형성된 수괴와는 혼합이 되지 않은 상태로 존재함을 밝혔다. 골의 서쪽사면과 비교해서, 동쪽사면 쪽으로 남극순환 심층수가 더욱 많이 분포하는데, 이러한 비대칭적 공간 분포에 대해서는 유속자료를 통한 심층적인 자료 분석이 요구된다. 또한, 폴리냐 해역 표층 30 m 까지 담수량을 계산한 결과 지난 관측 시기에 비해 저염화 되었으며, 이는 연구해역 남극순환 심층수 유입량의 연 변동에 의한 것으로 사료된다. 남극 아문젠해에서 최근 발생하고 있는 급속용융을 모니터링하기 위해, 1년이상의 장기 계류장비를 설치하였다. 국제공동연구의 일환으로, 기존에 구축된 타국가 (영국/스웨덴/미국)의 관측망과 연계한 현장조사를 실시하였다. 총 6개의 계류장비를 회수하였고, 총 15개의 신규 계류장비를 아문젠해 대륙사면, 대륙붕, 빙붕경계면에 설치하였다. 회수된 자료의 심층분석을 통해 남극순환 심층수의 분포와 빙붕용융과의 관계를 규명할 계획이다.

Abstract

In order to understand the role of CDW in controlling the hydrodynamics and related biochemical processes on the continental shelf of the Amundsen Sea, the shipborne measurements were conducted during the 2012 expedition (ANA02C). The overall purposes of physical oceanography are: (1) to identify the temporal and spatial distribution of CDW on the Amundsen shelf; (2) reveal the main forcing that affects the flow rate of CDW onto the Amundsen shelf; and (3) estimate the heat transport and its effect on the melting of ice shelves by CDW intrusions. In 2012, the location of the maximum fresh water content was almost the same as that in 2010/11, but the maximum fresh water content slightly increased about 0.2-0.3 m within the polynya area. As an international collaboration for monitoring the circumpolar deep water (CDW) and associated rapid melting of glaciers in the Amundsen Shelf, four institutes (Korea Polar Research

Institute, British Antarctic Survey, Marine Biological Laboratory and University of Gothenburg) developed a resource-sharing program. Recovered data will be further investigated to reveal hydrographic variability on the Amundsen Shelf.

1.1 Hydrographic Survey

T.W. Kim[1], H.K. Ha[1], and C.S. Hong[2]
[1]Korea Polar Research Institute, Incheon 406-840, South Korea
[2]Korea Ocean Research and Development Institute, Ansan 425-600, South Korea

1.1.1 Introduction

The widespread thinning of ice sheets in the coast around the Amundsen Sea that has been recorded in recent decades has recently been attributed to intrusions of warm circumpolar deep water (CDW) onto the continental shelf (Vaughan, 2008; Jenkins et al., 2010). The intrusion of relatively warm CDW, supplying heat onto the continental shelf, has led to an increase in the melting rate of ice shelves (Walker et al., 2007; Wahlin et al., 2010). As the CDW flows onto the shelf, it becomes colder and fresher by mixing with Antarctic surface water (AASW) and glacier melt water. Despite the importance of the spatial-temporal variability of CDW in continental shelf, vital knowledge for assessing the role of various forcing mechanisms is virtually unknown. This is mainly because the Amundsen Sea is remotely located and the extremely harsh weather and sea conditions limit the access to its inner shelf. Recently, Thoma et al. (2008) showed the relationship between temporal variability in the influx of CDW and regional wind forcing using a numerical model. The easterly winds over the shelf edge change to westerlies when the Amundsen Sea Low migrates west and south in winter/spring.

In order to understand the CDW's roles in controlling the hydrodynamics and related biochemical processes in the continental shelf of the Amundsen Sea, shipborne measurements were conducted during the 2012 expedition (ANA02C). The overall purposes of physical oceanography are:

- To identify the temporal and spatial distribution of CDW on the Amundsen shelf,
- To reveal the main forcing that affects the flow rate of CDW onto the Amundsen shelf,
- To estimate the heat transport and its effect on the melting of ice shelves by CDW intrusion.

1.1.2 Materials and methods

An intensive oceanographic survey was conducted in the period of January 31 - March 20, 2012 using the new Korean IBRV Araon to reveal the spatial distribution of CDW on the Amundsen shelf (Fig. 1.1). At each hydrographic station, the hydrocast of CTD/Rosette system with additional probes (e.g., transmissometer, PAR, altimeter, fluorometer, oxygen sensor and etc.) was conducted to measure the profiles of temperature, salinity, depth and other biochemical

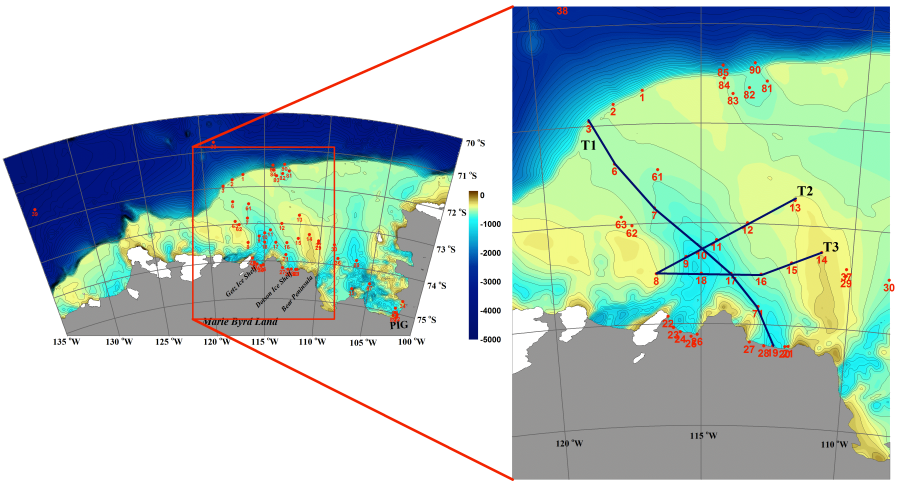

Figure 1.1: Map of study area. Red dots show the CTD stations during 2012 expedition. The numbers indicates the station numbers. Three transects (T-1, T-2 and T-3) were made to reveal the spatial distribution of CDW (right panel).

parameters. During the CTD upcasts, water samples were collected at several depths. A lowered acoustic Doppler current profiler (LADCP, RDI, 300 kHz) was attached to the CTD frame to measure the full profile of current velocities. The bin size was chosen as 5 m, and the number of bins was 20. On the cruise track, the vessel-mounted ADCP (RDI, 38 kHz) was continuously operated. In the shallow area (ca. $<$ 1000 m), the bottom tracking mode was applied. In order to avoid any signal interference with other acoustic systems, a synchronization unit was used during the entire running time.

1.1.3 Preliminary results

To investigate the spatial variability in CDW inflow and its significance for the water properties in the Amundsen Sea, a total of 52 CTD stations were occupied during the expedition. The main meridional transect (T-1) is along the western trough on the Amundsen Shelf. Offshore of the Amundsen Shelf the CDW was observed to be warmer than 1 °C, and its salinity was 34.7 psu. As the CDW enters onto the shelf region, it becomes colder and fresher as it interacts with Antarctic surface water (AASW) and glacier melt water. Next to the coast there is an open polynya where the observed maximum temperature and salinity of modified CDW (MCDW) were 0.6 °C and 34.5 psu, respectively (Fig. 1.2). The three different water masses are present along the western channel. The potential temperature and neutral density of AASW were lower than -1.6 °C and 27.75 kg m^{-3}, respectively, extending from the surface to 200-300 m depth. Near the bottom, the potential temperature and neutral density of the MCDW were higher than 0.6 °C and 28.00 kg m^{-3}. In the intermediate layer between AASW and MCDW, another different water mass was present.

Two zonal cross-transects (T-2 and T-3) clearly show the intrusion tongue of warm CDW (Fig. 1.3 and 1.4). The existence of warm, dense water suggests that

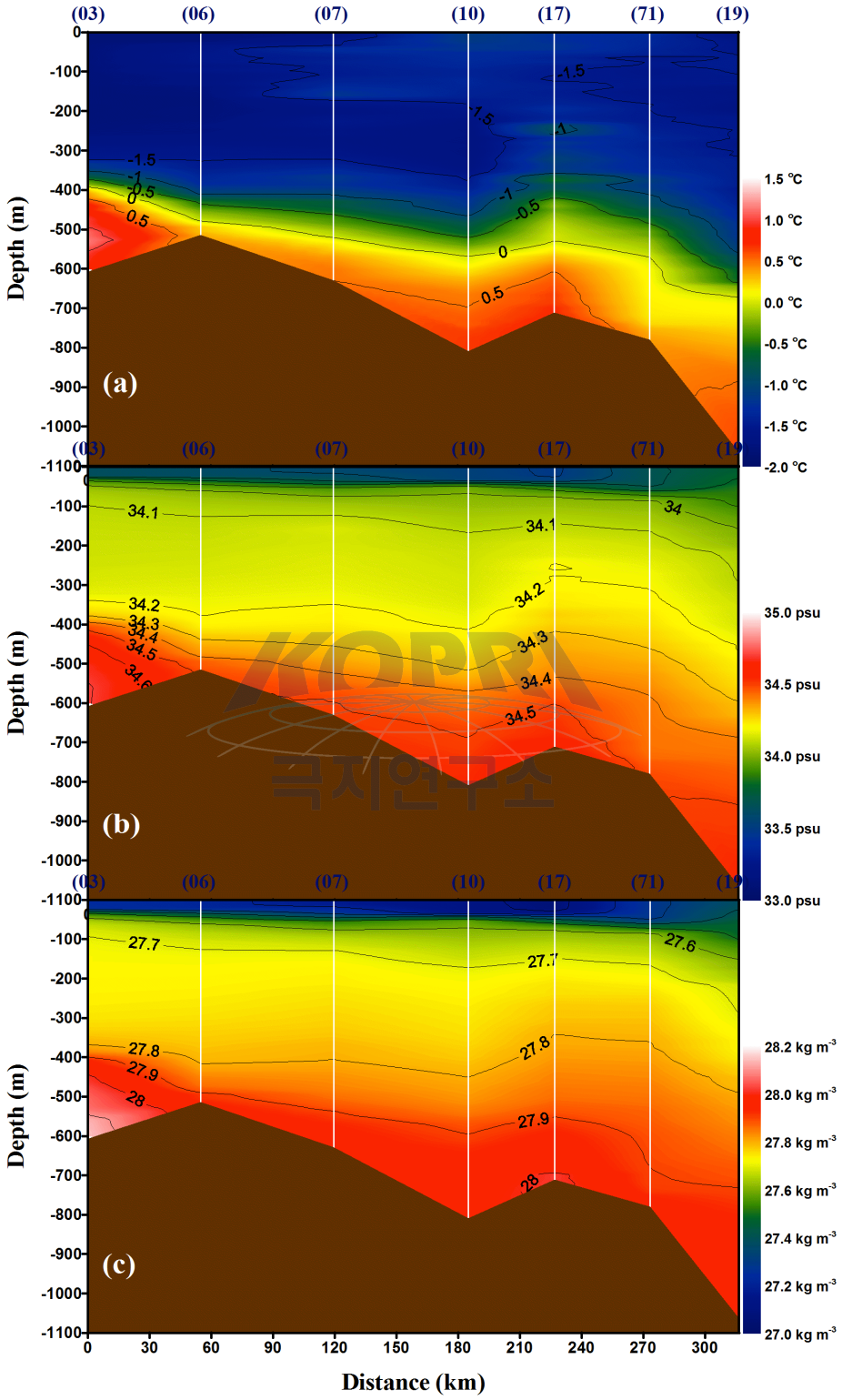

Figure 1.2: Vertical distribution of (a) temperature, (b) salinity and (c) neutral density along the channel (T-1).

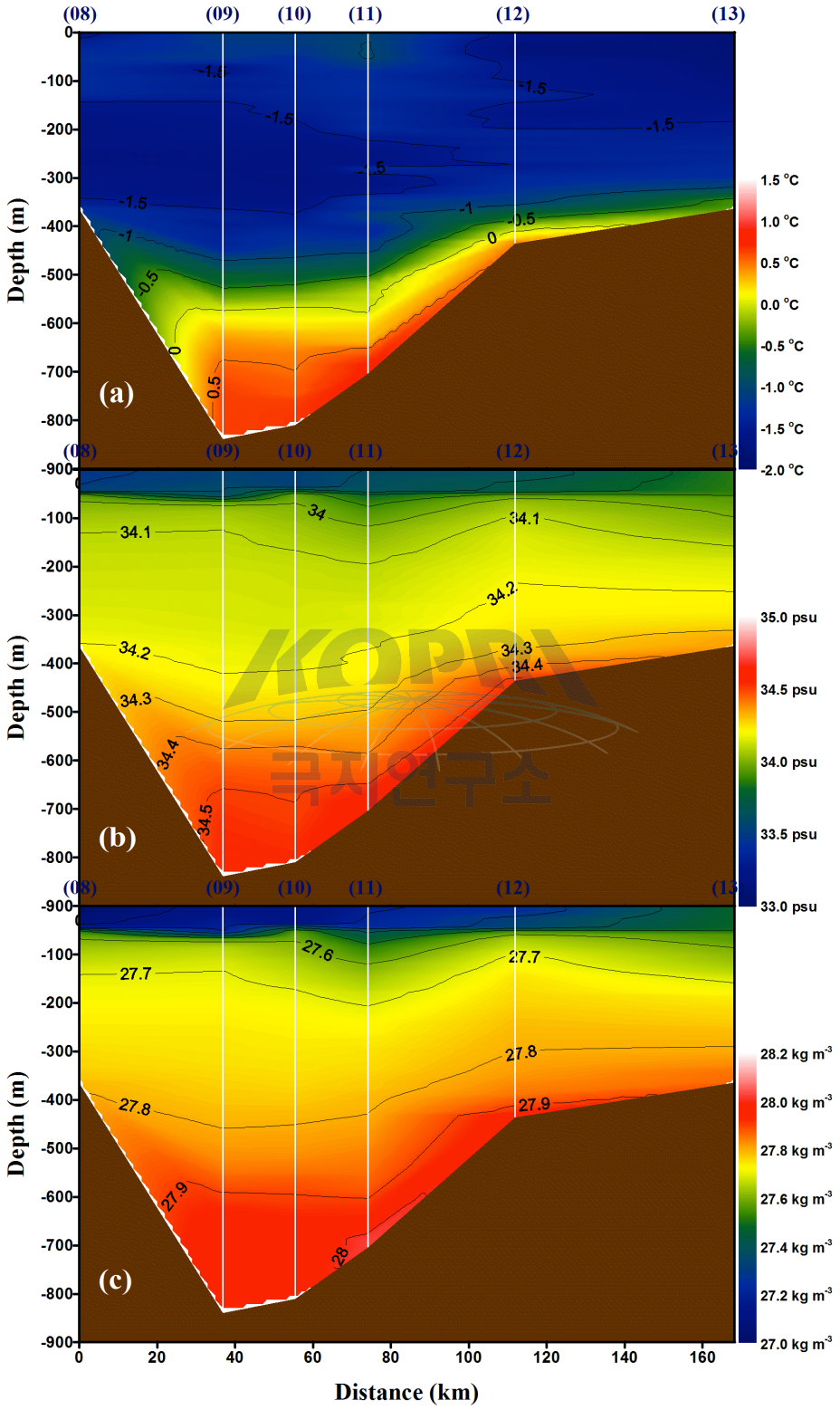

Figure 1.3: Vertical distribution of (a) temperature, (b) salinity and (c) neutral density across the channel (T-2).

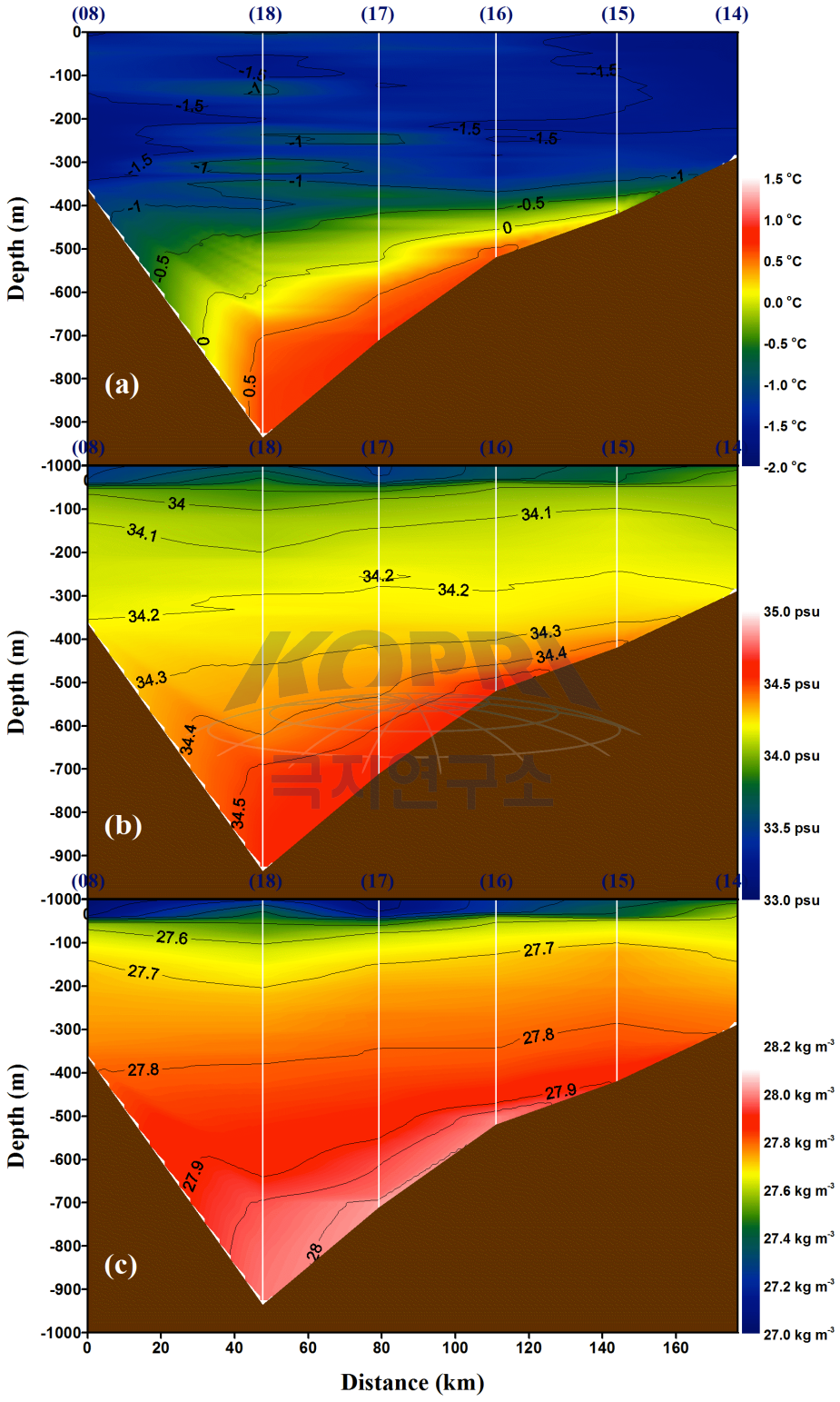

Figure 1.4: AVertical distribution of (a) temperature, (b) salinity and (c) neutral density across the channel (T-3).

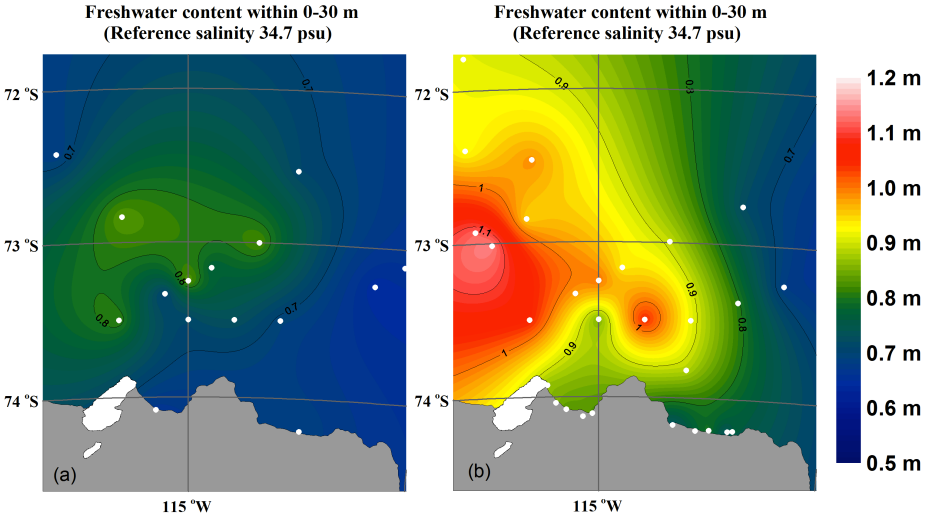

Figure 1.5: Spatial distribution of freshwater content within 0-30 m (upper): (a) 2010/11 and (b) 2012.

the trough geomorphology plays an important role in confining the flow pattern of CDW within shelf areas. It is noticeable that a warm tongue extended over the eastern flank of the trough, and that the eastern slope is slightly gentler than the western slope. It was found that the warm core is located at the depth of 800 m at St. 17 with a temperature and salinity of about 0.7 °C 34.6 psu, respectively. Also, the neutral density was higher than 28.01 kg m^{-3}. The warm core is not found along the channel except St. 03. This suggests that a different water mass might be transported into the polynya.

Fig. 1.5 shows the spatial distribution of freshwater content within 0-30 m in the polynya area. To calculate the freshwater content the reference salinity was used as 34.7 psu, which is upper boundary of CDW (neutral density is 28.03 kg m^{-3}). In 2010/11, the maximum of freshwater content was 0.8 m at St. 6. In 2012, the location of maximum fresh water content was almost the same as that in 2010/11 (Fig. 1.5), but the maximum fresh water content slightly increased about 0.2-0.3 m in the entire polynya area. The difference of freshwater content between 2010/11 and 2012 indicates the difference of volume loss of ice.

1.2 Moorings for ocean current and sediment trap

H.K. Ha[1], T.W. Kim[1], C.S. Hong[2], J.H. Jeong[2], E.P. Abrahamsen[3], and C. Stranne[4]
[1]Korea Polar Research Institute (KOPRI), Incheon 406-840, Korea
[2]Korea Ocean and Research Institute (KORDI), Ansan 425-600, Korea
[3]British Antarctic Survey (BAS), Cambridge, UK
[4]University of Gothenburg (UGOT), Sweden

As an international collaboration for monitoring the circumpolar deep water

(CDW) and associated rapid melting of glaciers in the Amundsen Shelf, four institutes (KOPRI, UGOT, BAS and Marine Biological Laboratory) launched a resource-sharing program. During the 2012 Amundsen Sea cruise (ANA02C), a total of 6 moorings were successfully recovered and 15 moorings were deployed at the shelf break, shelf troughs and near the ice shelf front. Only BSR-12 mooring failed to recover due to the high sea ice concentration and inherent weak buoyancy. Recovered raw data will be further investigated to reveal dynamic changes in the hydrography of the Amundsen Shelf.

1.2.1 KOPRI moorings

Recovery

Two stations, located at the northern entrance (K1) and the central polynya (K2), were retrieved during ANA02C (Table 1.1).

After arriving at the recovery station of K2 at 03:40 UTC, Feb. 12, 2012, we sent an enable command to underwater acoustic release (AR, SN: 841) transponder. We got ranges of more than 2000 m between the acoustic deck unit transducer and AR, suggesting an incorrect range due to low signal-to-noise. By sending the enable command to the second AR (SN 842) again, we concluded that we were located 3 km away from the original station. After moving exactly to K2, we tried to send the ranging signal to both ARs, but did not get reliable ranges, and then attempted to do a new trial using the echo sounder (EK60). By sending a release command, we finally found the mooring system floating on the surface. When all units were on deck, it was realized that the sediment trap had not worked at all during the entire deployment period.

Because the sea ice concentration at K1 was over 90%, it was difficult to access the target station by IBRV Araon from the east. We decided to attempt a detour to approach the mooring from the north. A 40-min helicopter survey confirmed that the detoured route was acceptable to recover the mooring system at K1. The first communication with AR failed, but we tried to communicate with the second AR again. The pinging between deck unit and AR gave reliable ranges. After cleaning up the heavy sea ice by swathing back and forth, an open area with a diameter of approximately 300 m was made, and then a release command was sent. Finally, all instruments were safely recovered, and the functions of sediment trap during the deployment had worked, as scheduled. Trap samples collected were treated, and then stored in the refrigerator for estimating annual flux of organic matter (Fig. 1.6).

Deployment

The location and details of deployed moorings are given in Table 1.2, 1.3, 1.4, 1.5, and 1.6. After the deployment, triangulation was done to confirm the settlement status of moorings and record the exact GPS location for future recovery. The design diagrams and triangulation results for individual moorings are given in Appendix II and III.

1.2.2 BAS and ASPIRE moorings

iSTAR is a directed research program, funded by the Natural Environment Research Council (NERC), UK, with the main goal of improving our understanding

Figure 1.6: Samples collected at K1 sediment trap

Table 1.1: Detail information of recovered moorings (KOPRI).

St.	Latitude (S)	Longitude (W)	Depth (m)	Deployment		Recovery	
				Date (YYYY/MM/DD)	Time (UTC)	Date (YYYY/MM/DD)	Time (UTC)
K1	72° 24.163′	117° 43.341′	530	2010/12/31	12:06	2012/03/02	23:07
K2	73° 16.280′	114° 58.230′	830	2011/01/01	08:00	2012/02/12	08:55

Table 1.2: Location and time of mooring stations at the anchor release on the surface (KOPRI)

St.	Latitude (S)	Longitude (W)	Depth (m)	Date (YYYY/MM/DD)	Time (UTC)	No. deployment	CTD Station
K1	72° 23.2374′	117° 42.8214′	525	2012/03/04	02:03	2nd	06
K2	73° 16.8265′	114° 57.2270′	823	2012/02/15	07:23	2nd	10
K3	74° 11.2019′	112° 31.7818′	1057	2012/02/16	18:27	1st	19

Table 1.3: Triangulation position of mooring stations (KOPRI)

St.	Depth (m)	Triangulation position (2D)		From anchor drop	
		Latitude (S)	Longitude (W)	Drift (m)	Direction (°)
K1	525	72° 23.210′	117° 42.634′	116	64
K2	823	73° 16.882′	114° 56.999′	159	130
K3	1057	74° 11.231′	112° 32.399′	316	260

Table 1.4: Detail information of acoustic release transponders (KOPRI).

St.	Depth/ Bottom (height)	Model (manufacture)	S/N	Frequency (kHz)		Command code		Battery packs (years)	Voltage	Remarks
				Rx	Tx	En	Re			
K1	473m/ 525m (52m)	865-A-DB-13 (Benthos) Old model	840	9.5	13.0	C	D	2 (2)	14.44, 14.35V	* change transmit frequency after recovery in K1, Mar., 2012 *Replace new alkaline battery packs of Benthos
			841	9.5	12.0	E	F	2 (2)	14.35, 14.36V	* recovery in K2, Feb. 2012 * passed the under-water test, Feb. 2012 *Replace new alkaline battery packs of Benthos
K2	796m/ 823m (27m)	865-A (Teledyne Benthos)	54244	9.0	12.0	D	F	1 (2)	Not open chassis	* new employment * passed the under-water test, Feb. 2012
			54246	10.0	12.0	B	D	1 (2)	Not open chassis	* new employment * passed the under-water test, Feb. 2012
K3	930m/ 1057m (127m)	865-A (Teledyne Benthos)	54245	9.5	12.0	C	E	1 (2)	Not open chassis	* new employment * passed the under-water test, Feb. 2012
			54247	10.5	12.0	A	C	1 (2)	Not open chassis	* new employment * replace the fuse because of damage at the underwater test, Feb. 2012 * no zinc anode bar

Table 1.5: Detail information of deployed mooring sensors (KOPRI)

St.	Depth (m)	Instruments (S/N)	Start Date (YYYY/MM/DD)	Time (UTC)	Interval (min)	Remark
K1	268	RCM-11 (277)	2012/03/03	03:00	60	*re-deployment *conductivity cell is not good (type 3619)
	269	MicroCAT, SBE37SM (7825)	2012/03/03	08:00	30	*re-deployment
	344	TR, SBE39 (5512)	2012/03/03	10:00	30	*new employment *broken clamp, fastening using steel cable band
	420	RCM-11 (227)	2012/03/03	03:00	60	*re-deployment
	421	MicroCAT, SBE37SM (8006)	2012/03/03	08:00	30	*re-deployment
K2	416	SEAGUARD RCM DW (156)	2012/02/15	00:00	60	*re-deployment
	417	MicroCAT, SBE37SM (8728)	2012/02/11	23:00	30	*new employment
	517	TR, SBE39 (5475)	2012/02/11	23:00	30	*new employment
	617	TR, SBE39 (5476)	2012/02/11	23:00	30	*new employment *broken clamp, replace new clamp
	716	RCM-11 (346)	2012/02/15	00:00	60	*re-deployment *change install depth 250m to 716m
	717	MicroCAT, SBE37SM (8729)	2012/02/11	23:00	30	*new employment
K3	259	RCM-11 (613)	2012/02/16	03:00	60	*new deployment
	260	MicroCAT, SBE37SM (8727)	2012/02/16	03:00	30	*new employment
	509	SEAGUARD RCM IW (502)	2012/02/16	03:00	60	*new employment
	857	SEA GUARD RCM DW (157)	2012/02/16	03:00	60	*new employment
	858	MicroCAT, SBE37SM (8046)	2012/02/16	03:00	30	*recovery at K2, Feb. 2012 *change the station and deployment

Table 1.6: Sediment trap time schedule.

Bottle	K1 YYYY/MM/DD hh:mm:ss	K2 YYYY/MM/DD hh:mm:ss	K3 YYYY/MM/DD hh:mm:ss
1	2012/03/07 00:00:00	2012/02/15 00:00:00	2012/02/17 00:00:00
2	2012/04/01 00:00:00	2012/03/01 00:00:00	2012/03/16 00:00:00
3	2012/05/01 00:00:00	2012/03/16 00:00:00	2012/04/01 00:00:00
4	2012/06/01 00:00:00	2012/04/01 00:00:00	2012/05/01 00:00:00
5	2012/07/01 00:00:00	2012/05/01 00:00:00	2012/06/01 00:00:00
6	2012/08/01 00:00:00	2012/06/01 00:00:00	2012/07/01 00:00:00
7	2012/09/01 00:00:00	2012/07/01 00:00:00	2012/08/01 00:00:00
8	2012/10/01 00:00:00	2012/08/01 00:00:00	2012/09/01 00:00:00
9	2012/11/01 00:00:00	2012/09/01 00:00:00	2012/10/01 00:00:00
10	2012/11/16 00:00:00	2012/10/01 00:00:00	2012/11/01 00:00:00
11	2012/12/01 00:00:00	2012/11/01 00:00:00	2012/11/16 00:00:00
12	2012/12/10 00:00:00	2012/11/16 00:00:00	2012/12/01 00:00:00
13	2012/12/19 00:00:00	2012/12/01 00:00:00	2012/12/10 00:00:00
14	2012/12/28 00:00:00	2012/12/10 00:00:00	2012/12/19 00:00:00
15	2013/01/06 00:00:00	2012/12/19 00:00:00	2012/12/28 00:00:00
16	2013/01/15 00:00:00	2012/12/28 00:00:00	2013/01/06 00:00:00
17	2013/01/24 00:00:00	2013/01/06 00:00:00	2013/01/15 00:00:00
18	2013/02/02 00:00:00	2013/01/15 00:00:00	2013/01/24 00:00:00
19	2013/02/11 00:00:00	2013/01/24 00:00:00	2013/02/02 00:00:00
20	2013/02/20 00:00:00	2013/02/02 00:00:00	2013/02/11 00:00:00
21	2013/03/01 00:00:00	2013/02/11 00:00:00	2013/02/20 00:00:00
22	2013/03/16 00:00:00	2013/02/20 00:00:00	2012/03/01 00:00:00

of the dynamics of ice sheet stability, and in turn improving our predictions for future mass loss rates and sea-level rise. To achieve this goal, the program has two main components, investigating ocean forcing on the West Antarctic Ice Sheet, specifically in the Amundsen Sea, and the ice sheet response to this forcing. A key tool in investigating the ocean forcing is the array of moorings, which have been deployed during the ANA02C.

EPA previously participated in cruise NBP10-05 on RV Nathaniel B. Palmer in Nov. 2010-Jan. 2011. Here the goal was to recover and deploy as many moorings as possible in Pine Island Bay (PIB), to kick-start the project. Unfortunately the Palmer was unable to reach PIB because of heavy sea ice conditions in the area north of iceberg B-22A. Two moorings were, however, deployed near the shelf break, BSR12 and BSR13. Attempts were made to recover these moorings during ANA02C, with one failure and one successful recovery. The ASPIRE mooring (PI: Hugh Ducklow, MBL) which was deployed on NBP10-05, and successfully recovered on ANA02C.

Recovery

Positions and dates for all mooring recovered and deployed on ANA02C are given in Table 1.7. The ASPIRE mooring recovery was uneventful; the mooring was released and sighted on the surface shortly afterwards. The sediment trap on the mooring had not rotated fully, but was stuck on the 23rd bottle. This means that there was no way for the water to drain out of the funnel, and consequently handling the trap on deck was quite difficult. The carousel was removed from the trap, releasing the water; the carousel was placed in the CTD room, where the bottles were removed and sealed. Some biological growth was evident near the tops of the bottles, and some of this sank into the bottles when they were removed.

The only unsuccessful recovery on the cruise was mooring BSR12. The ship arrived on the mooring position when it was still too dark to start the recovery. The triangulation was performed in the dark, and once light returned, around midnight local time (11:00 UTC), the ship began breaking ice. The ice was drifting westward at a rate of 0.4 kn. Because of very cold temperatures, thin ice quickly re-formed on the broken areas. A small iceberg was also present in the mooring area, but we estimated that it would pass north of the mooring position. There were some areas of new ice/black nilas cover, with approx. 80% second-year ice. When a hole had been broken, approx. 300x100 m, instructions were given to release the mooring. Unfortunately there were problems with the initial release command, and the command was re-sent at 12:39, four minutes after the first attempt. Because of miscommunication, the hydrophone was recovered shortly after the release command was sent, and the ship moved; we do not know how long the mooring took to rise to the surface. The mooring was not sighted on the surface, and the hydrophone was again deployed to listen for the mooring. Ranges of 360 m were obtained. Attempts were made to move in various directions, to locate the mooring, but there were problems communicating with the mooring at other positions. During these attempts, we attempted to use the hydrophone with the ship moving. Unfortunately we were unable to get any ranges because of noise from the ship's propellers. When the ship was coming to a stop, it drifted towards an ice floe, and when the hydrophone got caught between the hull and the ice, the hydrophone was ripped from the end of

Table 1.7: Sediment trap time schedule.

Mooring	Deployment date (YY/MM/DD)	Recovery date (YY/MM/DD)	Latitude	Longitude	Depth (m)	Vs_{eff}**
ASPIRE*	10/12/16 08:35	12/02/16 06:51	73°S 49.170'	113°W 04.324'	785	1451
BSR12* (failed)	11/01/0714:09	12/03/06 12:39	71°S 34.099'	113°W 00.418'	587	1452
BSR13*	11/01/07 05:12	12/03/06 20:28	71°S 23.575'	113°W 22.988'	958	1459

the cable and sank. Further ranging was attempted with the Benthos UDB-9000 deck unit, but after more ranges around 360 m, no further pings were heard from the acoustic release. The enable command was re-sent several times, and from several positions, but with no response. At this point, with the opening in the ice rapidly re-freezing, the recovery attempt was abandoned, at approximately 14:30 UTC.

Various factors probably contributed to the failed recovery. The high ice concentration complicated matters, and the cold temperatures meant that the area where ice had been broken started re-freezing very quickly. The trawl floats used on the mooring do not have enough buoyancy to break through any significant ice thickness, so they must be recovered at most into very thin nilas, or preferably in open water. The delay in releasing the mooring meant that the open water area may have drifted too far past the mooring position – and the size of the pool created was probably slightly too small for the recovery. The iceberg in the area may also have played a part; all ranges obtained were quite high, so it is possible that the mooring could have been caught on the keel of the iceberg. We do not know how long the mooring took to rise, as the transducer was recovered prematurely. It is probably a combination of several of these factors that contributed to the failed recovery.

BSR13 was recovered with much less incident. Again, a hole was broken in the ice, slightly larger than before. The mooring was sighted at the edge of the ice, and the zodiac deployed to bring the top of the mooring to the ship. The mooring was recovered by hand in the area in front of the CTD room. During NBP10-05 several deep moorings were not successfully recovered; one theory is that the buoyancy, provided by 9" trawl floats, had failed. As a test, a single 9" float was deployed at 950 m depth. When this float was recovered, it had broken in half roughly along the seam where it had been welded together. No damage to the line was observed in this area.

Deployment

Three of the iSTAR moorings were deployed anchor last. The remaining moorings, iSTAR1-6, were deployed anchor first (Table 1.8). During the deployment of iSTAR5, the deepest shelf break mooring, the outer cover of the rope became caught on a cotter pin on a shackle, and broke. Fortunately the inner core remained undamaged, and the rope was secured, the cover stretched back towards the break, and a knot tied to circumvent the damaged area, reducing the length of the rope by approx. 2 m. The deployment was able to proceed with no further problems.

Table 1.8: Detail information of deployed moorings (BAS-iSTAR)

Mooring	Deployment date (YY/MM/DD)	Latitude	Longitude	Depth (m)	Vs_{eff} **
iSTAR1	12/03/06 16:00	71°S 33.732'	113°W 02.759'	605	1452
iSTAR2	12/03/06 05:17	71°S 38.351'	113°W 32.146'	615	1451
iSTAR3	12/03/05 17:42	71°S 42.184'	114°W 02.613'	542	1449
iSTAR4	12/03/05 12:27	71°S 32.702'	114°W 18.208'	513	1450
iSTAR5	12/03/05 04:22	71°S 25.386'	114°W 18.890'	1465	1465
iSTAR6	12/02/27 05:46	73°S 48.759'	106°W 32.120'	913	1455
iSTAR7	12/02/23 02:53	74°S 21.701'	104°W 58.121'	1346	1460
iSTAR8*	12/02/23 18:26	74°S 51.798'	102°W 06.250'	954	1454
iSTAR9*	12/02/24 03:57	75°S 03.317'	102°W 09.262'	810	1452

1.2.3 UGOT (Sweden) moorings

Two moorings (S1_OLD, S2_OLD) were recovered, and three moorings were deployed. Detail information of each mooring is given in Appendix II.

Recovery

Table 1.9: Detail information of recovered moorings (UGOT)

Mooring	Deployment date (YY/MM/DD)	Recovery date	Latitude	Longitude	Depth (m)
S1_OLD*	10/12/24 19:12	01/03/12 20:32	72°S 27.345'	116°W 20.327'	557
S2_OLD*	10/12/25 02:24	11/02/12 12:48	73°S 0.948'	117°W 14.857'	537

Deployment

Table 1.10: Detail information of deployed moorings (UGOT)

Mooring	Deployment date (YY/MM/DD)	Latitude	Longitude	Depth (m)
S1_NEW*	12/03/02 01:29	72°S 27.286'	116°W 20.936'	561
S2_NEW*	12/03/04 12:28	71°S 57.061'	118°W 27.093'	620
S3	12/03/01 08:36	72°S 55.580'	117°W 34.888'	548

Acknowledgements

We are very grateful to the captain and crew of IBRV Araon for their technical assistance with all mooring works, and for their flexibility and ingenuity in making recoveries and deployments, including anchor-first, possible using the A-frame.

References

Jenkins, A., Dutrieux, P., Jacobs, S.S., McPhail, S.D., Perrett, J.R., Webb, A.T. and White, D., (2010) Observations beneath Pine Island Glacier in West Antarctica and implications for its retreat. Nature Geoscience, 3, 468-472.

Thoma, M., Jenkins, A., Holland, D. and Jacobs, S., (2008) Modelling Circumpolar deep water intrusions on the Amundsen Sea continental shelf, Antarctica. Geophysical Research Letters, 35(L18602), doi:10.1029/2008GL034939.

Vaughan, D.G., (2008) West Antarctic Ice Sheet collapse-the fall and rise of a paradigm. Climate Change, 91, 65-79.

Wahlin, A.K., Yuan, X., Bjork, G. and Nohr, C., (2010) Inflow of warm circumpolar deep water in the central Amundsen Shelf. Journal of Physical Oceanography, 40, 1427- 1434.

Walker, D.P., Brandon, M.A., Jenkins, A., Allen, J.T., Dowdeswell, J.A. and Evans, J., (2007) Oceanic heat transport onto the Amundsen Sea shelf through a submarine glacial trough. Geophysical Research Letters, 37(L02602), doi:10.1029/2006GL028154.

1.3 Appendix I. ANA02C cruise log spreadsheet.

See the following pages.

Scientific Cruise Daily Log

Ship: R/V Araon **Cruise:** ANA02 **Leg:** C

Prepared by T.W. Kim (KOPRI) twkim@kopri.re.kr

STN No.	Gear	Cast No.	Date	Cast start	Bottom or at depth	Cast end	Latitude	Longitude	Water depth	Cast depth	Cable payout	No. of cnl Core length	Wind speed	Wind direction	Ship speed	Heading	Remarks	Device Driver
			(UTC)	(UTC)	(UTC)	(UTC)			(m)	(m)	(m)		knot	(°)	knot	(°)		
Amundsen Sea																		
CTD: CTD;**XBT**: XBT;**GFO**: GO-FLO;**ZOO**: Zooplankton; **PHY**: Phytoplankton; **BON**: Bongo net; **MOC**: Mocness; **MUC**: multi-core; **BOX**: Box core; **GVC**: gravity core; **PSC**: piston core; **ICE**: work on sea-ice; **IBY**: ice buoy; **OBY**: ocean buoy; **SUF**: surface water; **OCL**: ocean color																		
	XBT	1	1-1-2012	2:12		2:17	47°56.47'S	177°31.90'E	1147	780							XBT	TW Kim
	XBT	2	2-2-2012	2:10		2:15	51°40.74'S	178°32.71'W	533	780							XBT	TW Kim
	XBT	3	2-3-2012	2:03		2:08	54°14.78'S	172°05.96'W	5025	780							XBT	TW Kim
	XBT	4	2-4-2012	0:35		0:40	56°48.59'S	165°24.34'W	4890	780							XBT	TW Kim
	XBT	5	2-5-2012	0:33		0:38	59°44.80'S	157°43.14'W	3460	780							XBT	TW Kim
	XBT	6	2-5-2012	20:02		20:07	62°05.70'S	151°04.12'W	3043	780							XBT	TW Kim
	XBT	7	2-6-2012	7:57		8:53	63°30.51'S	146°42.06'W	3868	780							XBT	TW Kim
	XBT	8	2-6-2012	19:57		20:02	64°47.56'S	142°11.51'W	3707	780							XBT	TW Kim
	XBT	9	2-7-2012	7:58		8:03	66°17.67'S	137°48.67'W	4556	780							XBT	TW Kim
	XBT	10	2-8-2012	7:55		8:00	68°50.64'S	129°49.91'W	3990	780							XBT	TW Kim
	XBT	11	2-8-2012	19:52		19:57	69°53.45'S	124°10.92'W	3070	780							XBT	TW Kim
1	OCL	1	2-09-2012	17:50		18:40				70							HPRO II	JM Han
1	PHY	1	2-10-2012	7:13		7:22	71°39.63'S	116°46.67'W			150						20 micron mesh	EJ Yang
1	BON	1	2-10-2012	7:30		7:42					200						Vertical towing	DB Lee
1	BON	2	2-10-2012	7:48		8:00					200						Vertical towing	DB Lee
1	CTD	1	2-10-2012	9:48		10:18	71°39.63'S	116°46.67'W	473	470		24	6.1	227	0.3	169	First casting failed due to cable problem, the second cast overwrite the first	TW Kim
1	GFO	1	2-10-2012	10:30		10:40				15							GO-FLO	JS Park
1	CTD	2	2-10-2012	11:46		12:05	71°38.83'S	116°47.10'W	580	100		24	5.9	222	0.4	173	Second shallow casting	HC Kim
1	CTD	3	2-10-2012	12:54		13:04	71°38.39'S	116°47.66'W	669	40		24	6.2	230	0.4	174	Third shallow casting	TW Kim
2	CTD	1	02-10-2012	16:43		17:29	71°47.46'S	117°40.34'W	547	540		24	7	244	0	242	Only deep casting (no shallow)	TW Kim
2	OCL	1	02-10-2012	17:30		17:50				102							HPRO II	JM Han
7	GFO	1	02-11-2012	3:20		3:30				15							GO-FLO	JS Park
7	CTD	1	02-11-2012	3:32		4:19	72°50.74'S	116°30.18'W	638	636		24	3	120	0		First deep casting	CS Hong
7	OCL	1	02-11-2012	4:40		5:10				108							HPRO II	JM Han
7	CTD	2	02-11-2012	5:30		5:48	72°50.77'S	116°29.76'W	638	100		24					Second shallow casting	CS Hong
7	PHY	1	02-11-2012	6:04		6:17					150						20 micron mesh	EJ Yang
7	BON	1	02-11-2012	6:25		6:39					200						Vertical towing	DB Lee
7	BON	2	02-11-2012	6:45		7:00					200						Vertical towing	DB Lee
7	CTD	3	02-11-2012	7:22		7:29	72°50.77'S	116°29.74'W	638	20		24	5.4	131	0	197	Third shallow casting	TW Kim
62	CTD	1	02-11-2012	9:48		10:23	73°00.98'S	117°14.95'W	530	530		24	9	115	0.1	140	Only deep casting (no shallow)	TW Kim
62	BON	1	02-11-2012	10:35		11:05				200							Oblique towing	DB Lee
62	OBY	1	02-11-2012	12:47		14:05	73°00.99'S	117°14.95'W	530								u	HK Ha
8	CTD	1	02-11-2012	18:04		18:35	73°30.00'S	116°29.99'W	372	365		24	8	156	0	162	First deep casting	TW Kim
8	OCL	1	02-11-2012	18:40		19:05				101							HPRO II	JM Han
8	CTD	2	02-11-2012	19:38		19:52	73°29.88'S	116°30.90'W	372	100		24	7.5	180	0.1	171	Second shallow casting	TW Kim
8	PHY	1	02-11-2012	20:01		20:14					150						20 micron mesh	EJ Yang
8	BON	1	02-11-2012	20:20		20:32					200						Vertical towing	DB Lee
8	BON	2	02-11-2012	20:43		21:13					200						Vertical towing	DB Lee
9	CTD	1	02-11-2012	23:51		1:14	73°20.01'S	115°29.94'W	840	838		24	7.1	169			Only deep casting (no shallow)	CS Hong
9	OCL	1	02-11-2012	1:20		1:50				105							HPRO II	JM Han
10	OBY	1	02-12-2012	2:52		8:55	73°16.28S	114°58.23'W	830								K2 KOPRI buoy recovery	HK Ha
10	GFO	1	02-12-2012	9:35		9:45				15							GO-FLO	JS Park
10	CTD	1	02-12-2012	9:49		10:35	73°15.02'S	114°59.88'W	825	810		24	11.3	165	0.1	353	First deep casting	TW Kim
10	PHY	1	02-12-2012	10:44		10:55					150						20 micron mesh	EJ Yang
10	BON	1	02-12-2012	11:07		11:15					200						Vertical towing	DB Lee
10	BON	2	02-12-2012	11:20		11:34					200						Vertical towing	DB Lee
10	CTD	2	02-12-2012	11:53		12:10	73°15.02'S	114°59.88'W	825	100		24	7.8	159	0.1	169	Second shallow casting	TW Kim
10	OCL	1	02-12-2012	12:20		12:55				100							HPRO II	JM Han
10	CTD	3	02-12-2012	13:14		13:24	73°14.99'S	114°59.75'W	825	34		24	7.5	191	0.1	357	Third shallow casting	TW Kim
10	MUC	1	02-12-2012	15:00	15:30	15:50	73°14.09'S	114°54.56'W	802								Multiple core	HS Moon
10	BOX	1	02-12-2012	16:00	16:20	16:40	73°14.09'S	114°54.56'W	802								Box core	HS Moon
10	BOX	2	02-12-2012	16:50	17:10	17:30	73°14.09'S	114°54.56'W	802								Box core	HS Moon
10	BOX	3	02-12-2012	17:40	18:00	18:20	73°14.09'S	114°54.56'W	802								Box core	HS Moon
11	CTD	1	02-12-2012	20:32		21:17	73°09.98'S	114°29.95'W	710	705		24	8.8	173	0.1	194	Only deep casting (During upcasting, miss bottle fire at 110m return 110m & Salinity sensor problem due to see	TW Kim
11	OCL	1	02-12-2012	21:25		22:00				105							HPRO II	JM Han
12	CTD	1	02-13-2012	2:23		3:04	72°59.59'S	113°30.02'W	440	436		24	10	209			First deep casting	CS Hong
12	OCL	1	02-13-2012	3:05		3:30				101							HPRO II	JM Han
12	CTD	2	02-13-2012	4:11		4:27	72°59.40'S	113°29.44'W	438	100		24	8	214			Second shallow casting	CS Hong
12	PHY	1	02-13-2012	5:03		5:14					150						20 micron mesh	EJ Yang
12	BON	1	02-13-2012	5:21		5:34					200						Vertical towing	DB Lee
12	BON	2	02-13-2012	5:40		5:52					200						Vertical towing	DB Lee
12	MOC	1	02-13-2012	7:30		8:37	72°59.61'S	113°30.43'W	426	400							Mocness towing	HS Na

Scientific Cruise Daily Log

Ship: R/V Araon | **Cruise:** ANA02 | **Leg:** C | Prepared by T.W. Kim (KOPRI) twkim@kopri.re.kr

STN No.	Gear	Cast No.	Date (UTC)	Cast start (UTC)	Bottom or at depth (UTC)	Cast end (UTC)	Latitude	Longitude	Water depth (m)	Cast depth (m)	Cable payout (m)	No. of sal Core length	Wind speed knot	Wind direction (°)	Ship speed knot	Heading (°)	Remarks	Device Driver
Amundsen Sea																		
CTD: CTD;**XBT**: XBT;**GFO**: GO-FLO;**ZOO**: Zooplankton; **PHY**: Phytoplankton; **BON**: Bongo net; **MOC**: Mocness; **MUC**: multi-core; **BOX**: Box core; **GVC**: gravity core; **PSC**: piston core; **ICE**: work on sea-ice; **IBY**: ice buoy; **OBY**: ocean buoy; **SUF**: surface water; **OCL**: ocean color																		
12	BON	1	02-13-2012	5:21		5:34					200						Vertical towing	DB Lee
12	BON	2	02-13-2012	5:40		5:52					200						Vertical towing	DB Lee
12	MOC	1	02-13-2012	7:30		8:37	72°59.61'S	113°30.43'W	426	400							Mocness towing	HS Na
	XBT	12	02-13-2012	11:12		11:17	72°54.94'S	112°59.97'W	439	439							XBT	TW Kim
	XBT	13	02-13-2012	13:04		13:09	72°49.95'S	112°30.17'W	458	458							XBT	TW Kim
13	CTD	1	02-13-2012	15:01		15:38	72°45.08'S	111°59.82'W	369	364		24	9.9	180	0	350	Only deep casting	TW Kim
13	OCL	1	02-13-2012	15:45		16:15				105							HPRO II	JM Han
	XBT	14	2-13-2011	18:26		18:31	72°55.20'S	111°39.41'W	346	346							XBT	CS Hong
	XBT	15	2-13-2011	20:27		20:32	73°04.90'S	111°20.40'W	311	311							XBT	CS Hong
14	CTD	1	02-13-2012	22:40		23:17	73°15.26'S	111°01.99'W	294	291		24	9.8	170			Only deep casting (no shallow)	TW Kim
14	OCL	1	02-13-2012	23:25		23:55				110							HPRO II	JM Han
15	CTD	1	02-14-2012	3:37		4:15	73°22.47'S	112°00.07'W	424	420		24	8	182			Only deep casting (during downcasting ctd problem, the second cast overwrite the first cast file)	CS Hong
15	OCL	1	02-14-2012	4:20		4:40				100							HPRO II	JM Han
16	GFO	1	02-14-2012	9:30		11:00				10		5					GO-FLO	JH Hyun
16	CTD	1	02-14-2012	11:00		11:46	73°29.97'S	113°00.02'W	525	520		24	12	169	0.2	191	First deep casting	TW Kim
16	PHY	1	02-14-2012	12:00		12:13					150						20 micron mesh	EJ Yang
16	BON	1	02-14-2012	12:19		12:34					200						Vertical towing	DB Lee
16	CTD	2	02-14-2012	12:55		13:11	73°29.97'S	113°00.02'W	519	100		24	10.2	171	0.1	185	Second shallow casting	TW Kim
16	OCL	1	02-14-2012	13:20		14:00				60							HPRO II	JM Han
16	CTD	3	02-14-2012	14:26		14:36	73°29.34'S	112°59.63'W	520	30		24	10	188	1.4	90	Third shallow casting	TW Kim
16	BON	2	02-14-2012	14:50		15:13					250						Oblique towing	DB Lee
17	GFO	1	02-14-2012	18:25		18:35				15							GO-FLO	JS Park
17	CTD	1	02-14-2012	18:37		19:17	73°29.98'S	114°00.20'W	711	711		24	8.3	144	0.1	153	First deep casting	CS Hong
17	OCL	1	02-14-2012	19:20		19:55				100							HPRO II	JM Han
17	CTD	2	02-14-2012	20:29		20:45	73°29.79'S	114°00.53'W	711	100		24					Second shallow casting	CS Hong
18	CTD	1	02-15-2012	0:05		1:22	73°29.99'S	114°59.97'W	938	935		24	1.5	250	0.1	295	Only deep casting (no shallow)	HK Ha
18	OCL	1	02-15-2012	1:30		2:40				100							HPRO II	JM Han
10	OBY	1	02-15-2012	5:51		7:23	73°16.83'S	114°57.23'W	823								K2 KOPRI buoy redeploy	HK Ha
10	BOX	1	02-15-2012	8:00	8:30	8:50	73°14.09'S	114°54.56'W	802								Box core	HS Moon
10	GVC	1	02-15-2012	10:00	10:30	11:00	73°14.09'S	114°54.56'W	802								Gravity core	HS Moon
	BOX	1	02-15-2012	15:00	15:25	15:50	73°37.42'S	113°48.28'W	777								Box core	HS Moon
	BOX	2	02-15-2012	16:00	16:25	16:50	73°37.42'S	113°48.28'W	777								Box core	HS Moon
	MUC	1	02-15-2012	17:00	17:25	17:50	73°37.42'S	113°48.28'W	777								Multiple core	HS Moon
	MUC	2	02-15-2012	18:00	18:25	18:50	73°37.42'S	113°48.28'W	777								Multiple core (failed)	HS Moon
	BOX	3	02-15-2012	19:00	19:25	19:50	73°37.42'S	113°48.28'W	777								Box core	HS Moon
	BOX	4	02-15-2012	20:00	20:25	20:50	73°37.42'S	113°48.28'W	777								Box core	HS Moon
	BOX	5	02-15-2012	21:00	21:25	21:50	73°37.42'S	113°48.28'W	777								Box core	HS Moon
	MOC	1	02-15-2012	21:50		23:11	73°37.65'S	113°48.08'W	700	400							MOCNESS towing	HS Na
71	GFO	1	02-16-2012	2:20		2:30				15							GO-FLO	JS Park
71	CTD	1	02-16-2012	2:34		3:35	73°49.26'S	113°03.99'W	783	780		24	3.4	315	0.1	152	First deep casting	TW Kim
71	OCL	1	02-16-2012	3:35		4:00				100							HPRO II	JM Han
71	CTD	2	02-16-2012	4:42		5:00	73°49.30'S	113°03.67'W	783	100		24	5.18	270	0	282	Second shallow casting	TW Kim
71	PHY	1	02-16-2012	5:16		5:26					150						20 micron mesh	EJ Yang
71	BON	1	02-16-2012	5:38		5:49					200						Vertical towing	DB Lee
71	BON	2	02-16-2012	5:55		6:07					200						Vertical towing	DB Lee
71	OBY	1	02-16-2012	6:15		8:11	73°49.17'S	113°04.33'W	785								ASPIRE buoy recovery	HK Ha
19	GFO	1	02-16-2012	11:30		11:35				15							GO-FLO	JS Park
19	CTD	1	02-16-2012	11:40		12:53	74°12.13'S	112°30.67'W	1064	1064		24	3.8	182	0	151	First deep casting	TW Kim
19	PHY	1	02-16-2012	13:10		13:22					150						20 micron mesh	EJ Yang
19	BON	1	02-16-2012	13:28		13:40					200						Vertical towing	DB Lee
19	BON	2	02-16-2012	13:45		13:58					200						Vertical towing	DB Lee
19	CTD	2	02-16-2012	14:23		14:41	74°12.13'S	112°30.67'W	1064	100		24	7.5	180	0	140	Second shallow casting	TW Kim
19	OCL	1	02-16-2012	14:50		15:20				90							HPRO II	JM Han
19	CTD	3	02-16-2012	15:48		16:00	74°11.96'S	112°30.82'W	1060	50		24	5.3	194	0.5	105	Third shallow casting (salinity pump is not work due to freezing, the fourth cast overwrite the third)	TW Kim
19	OBY	1	02-16-2012	16:30		18:27	74°11.20'S	112°31.78'W	1057								K3 KOPRI buoy deploy	HK Ha
20	CTD	1	02-16-2012	21:22		22:07	74°12.41'S	112°05.51'W	742	737		24	6.4	177	0	179	Only deep casting	TW Kim
			02-16-2012	21:41													Bear Penninsula; Dispatch AWS team by heli	TJ Choi
20	OCL	1	02-16-2012	22:35		23:30				102							HPRO II	JM Han
19	BOX	1	02-17-2012	2:30	2:55	3:20	74°12.00'S	112°31.25'W	1080								Box core (failed)	HS Moon
19	BOX	2	02-17-2012	2:30	2:55	3:20	74°12.00'S	112°31.25'W	1080								Box core	HS Moon

Scientific Cruise Daily Log

Ship: R/V Araon **Cruise:** ANA02 **Leg:** C Prepared by T.W. Kim (KOPRI) twkim@kopri.re.kr

STN No.	Gear	Cast No.	Date (UTC)	Cast start (UTC)	Bottom or at depth (UTC)	Cast end (UTC)	Latitude	Longitude	Water depth (m)	Cast depth (m)	Cable payout (m)	No. of sal Core length	Wind speed knot	Wind direction (°)	Ship speed knot	Heading (°)	Remarks	Device Driver
Amundsen Sea																		
CTD: CTD;**XBT**: XBT;**GFO**: GO-FLO;**ZOO**: Zooplankton; **PHY**: Phytoplankton; **BON**: Bongo net; **MOC**: Mocness; **MUC**: multi-core; **BOX**: Box core; **GVC**: gravity core; **PSC**: piston core; **ICE**: work on sea-ice; **IBY**: ice buoy; **OBY**: ocean buoy; **SUF**: surface water; **OCL**: ocean color																		
19	BOX	3	02-17-2012	2:30	2:55	3:20	74°12.00'S	112°31.25'W	1080								Box core	HS Moon
19	MUC	1	02-17-2012	2:30	2:55	3:20	74°12.00'S	112°31.25'W	1080								Multiple core (failed)	HS Moon
19	BOX	4	02-17-2012	2:30	2:55	3:20	74°12.00'S	112°31.25'W	1080								Box core	HS Moon
19	BOX	5	02-17-2012	7:33	7:58	8:23	74°12.00'S	112°31.25'W	1080								Box core	HS Moon
19	GVC	1	02-17-2012	9:15	9:35	10:05	74°12.00'S	112°31.25'W	1080								Gravity core	HS Moon
28	CTD	1	02-17-2012	11:58		12:56	74°12.48'S	112°49.26'W	794	790		24	1.9	120	0	201	Only deep casting	TW Kim
27	CTD	1	02-17-2012	14:56		16:02	74°10.46'S	113°19.75'W	683	680		24	2.85	197	0	308	Only deep casting	TW Kim
27	OCL	1	02-17-2012	16:10		16:30				110							HPRO II	JM Han
26	CTD	1	02-17-2012	22:04		22:48	74°06.31'S	115°08.54'W	648	645		24	2.4	260	0	156	Only deep casting (no shallow)	TW Kim
26	OCL	1	02-17-2012	22:55		23:25				110							HPRO II	JM Han
25	CTD	1	02-18-2012	1:01		2:06	74°07.51'S	115°21.28'W	1136	1111		24	2.5	190	0	276	Only deep casting (no shallow)	CS Hong
25	OCL	1	02-18-2012	2:25		2:40				100							HPRO II	JM Han
24	GFO	1	02-18-2012	4:00		4:05				15							GO-FLO	JS Park
24	CTD	1	02-18-2012	4:08		5:10	74°04.80'S	115°43.49'W	1076	1055		24	5	170	0	268	First deep casting	CS Hong
24	PHY	1	02-18-2012	5:24		5:34					150						20 micron mesh	EJ Yang
24	BON	1	02-18-2012	5:41		5:55					200						Vertical towing	DB Lee
24	BON	2	02-18-2012	6:00		6:13					200						Vertical towing	DB Lee
24	CTD	2	02-18-2012	6:31		6:47	74°04.80'S	115°43.46'W	1077	100		24	2.7	180	0	167	Second shallow casting	CS Hong
24	BON	3	02-18-2012	7:13		7:58					300						Oblique towing	DB Lee
23	CTD	1	02-18-2012	8:50		9:39	74°02.22'S	115°57.39'W	1006	1003		24	1	150	0	265	Only deep casting (no shallow)	CS Hong
22	CTD	1	02-18-2012	11:22		12:03	73°55.46'S	116°08.22'W	637	635		24	2	170	0	298	First deep casting	CS Hong
22	OCL	1	02-18-2012	12:10		12:25				105							HPRO II	JM Han
22	CTD	2	02-18-2012	13:12		13:24	73°55.46'S	116°08.22'W	636	100		24	2.4	214	0	296	Second shallow casting	TW Kim
21	CTD	1	02-18-2012	21:30		22:10	74°12.15'S	111°58.50'W	630	626		24	5.4	186	0	199	Only deep casting (no shallow)	TW Kim
			02-18-2012	22:20													Dispatch heli for picking up AWS team	TJ Choi
21	OCL	1	02-18-2012	22:35		22:50				102							HPRO II	JM Han
19	CTD	4	02-19-2012	1:37		1:50	74°11.98'S	112°29.82'W	1037	100		24	5.6	182	0	7.5	Only shallow casting	TW Kim
	MOC	1	02-19-2012	14:35		16:08	73°22.03'S	111°16.70'W	330								Mocness towing	HS Na
29	ICE	1	02-20-2012	0:30		17:00	73°28.25'S	110°02.20'W									Sea ice mechanics team work at first sea ice station	MOERI
29	CTD	1	02-20-2012	7:22		7:50	73°28.24'S	110°09.96'W	331	325		24	2.9	72	0	37	Only deep casting (no shallow)	TW Kim
30	ICE	1	02-21-2012	0:00		22 12:30	73°30.73'S	109°02.20'W									Sea ice mechanics team work at second sea ice station	MOERI
30	ICE	1	02-21-2012	7:00		22 09:00	73°31.69'S	109°07.56'W	515	30							KOPRI sea ice work at first sea ice station (ADCP, LISST-HOLO, MicroCat, pCO2 and DO mooring)	HK Ha
30	ICE	1	02-21-2012	14:10		14:30	73°31.69'S	109°07.56'W		100							KOPRI sea ice work at first sea ice station (HPRO II)	JM Han
30	ICE	1	02-21-2012	21:00		22 02:00	73°31.69'S	109°07.56'W		25							Hydrocasting at KOPRI sea ice work	D Hahm
30	CTD	1	02-22-2012	9:28		10:01	73°28.13'S	108°43.65'W	515	510		24	6.3	35	0.1	54	Only deep casting (no shallow)	TW Kim
87	CTD	1	02-22-2012	22:28		23:33	74°21.98'S	105°00.00'W	1289	1278		24	14	73	0.1	88	First deep casting	CS Hong
87	OCL	1	02-22-2012	23:40		23 00:25				110							HPRO II	JM Han
87	OBY	1	02-23-2012	1:39		2:53	73°21.70'S	104°58.12'W	1346								ISTAR 7 buoy deploy	P. Abrahamsen
88	GFO	1	02-23-2012	16:30		16:45				15							GO-FLO	JS Park
88	OBY	1	02-23-2012	16:53		18:26	74°51.58'S	102°06.16'W	957								ISTAR 8 buoy deploy	P. Abrahamsen
88	PHY	1	02-23-2012	20:32		20:44					150						20 micron mesh	EJ Yang
88	BON	1	02-23-2012	20:50		21:19					150						Vertical towing	DB Lee
88	OCL	1	02-23-2012	21:25		21:55				100							HPRO II	JM Han
88	CTD	1	02-23-2012	22:16		23:08	74°51.83'S	102°05.71'W	942	935		24	16.8	359	0.2	2.3	Only deep casting (CTD cable problem, cable molding)	TW Kim
89	OBY	1	02-24-2012	3:03		3:57	75°03.23'S	102°09.24'W	830								ISTAR 9 buoy deploy	P. Abrahamsen
89	CTD	1	02-24-2-12	6:57		7:50	75°03.88'S	102°08.82'W	783	740		24	12	347	0.5	350	Only deep casting (Using SCS winch and A-frame, the second cast overwrite the first cast file)	TW Kim
31	GFO	1	02-24-2012	9:30		10:50				15							GO-FLO	JS Park
31	CTD	1	02-24-2012	11:12		12:18	75°05.24'S	101°45.56'W	947	943		24	9	350	0.2	344	First deep casting	HK Ha
31	PHY	1	02-24-2012	12:34		12:45					150						20 micron mesh	EJ Yang
31	BON	1	02-24-2012	12:50		13:17					165						Vertical towing	DB Lee
31	CTD	2	02-24-2012	13:47		14:03	75°05.24'S	101°45.56'W	939	100		24	7.8	8	0.1	350	Second shallow casting	HK Ha
31	OCL	1	02-24-2012	14:10		14:30				100							HPRO II	JM Han
31	CTD	3	02-24-2012	15:03		15:19	75°05.24'S	101°45.56'W	939	100		24	7.5	330	0	350	Third shallow casting	HK Ha
31	BON	3	02-24-2012	16:05		16:45					300						Oblique towing	DB Lee
32	CTD	1	02-24-2012	17:47		19:01	75°01.07'S	101°46.67'W	1017	1015		24	8.5	340	0	349	Only deep casting	HK Ha
33	CTD	1	02-24-2012	20:32		21:31	74°58.49'S	102°01.05'W	917	910		24	6	320	0	317	Only deep casting	CS Hong
34	GFO	1	02-25-2012	0:00		0:05				15							GO-FLO	JS Park
34	OCL	1	02-25-2012	0:45		1:05				100							HPRO II	JM Han
34	PHY	1	02-25-2012	1:45		1:57					150						20 micron mesh	EJ Yang
34	BON	1	02-25-2012	2:04		2:34					200						Vertical towing	DB Lee

Scientific Cruise Daily Log

Ship: R/V Araon **Cruise:** ANA02 **Leg:** C **Prepared by T.W. Kim (KOPRI) twkim@kopri.re.kr**

STN No.	Gear	Cast No.	Date (UTC)	Cast start (UTC)	Bottom or at depth (UTC)	Cast end (UTC)	Latitude	Longitude	Water depth (m)	Cast depth (m)	Cable payout (m)	No. of sal Core length	Wind speed knot	Wind direction (°)	Ship speed knot	Heading (°)	Remarks	Device Driver
Amundsen Sea																		
CTD: CTD;**XBT**: XBT;**GFO**: GO-FLO;**ZOO**: Zooplankton; **PHY**: Phytoplankton; **BON**: Bongo net; **MOC**: Mocness; **MUC**: multi-core; **BOX**: Box core; **GVC**: gravity core; **PSC**: piston core; **ICE**: work on sea-ice; **IBY**: ice buoy; **OBY**: ocean buoy; **SUF**: surface water; **OCL**: ocean color																		
34	CTD	1	02-25-2012	4:28		5:19	74°38.83'S	101°31.97'W	541	540		24	7	331	0.1	335	Only deep casting (Conductivity and Temperature sensors problem, change the sensors)	TW Kim
		1	02-25-2012	14:05													B22; Dispatch SAR team by heli (Corner Reflector installation)	JW Kim
35	BON	1	02-25-2012	16:01		16:25			1369		200						Target trawl	HS Na
35	CTD	1	02-25-2012	17:20		18:23	74°34.26'S	106°35.97'W	1369	1355		24	7.1	254	0	267	Only deep casting at SAR-1 station	TW Kim
		1	02-25-2012	18:22													Dispatch heli for picking up SAR team	JW Kim
		2	02-25-2012	22:32													B22; Dispatch SAR team by heli (Corner Reflector installation)	JW Kim
	BON	1	02-26-2012	0:00		0:40	74°12.64'S	107°25.82'W	696								Oblique towing	HS Na
	BON	2	02-26-2012	0:50		1:30	74°12.64'S	107°25.82'W	696								Oblique towing	HS Na
		2	02-26-2012	1:45													Dispatch heli for picking up SAR team	JW Kim
87	GFO	1	02-26-2012	6:18		6:42				15							GO-FLO	JH Hyun
87	CTD	2	02-26-2012	6:46		6:59	74°21.99'S	104°59.93'W	1273	100		24	6.7	263	0	91	Only shallow casting	TW Kim
87	PHY	1	02-26-2012	7:13		7:25					150						20 micron mesh	EJ Yang
87	BON	1	02-26-2012	7:35		8:00					200						Vertical towing	DB Lee
		2	02-26-2012	17:15													Lindsey island; Dispatch AWS team by heli	TJ Choi
86	GFO	1	02-27-2012	4:00		4:05				15							GO-FLO	JS Park
86	OCL	1	02-27-2012	4:00		4:15				100							HPRO II	JM Han
86	OBY	1	02-27-2012	4:48		5:46	73°48.76'S	106°32.12'W	913								ISTAR 6 buoy deploy	HK Ha
86	CTD	1	02-27-2012	6:37		7:28	73°48.71'S	106°32.14'W	933	920		24	3.7	192	0.1	56	First deep casting	TW Kim
86	PHY	1	02-27-2012	7:43		7:55					150						20 micron mesh	EJ Yang
86	BON	1	02-27-2012	8:02		8:30					200						Vertical towing	DB Lee
86	CTD	2	02-27-2012	8:45		8:59	73°48.56'S	106°32.13'W	933	100		24	5.4	192	0	49	Second shallow casting	TW Kim
86	CTD	3	02-27-2012	9:38		9:47	73°48.53'S	106°32.09'W	933	35		24	5.8	170	0	49	Third shallow casting	TW Kim
		2	02-27-2012	18:50													Dispatch heli for picking up AWS team	TJ Choi
36	CTD	1	02-28-2012	8:11		8:52	73°49.20'S	108°16.28'W	742	735		24	11	174	0	171	First deep casting (pump not work, second cast overwrite the first cast file)	TW Kim
	XBT	16	02-28-2012	9:12			73°49.20'S	108°16.29'W	741.4								XBT	HK Ha
		17	02-28-2012	12:00			73°40.80'S	109°06.6'W	420								XBT	TW Kim
		18	02-28-2012	18:40			73°30.93'S	109°44.48'W	392								XBT	HK Ha
37	CTD	1	02-29-2012	9:10		9:40	73°24.35'S	110°10.36'W	351	340		24	11.2	160	0	166	Only deep casting	CS Hong
		19	02-29-2012	14:55			73°14.93'S	111°16.87'W	322								XBT	TW Kim
		20	02-29-2012	18:07			73°21.88'S	113°03.64'W	510								XBT	CS Hong
17	CTD	3	02-29-2012	20:32		21:11	73°30.02'S	114°00.60'W	712	710		24	9.2	149	0	159	Revisit Station 17 for comparison between 2/14 and 2/19	MK Kim
17	PHY	1	02-29-2012	20:32		20:44					150						20 micron mesh	EJ Yang
17	BON	1	02-29-2012	20:50		21:19					150						Vertical towing	DB Lee
17	CTD	4	02-29-2012	23:51		0:04	73°28.64'S	114°13.46'W	781	100		24	8.5	80	0	345	Revisit Station 17 for comparison between 2/14 and 2/19	TW Kim
		21	03-01-2012	2:54			73°14.75'S	115°41.84'W	743								XBT	HK Ha
		22	03-01-2012	6:10			72°57.36'S	117°20.10'W	575								XBT	CS Hong
63	GFO	1	03-01-2012	7:05		7:35				15							GO-FLO	JS Park
63	OBY	1	03-01-2012	7:35		8:36	72°55.58'S	117°34.89'W	830								UG S3 buoy deploy	C. Stranne
63	CTD	1	03-01-2012	9:05		9:39	72°55.60'S	117°35.01'W	542	535		24	4.8	97	0	302	First deep casting	TW Kim
63	CTD	2	03-01-2012	10:29		10:44	72°55.63'S	117°35.21'W	540	100		24	3.9	118	0	302	Second shallow casting	SA Hwang
		23	03-01-2012	12:07			72°50.10'S	117°26.71'W	614	500							XBT	TW Kim
		24	03-01-2012	15:00			72°33.83'S	116°39.49'W	573								XBT	HK Ha
61	OBY	1	03-01-2012	20:14		20:32	72°27.41'S	116°20.76'W	555								UG S1 buoy recovery	C. Stranne
61	CTD	1	03-01-2012	21:17		21:54	72°27.65'S	116°22.12'W	555	545		24	4.4	120	0	30	First deep casting	TW Kim
61	PHY	1	03-01-2012	22:11		22:22					150						20 micron mesh	EJ Yang
61	BON	1	03-01-2012	22:29		22:58					200						Vertical towing	DB Lee
61	CTD	2	03-01-2012	23:13		23:28	72°27.81'S	116°23.45'W	556	100		24	5.7	165	0	39	Second shallow casting	TW Kim
61	OCL	1	03-01-2012	23:30		23:50				100							HPRO II	JM Han
61	OBY	2	03-02-2012	0:42		1:29	72°27.30'S	116°21.04'W	556								UG S1 buoy redeploy	C. Stranne
		25	03-02-2012	12:04			72°02.43'S	116°52.69'W	489								XBT	CS Hong
6	OBY	1	03-02-2012	20:23		23:07	72°24.16'S	117°43.34'W	530								KOPRI K1 buoy recovery	HK Ha
6	CTD	1	03-03-2012	0:22		0:59	72°23.40'S	117°43.16'W	521	515		24	6.5	246	0	89	First deep casting	TW Kim
6	PHY	1	03-03-2012	1:16		1:28					150						20 micron mesh	EJ Yang
6	BON	1	03-03-2012	1:30		2:05					200						Vertical towing	DB Lee
6	CTD	2	03-03-2012	2:24		2:38	72°23.17'S	117°43.21'W	523	100		24	3.5	241	0	90	Second shallow casting	TW Kim
6	OCL	1	03-03-2012	2:45		3:10				100							HPRO II	JM Han
6	EK60	1	03-03-2012	8:20		14:27											EK60 Calibration	HS Na
6	OBY	2	03-04-2012	1:08		2:03	72°23.24'S	117°42.82'W	525								KOPRI K1 buoy redeploy	HK Ha
	ICE	1	03-03-2012	10:00		04 05:30	72°13.56'S	117°47.82'W									Sea ice mechanics team work at first sea ice station	MOERI
3	GFO	1	03-04-2012	8:20		8:30				15							GO-FLO	JS Park

Scientific Cruise Daily Log

Ship: R/V Araon **Cruise:** ANA02 **Leg:** C Prepared by T.W. Kim (KOPRI) twkim@kopri.re.kr

STN No.	Gear	Cast No.	Date	Cast start	Bottom or at depth	Cast end	Latitude	Longitude	Water depth	Cast depth	Cable payout	No. of sal Core length	Wind speed	Wind direction	Ship speed	Heading	Remarks	Device Driver
			(UTC)	(UTC)	(UTC)	(UTC)			(m)	(m)	(m)		knot	(°)	knot	(°)		
Amundsen Sea																		
CTD: CTD;**XBT**: XBT;**GFO**: GO-FLO;**ZOO**: Zooplankton; **PHY**: Phytoplankton; **BON**: Bongo net; **MOC**: Mocness; **MUC**: multi-core; **BOX**: Box core; **GVC**: gravity core; **PSC**: piston core; **ICE**: work on sea-ice; **IBY**: ice buoy; **OBY**: ocean buoy; **SUF**: surface water; **OCL**: ocean color																		
3	CTD	1	03-04-2012	9:00		9:37	71°57.11'S	118°26.73'W	610	609		24	1.8	72	0.1	121	First deep casting	TW Kim
3	PHY	1	03-04-2012	9:51		10:02					150						20 micron mesh	EJ Yang
3	BON	1	03-04-2012	10:10		10:39					200						Vertical towing	DB Lee
3	CTD	2	03-04-2012	11:08		11:22	71°56.73'S	118°27.26'W	645	100		24	3.2	140	0	119	Second shallow casting	TW Kim
3	OCL	1	03-04-2012	13:45		14:00				88							HPRO II	JM Han
3	OBY	1	03-04-2012	12:28		13:26	71°57.06'S	118°27.09'W	645								UG S2 buoy deploy	C. Stranne
85	OBY	1	03-05-2012	2:38		4:22	71°25.39'S	114°18.89'W	1465								ISTAR 5 buoy deploy	P. Abrahamsen
85	GFO	1	03-05-2012	4:40		5:35				15							GO-FLO	JS Park
85	CTD	1	03-05-2012	6:47		7:54	71°25.20'S	114°19.44'W	1510	1500		24	2.9	134	0	307	First shallow casting (Pump is not work during first cast, second cast overwrite the first cast file, salinity not co	TW Kim
85	CTD	2	03-05-2012	8:50			71°25.02'S	114°20.71'W	1528	1523		24	3.2	147	0.2	314	Second deep casting	HK Ha
84	OBY	1	03-05-2012	11:42		12:27	71°32.70'S	114°18.21'W	513								ISTAR 4 buoy deploy	P. Abrahamsen
84	CTD	1	03-05-2012	13:18		13:50	71°32.73'S	114°18.56'W	506	500		24	4.8	102	0.2	161	Only deep casting	HK Ha
83	CTD	1	03-05-2012	15:52		16:34	71°42.00'S	114°02.26'W	537	532		24	7.1	125	0.2	63	Only deep casting	HK Ha
83	OBY	1	03-05-2012	16:59		17:42	71°42.18'S	114°02.61'W	542								ISTAR 3 buoy deploy	P. Abrahamsen
83	OCL	1	03-05-2012	18:40		19:00				100							HPRO II	JM Han
	BOX	1	03-05-2012	23:40	0:00	0:15	71°41.88'S	114°02.41'W	543								Box core	HS Moon
	BOX	2	03-06-2012	0:58	1:11	1:25	71°41.88'S	114°02.41'W	543								Box core	HS Moon
	BOX	3	03-06-2012	1:45	1:57	2:12	71°41.88'S	114°02.41'W	543								Box core	HS Moon
	BOX	4	03-06-2012	2:32	2:45	3:00	71°41.88'S	114°02.41'W	543								Box core	HS Moon
	GVC	1	03-06-2012	3:22	3:33	3:50	71°41.88'S	114°02.41'W	543								Gravity core	HS Moon
82	OBY	1	03-06-2012	4:36		5:17	71°38.35'S	113°32.15'W	615								ISTAR 2 buoy deploy	P. Abrahamsen
82	CTD	1	03-06-2012	6:04		6:48	71°38.23'S	113°32.73'W	609	605		24	8.6	144	0.4	131	Only deep casting	TW Kim
81	OBY	1	03-06-2012	9:07													BSR 12 buoy recovery (Release enabled 09:07, Released 12:39, Mooring not sighted)	P. Abrahamsen
81	CTD	1	03-06-2012	10:34		11:11	71°34.04'S	113°00.82'W	594	592		24	7.6	152	0.4	38	Only deep casting	TW Kim
81	OBY	2	03-06-2012	15:15		16:00	71°38.35'S	113°32.15'W	615								ISTAR 1 buoy deploy	P. Abrahamsen
90	OBY	1	03-06-2012	18:48		21:30											BSR 13 buoy recovery	P. Abrahamsen
90	CTD	1	03-06-2012	21:46		22:40	71°23.18'S	113°23.79'W	1089	1080		24	5.2	187	0.3	75	Only deep casting	HK Ha
	BON	1	03-07-2012	12:40		13:10	70°45.74'S	117°22.52'W									Target trawl	HS Na
	BON	2	03-07-2012	13:20		13:34	70°47.18'S	117°23.72'W									Target trawl	HS Na
	MOC	1	03-07-2012	19:05		20:13	70°44.97'S	118°49.85'W									Mocness towing	HS Na
38	GFO	1	03-07-2012	20:40		20:50				15							GO-FLO	JS Park
38	CTD	1	03-07-2012	20:58		21:30	70°45.01'S	119°00.03'W	3110	1692			5.5	35	0	84	CTD saved only downcasting (0~1692m) due to the winch cable problem, no water samples.	CS Hong
39	GFO	1	03-09-2012	6:00		6:10				15							GO-FLO	JS Park
39	CTD	1	03-09-2012	6:18		9:02	71°34.84'S	133°59.30'W	3965	3960		24	9.2	83	0.3	74	First deep casting	TW Kim
39	PHY	1	03-09-2012	9:13		9:25					150						20 micron mesh	EJ Yang
39	BON	1	03-09-2012	9:34		10:05					200						Vertical towing	DB Lee
39	CTD	2	03-09-2012	10:41		10:56	71°34.85'S	133°59.30'W	3913	100		24	7.5	113	0	101	Second shallow casting	TW Kim
39	CTD	3	03-09-2012	11:30		11:37	71°34.84'S	133°59.30'W	3914	30		24	11	131	0.5	98	Third shallow casting	TW Kim
40	CTD	1	03-10-2012	6:42		7:00	73°41.08'S	136°58.44'W	2520	100		24	13	81	0.4	343	First shallow casting	TW Kim
		3	03-10-2012	15:05													Cape Bucks; Dispatch AWS team by heli	TJ Choi
40	CTD	2	03-10-2012	18:59		20:44	73°42.56'S	137°10.76'W	2578	2570		24	3.6	142	0.2	334	Second deep casting	TW Kim
		3	03-10-2012	20:52													Dispatch heli for picking up AWS team	TJ Choi
40	OCL	1	03-10-2012	20:55		21:10				100							HPRO II	JM Han

1.4 Appendix II. All layout diagrams of moorings serviced by KOPRI, BAS, MBL and UGOT.

See the following pages.

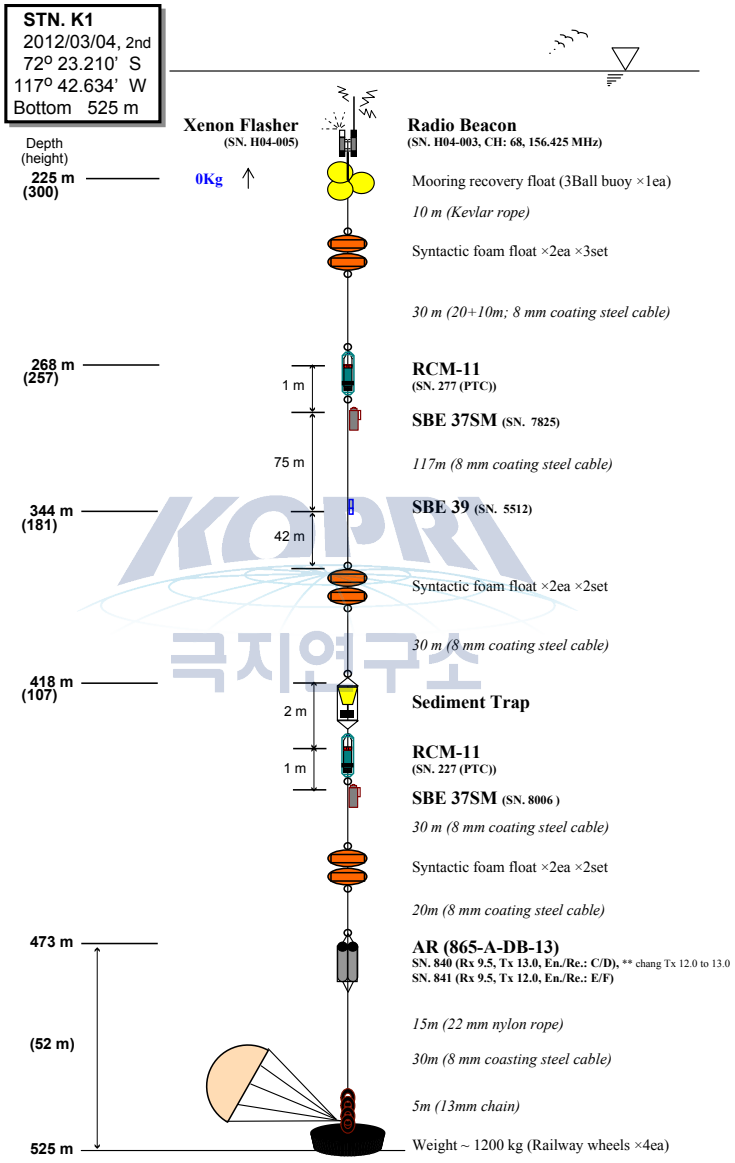
STN. K1
2012/03/04, 2nd
72° 23.210' S
117° 42.634' W
Bottom 525 m
Depth (height)
225 m (300)
Xenon Flasher
(SN. H04-005)
0Kg
Radio Beacon
(SN. H04-003, CH: 68, 156.425 MHz)
Mooring recovery float (3Ball buoy ×1ea)
10 m (Kevlar rope)
Syntactic foam float ×2ea ×3set
30 m (20+10m; 8 mm coating steel cable)
268 m (257)
1 m
RCM-11
(SN. 277 (PTC))
SBE 37SM (SN. 7825)
75 m
117m (8 mm coating steel cable)
344 m (181)
SBE 39 (SN. 5512)
42 m
Syntactic foam float ×2ea ×2set
30 m (8 mm coating steel cable)
418 m (107)
2 m
Sediment Trap
1 m
RCM-11
(SN. 227 (PTC))
SBE 37SM (SN. 8006)
30 m (8 mm coating steel cable)
Syntactic foam float ×2ea ×2set
20m (8 mm coating steel cable)
473 m
AR (865-A-DB-13)
SN. 840 (Rx 9.5, Tx 13.0, En./Rc.: C/D), ** chang Tx 12.0 to 13.0
SN. 841 (Rx 9.5, Tx 12.0, En./Rc.: E/F)
15m (22 mm nylon rope)
(52 m)
30m (8 mm coasting steel cable)
5m (13mm chain)
525 m
Weight ~ 1200 kg (Railway wheels ×4ea)

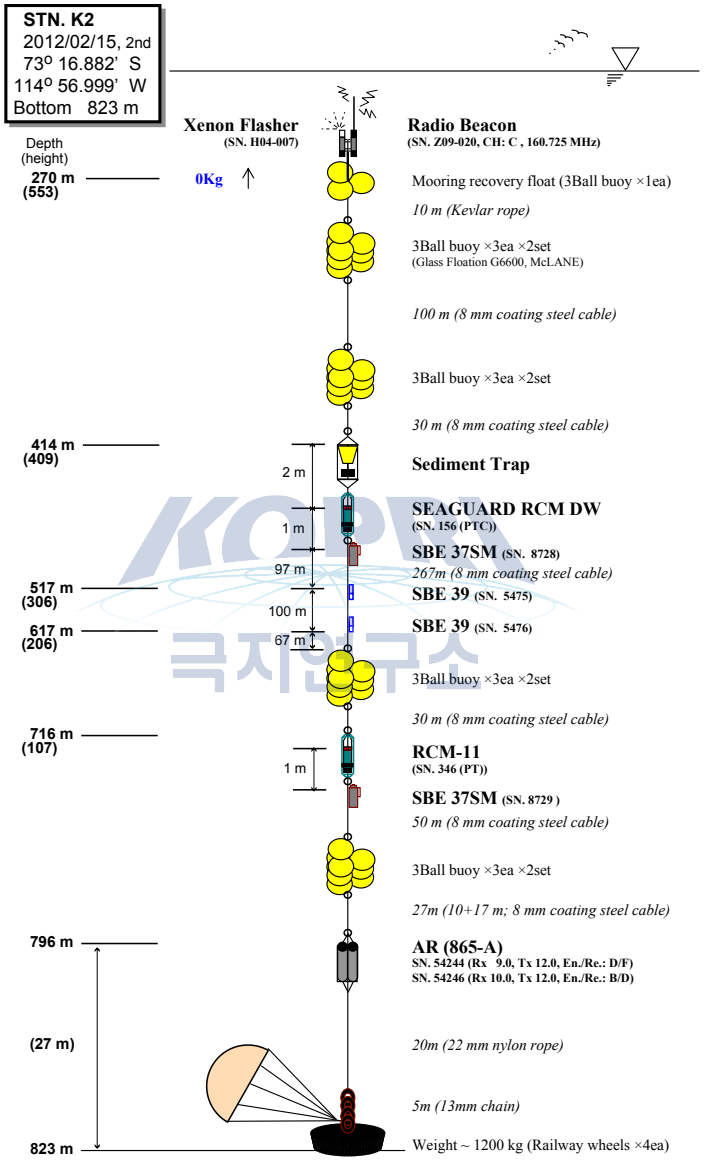
STN. K2
2012/02/15, 2nd
73° 16.882' S
114° 56.999' W
Bottom 823 m
Xenon Flasher
(SN. H04-007)
Radio Beacon
(SN. Z09-020, CH: C , 160.725 MHz)
Depth
(height)
270 m
(553)
0Kg
Mooring recovery float (3Ball buoy ×1ea)
10 m (Kevlar rope)
3Ball buoy ×3ea ×2set
(Glass Floation G6600, McLANE)
100 m (8 mm coating steel cable)
3Ball buoy ×3ea ×2set
30 m (8 mm coating steel cable)
414 m
(409)
2 m
Sediment Trap
1 m
SEAGUARD RCM DW
(SN. 156 (PTC))
SBE 37SM (SN. 8728)
97 m
267m (8 mm coating steel cable)
517 m
(306)
SBE 39 (SN. 5475)
100 m
617 m
(206)
67 m
SBE 39 (SN. 5476)
3Ball buoy ×3ea ×2set
30 m (8 mm coating steel cable)
716 m
(107)
1 m
RCM-11
(SN. 346 (PT))
SBE 37SM (SN. 8729)
50 m (8 mm coating steel cable)
3Ball buoy ×3ea ×2set
27m (10+17 m; 8 mm coating steel cable)
796 m
AR (865-A)
SN. 54244 (Rx 9.0, Tx 12.0, En./Re.: D/F)
SN. 54246 (Rx 10.0, Tx 12.0, En./Re.: B/D)
(27 m)
20m (22 mm nylon rope)
5m (13mm chain)
823 m
Weight ~ 1200 kg (Railway wheels ×4ea)

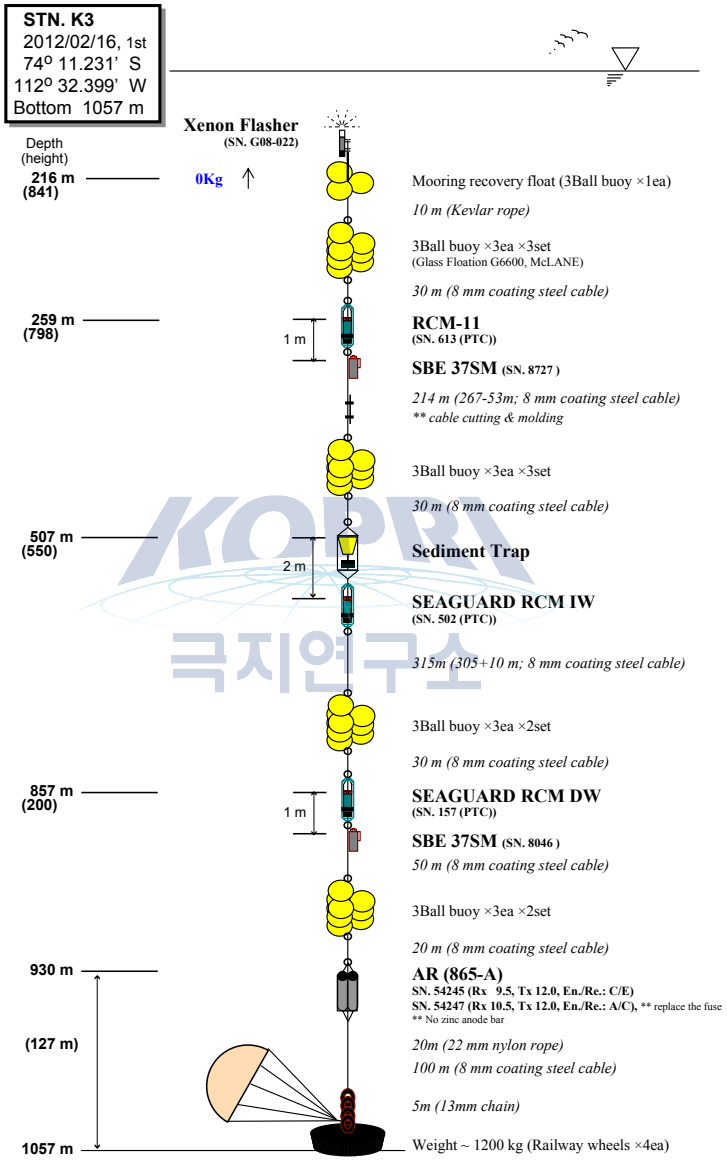
STN. K3
2012/02/16, 1st
74° 11.231' S
112° 32.399' W
Bottom 1057 m
Xenon Flasher
(SN. G08-022)
Depth
(height)
216 m
(841)
0Kg
Mooring recovery float (3Ball buoy ×1ea)
10 m (Kevlar rope)
3Ball buoy ×3ea ×3set
(Glass Floation G6600, McLANE)
30 m (8 mm coating steel cable)
259 m
(798)
1 m
RCM-11
(SN. 613 (PTC))
SBE 37SM (SN. 8727)
214 m (267-53m; 8 mm coating steel cable)
** cable cutting & molding
3Ball buoy ×3ea ×3set
30 m (8 mm coating steel cable)
507 m
(550)
2 m
Sediment Trap
SEAGUARD RCM IW
(SN. 502 (PTC))
315m (305+10 m; 8 mm coating steel cable)
3Ball buoy ×3ea ×2set
30 m (8 mm coating steel cable)
857 m
(200)
1 m
SEAGUARD RCM DW
(SN. 157 (PTC))
SBE 37SM (SN. 8046)
50 m (8 mm coating steel cable)
3Ball buoy ×3ea ×2set
20 m (8 mm coating steel cable)
930 m
AR (865-A)
SN. 54245 (Rx 9.5, Tx 12.0, En./Re.: C/E)
SN. 54247 (Rx 10.5, Tx 12.0, En./Re.: A/C), ** replace the fuse
** No zinc anode bar
(127 m)
20m (22 mm nylon rope)
100 m (8 mm coating steel cable)
5m (13mm chain)
1057 m
Weight ~ 1200 kg (Railway wheels ×4ea)

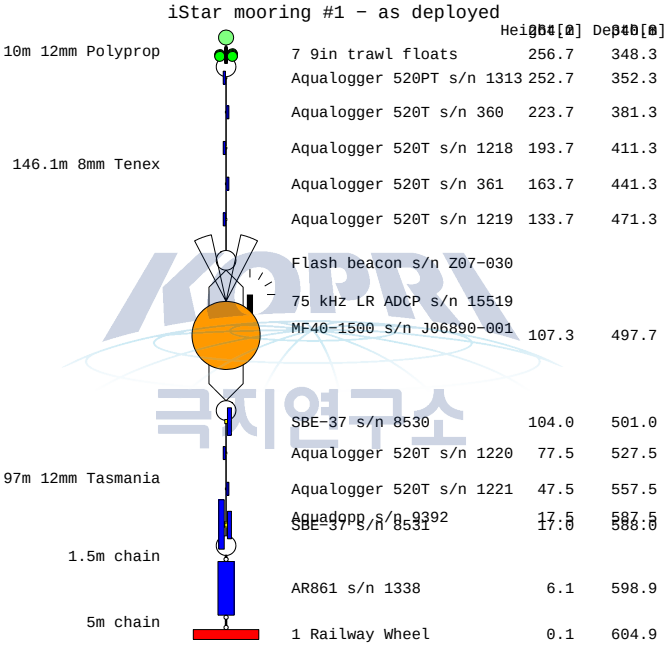
iStar mooring #1 – as deployed
Height [m] Depth [m]
10m 12mm Polyprop
7 9in trawl floats 256.7 348.3
Aqualogger 520PT s/n 1313 252.7 352.3
Aqualogger 520T s/n 360 223.7 381.3
Aqualogger 520T s/n 1218 193.7 411.3
146.1m 8mm Tenex
Aqualogger 520T s/n 361 163.7 441.3
Aqualogger 520T s/n 1219 133.7 471.3
Flash beacon s/n Z07-030
75 kHz LR ADCP s/n 15519
MF40-1500 s/n J06890-001 107.3 497.7
SBE-37 s/n 8530 104.0 501.0
Aqualogger 520T s/n 1220 77.5 527.5
97m 12mm Tasmania
Aqualogger 520T s/n 1221 47.5 557.5
Aquadopp s/n 9392 17.5 587.5
SBE-37 s/n 8531 17.0 588.0
1.5m chain
AR861 s/n 1338 6.1 598.9
5m chain
1 Railway Wheel 0.1 604.9

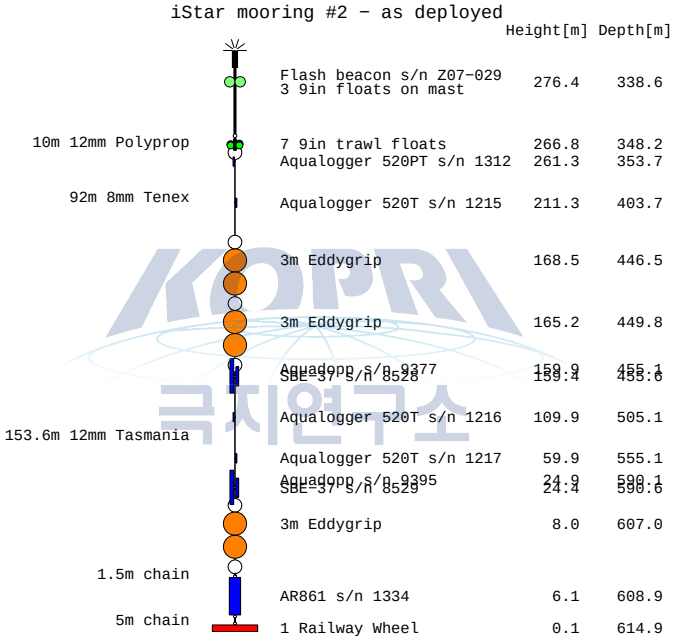
iStar mooring #2 – as deployed
Height[m] Depth[m]
Flash beacon s/n Z07-029
3 9in floats on mast 276.4 338.6
10m 12mm Polyprop
7 9in trawl floats 266.8 348.2
Aqualogger 520PT s/n 1312 261.3 353.7
92m 8mm Tenex
Aqualogger 520T s/n 1215 211.3 403.7
3m Eddygrip 168.5 446.5
3m Eddygrip 165.2 449.8
Aquadopp s/n 9377 159.9 445.1
SBE 37 s/n 8528 159.4 445.6
Aqualogger 520T s/n 1216 109.9 505.1
153.6m 12mm Tasmania
Aqualogger 520T s/n 1217 59.9 555.1
Aquadopp s/n 9395 24.9 590.1
SBE 37 s/n 8529 24.4 590.6
3m Eddygrip 8.0 607.0
1.5m chain
AR861 s/n 1334 6.1 608.9
5m chain
1 Railway Wheel 0.1 614.9

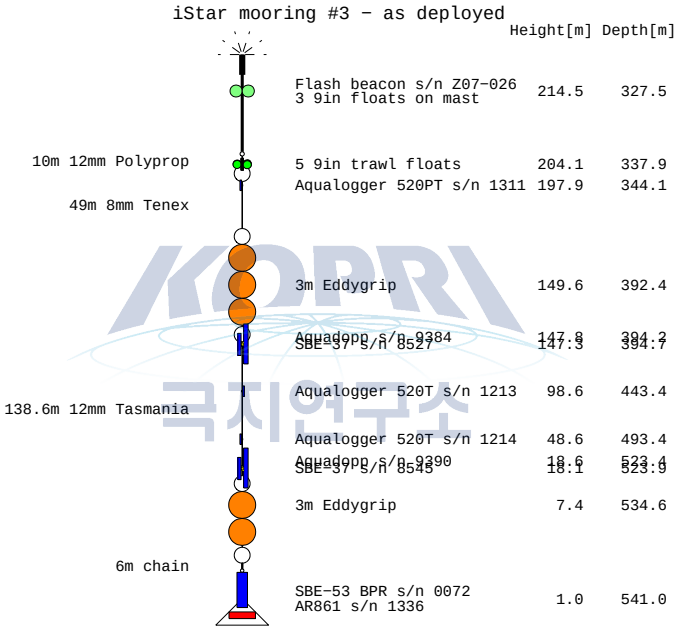
iStar mooring #3 – as deployed
Height[m]
Depth[m]
Flash beacon s/n Z07-026
3 9in floats on mast
214.5
327.5
10m 12mm Polyprop
5 9in trawl floats
204.1
337.9
Aqualogger 520PT s/n 1311
197.9
344.1
49m 8mm Tenex
3m Eddygrip
149.6
392.4
Aquadopp s/n 9384
147.8
394.2
SBE-37 s/n 8527
147.3
394.7
Aqualogger 520T s/n 1213
98.6
443.4
138.6m 12mm Tasmania
Aqualogger 520T s/n 1214
48.6
493.4
Aquadopp s/n 9390
18.6
523.4
SBE-37 s/n 8545
18.1
523.9
3m Eddygrip
7.4
534.6
6m chain
SBE-53 BPR s/n 0072
AR861 s/n 1336
1.0
541.0

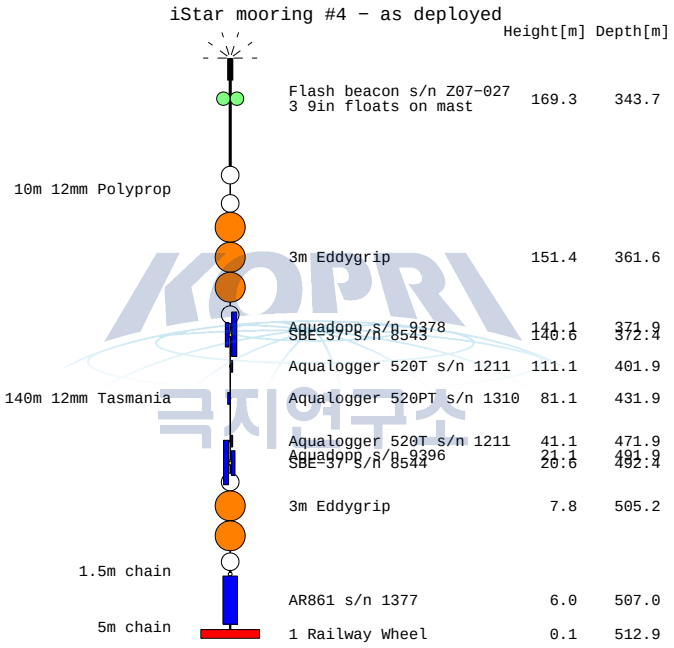
iStar mooring #4 – as deployed
Height[m] Depth[m]
Flash beacon s/n Z07–027
3 9in floats on mast 169.3 343.7
10m 12mm Polyprop
3m Eddygrip 151.4 361.6
Aquadopp s/n 9378 141.1 371.9
SBE–37 s/n 8543 140.6 372.4
Aqualogger 520T s/n 1211 111.1 401.9
140m 12mm Tasmania
Aqualogger 520PT s/n 1310 81.1 431.9
Aqualogger 520T s/n 1211 41.1 471.9
Aquadopp s/n 9396 21.1 491.9
SBE–37 s/n 8544 20.6 492.4
3m Eddygrip 7.8 505.2
1.5m chain
AR861 s/n 1377 6.0 507.0
5m chain
1 Railway Wheel 0.1 512.9

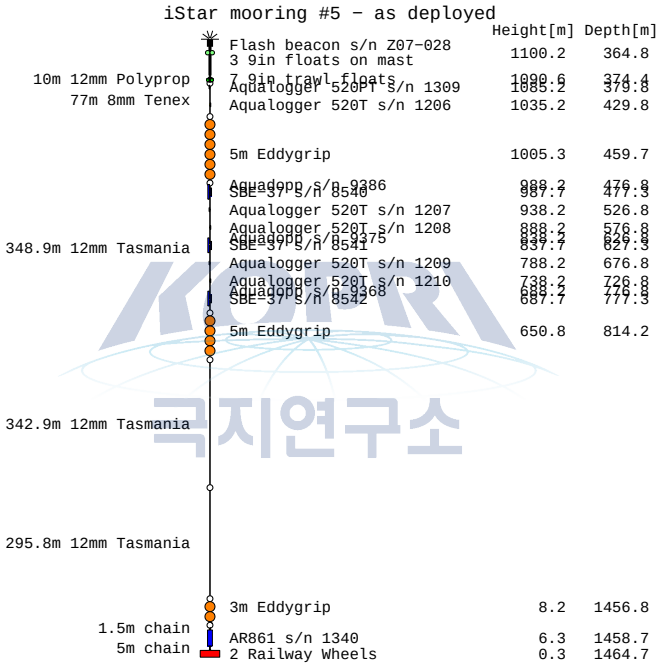
iStar mooring #5 – as deployed
Height[m]
Depth[m]
Flash beacon s/n Z07-028
3 9in floats on mast
1100.2
364.8
10m 12mm Polyprop
7 9in trawl floats
1090.6
374.4
Aqualogger 520PT s/n 1309
1085.2
379.8
77m 8mm Tenex
Aqualogger 520T s/n 1206
1035.2
429.8
5m Eddygrip
1005.3
459.7
Aquadopp s/n 9386
988.2
476.8
SBE 37 s/n 8540
987.7
477.3
Aqualogger 520T s/n 1207
938.2
526.8
Aqualogger 520T s/n 1208
888.2
576.8
Aquadopp s/n 9475
838.2
626.8
348.9m 12mm Tasmania
SBE 37 s/n 8541
837.7
627.3
Aqualogger 520T s/n 1209
788.2
676.8
Aqualogger 520T s/n 1210
738.2
726.8
Aquadopp s/n 9368
688.2
776.8
SBE 37 s/n 8542
687.7
777.3
5m Eddygrip
650.8
814.2
342.9m 12mm Tasmania
295.8m 12mm Tasmania
3m Eddygrip
8.2
1456.8
1.5m chain
AR861 s/n 1340
6.3
1458.7
5m chain
2 Railway Wheels
0.3
1464.7

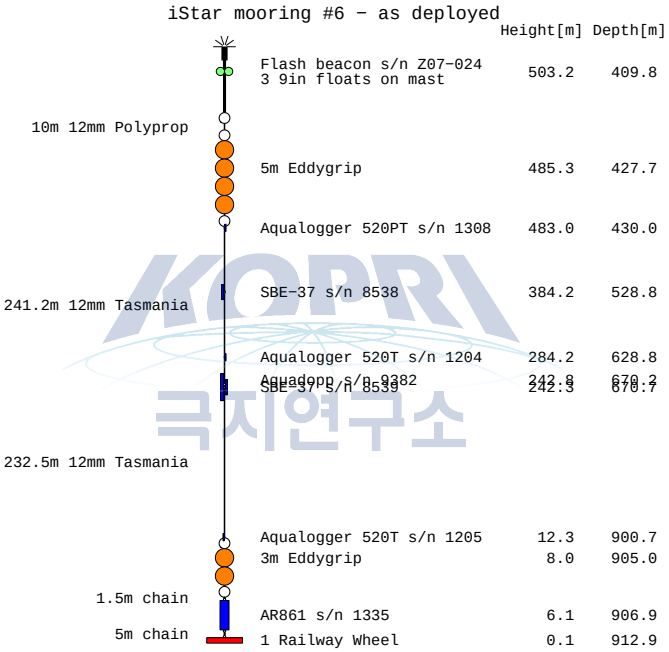
iStar mooring #6 – as deployed
Height[m]
Depth[m]
Flash beacon s/n Z07-024
3 9in floats on mast
503.2
409.8
10m 12mm Polyprop
5m Eddygrip
485.3
427.7
Aqualogger 520PT s/n 1308
483.0
430.0
SBE-37 s/n 8538
384.2
528.8
241.2m 12mm Tasmania
Aqualogger 520T s/n 1204
284.2
628.8
Aquadopp s/n 9382
242.8
670.2
SBE-37 s/n 8539
242.3
670.7
232.5m 12mm Tasmania
Aqualogger 520T s/n 1205
12.3
900.7
3m Eddygrip
8.0
905.0
1.5m chain
AR861 s/n 1335
6.1
906.9
5m chain
1 Railway Wheel
0.1
912.9

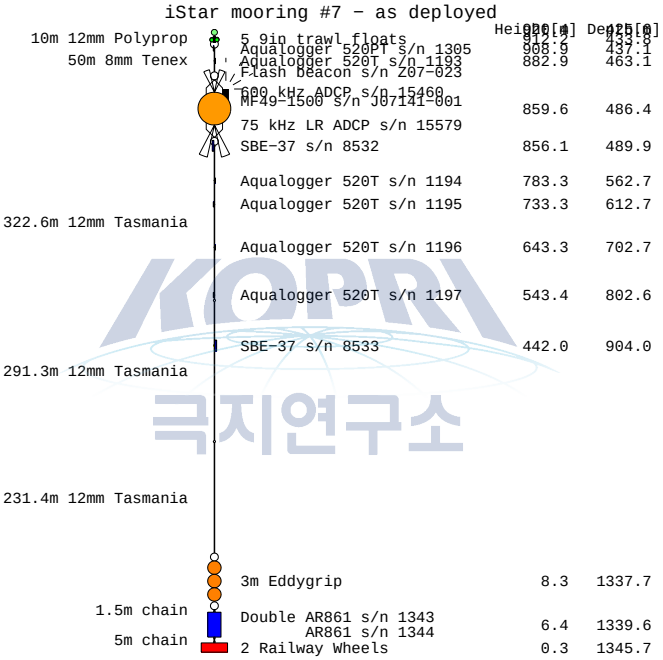
iStar mooring #7 – as deployed
Height[m] Depth[m]
10m 12mm Polyprop
50m 8mm Tenex
5 9in trawl floats 912.9 433.8
Aqualogger 520PT s/n 1305 908.9 437.1
Aqualogger 520T s/n 1193 882.9 463.1
Flash Beacon s/n Z07-023
600 kHz ADCP s/n 15460
MF49-1500 s/n J07141-001 859.6 486.4
75 kHz LR ADCP s/n 15579
SBE-37 s/n 8532 856.1 489.9
Aqualogger 520T s/n 1194 783.3 562.7
Aqualogger 520T s/n 1195 733.3 612.7
322.6m 12mm Tasmania
Aqualogger 520T s/n 1196 643.3 702.7
Aqualogger 520T s/n 1197 543.4 802.6
SBE-37 s/n 8533 442.0 904.0
291.3m 12mm Tasmania
231.4m 12mm Tasmania
3m Eddygrip 8.3 1337.7
1.5m chain
Double AR861 s/n 1343
AR861 s/n 1344 6.4 1339.6
5m chain
2 Railway Wheels 0.3 1345.7

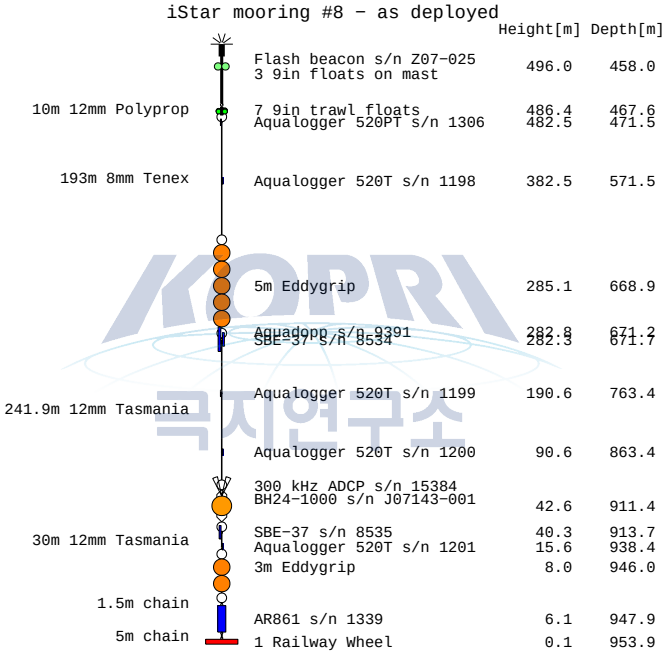
iStar mooring #8 – as deployed
Height[m] Depth[m]
Flash beacon s/n Z07-025
3 9in floats on mast
496.0 458.0
10m 12mm Polyprop
7 9in trawl floats
Aqualogger 520PT s/n 1306
486.4 467.6
482.5 471.5
193m 8mm Tenex
Aqualogger 520T s/n 1198
382.5 571.5
5m Eddygrip
285.1 668.9
Aquadopp s/n 9391
SBE-37 s/n 8534
282.8 671.2
282.3 671.7
Aqualogger 520T s/n 1199
190.6 763.4
241.9m 12mm Tasmania
Aqualogger 520T s/n 1200
90.6 863.4
300 kHz ADCP s/n 15384
BH24-1000 s/n J07143-001
42.6 911.4
SBE-37 s/n 8535
40.3 913.7
30m 12mm Tasmania
Aqualogger 520T s/n 1201
15.6 938.4
3m Eddygrip
8.0 946.0
1.5m chain
AR861 s/n 1339
6.1 947.9
5m chain
1 Railway Wheel
0.1 953.9

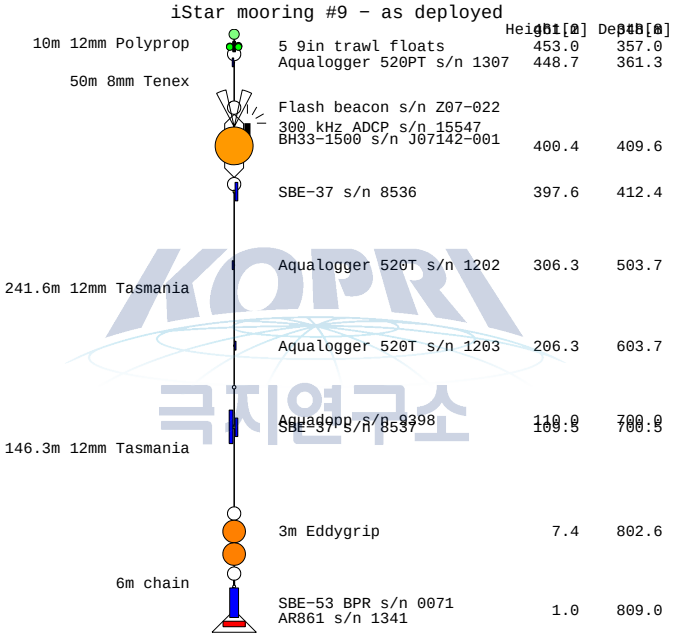
iStar mooring #9 – as deployed
Height [m]
Depth [m]
10m 12mm Polyprop
5 9in trawl floats
453.0
357.0
Aqualogger 520PT s/n 1307
448.7
361.3
50m 8mm Tenex
Flash beacon s/n Z07-022
300 kHz ADCP s/n 15547
BH33-1500 s/n J07142-001
400.4
409.6
SBE-37 s/n 8536
397.6
412.4
Aqualogger 520T s/n 1202
306.3
503.7
241.6m 12mm Tasmania
Aqualogger 520T s/n 1203
206.3
603.7
Aquadopp s/n 9398
110.0
700.0
SBE-37 s/n 8537
109.5
700.5
146.3m 12mm Tasmania
3m Eddygrip
7.4
802.6
6m chain
SBE-53 BPR s/n 0071
AR861 s/n 1341
1.0
809.0

ASPIRE Sediment Trap Mooring Diagram

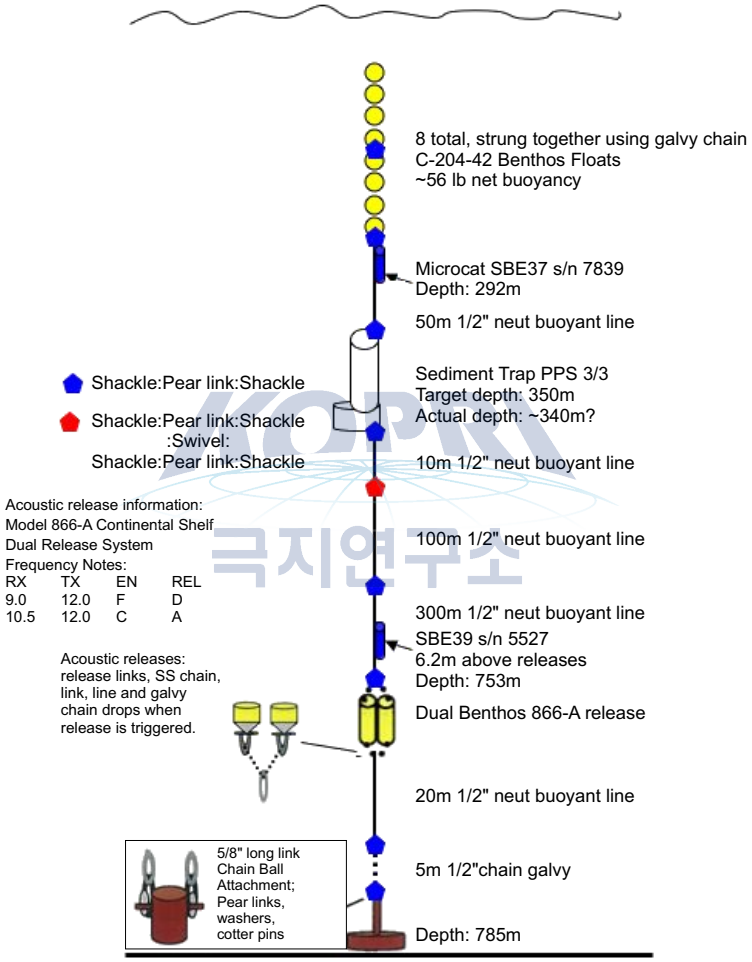

Outer/Shallow
Shelf (6)

NBP1005

Mooring ID: BSR12

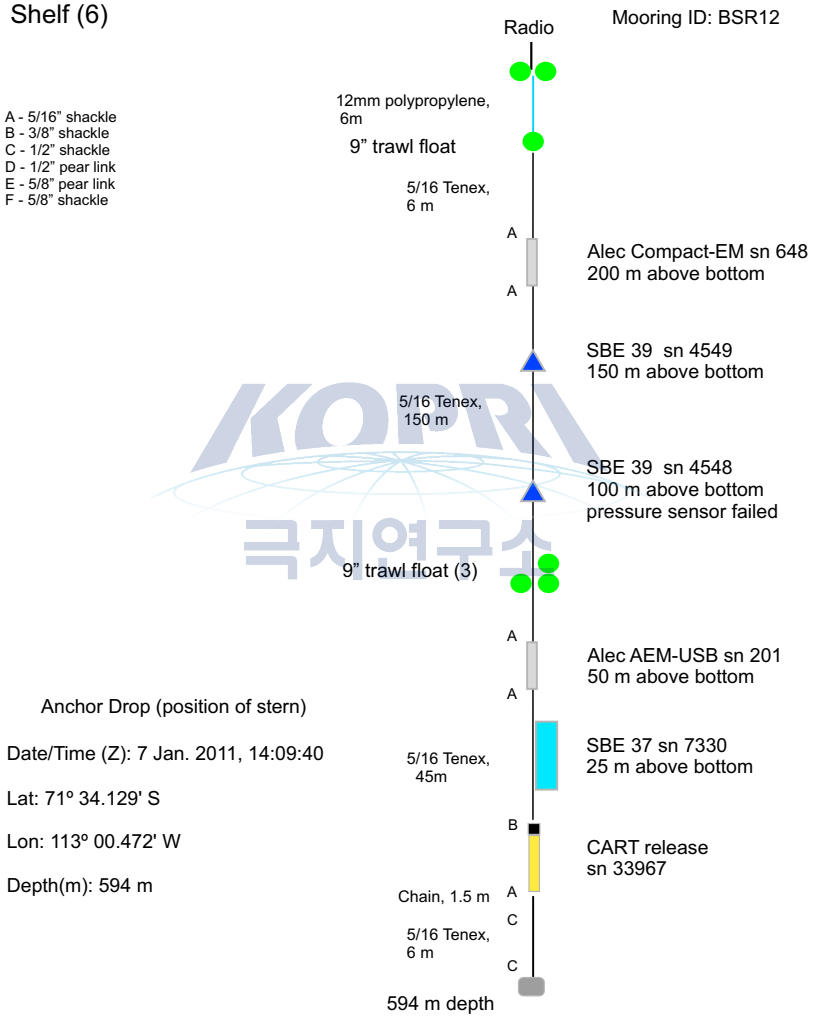

Anchor Drop (position of stern)

Date/Time (Z): 7 Jan. 2011, 14:09:40

Lat: 71º 34.129' S

Lon: 113º 00.472' W

Depth(m): 594 m

Slope (2)

NBP1005

Mooring ID: BSR13

A - 5/16” shackle
B - 3/8” shackle
C - 1/2” shackle
D - 1/2” pear link
E - 5/8” pear link
F - 5/8” shackle

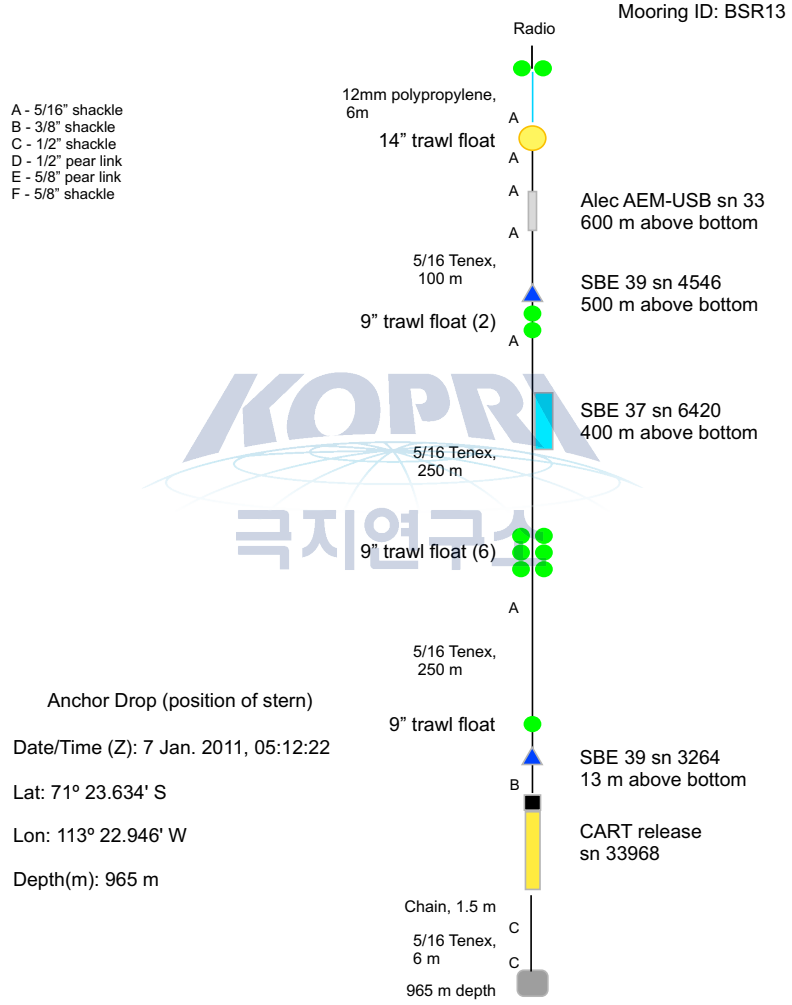

Anchor Drop (position of stern)

Date/Time (Z): 7 Jan. 2011, 05:12:22

Lat: 71º 23.634' S

Lon: 113º 22.946' W

Depth(m): 965 m

Mooring S1 OLD **Lat:** -72.4569N **Lon:** -116.346E **Depth:** 557 m

Depl. date/time: ---------- **Recov. date/time:** ----------

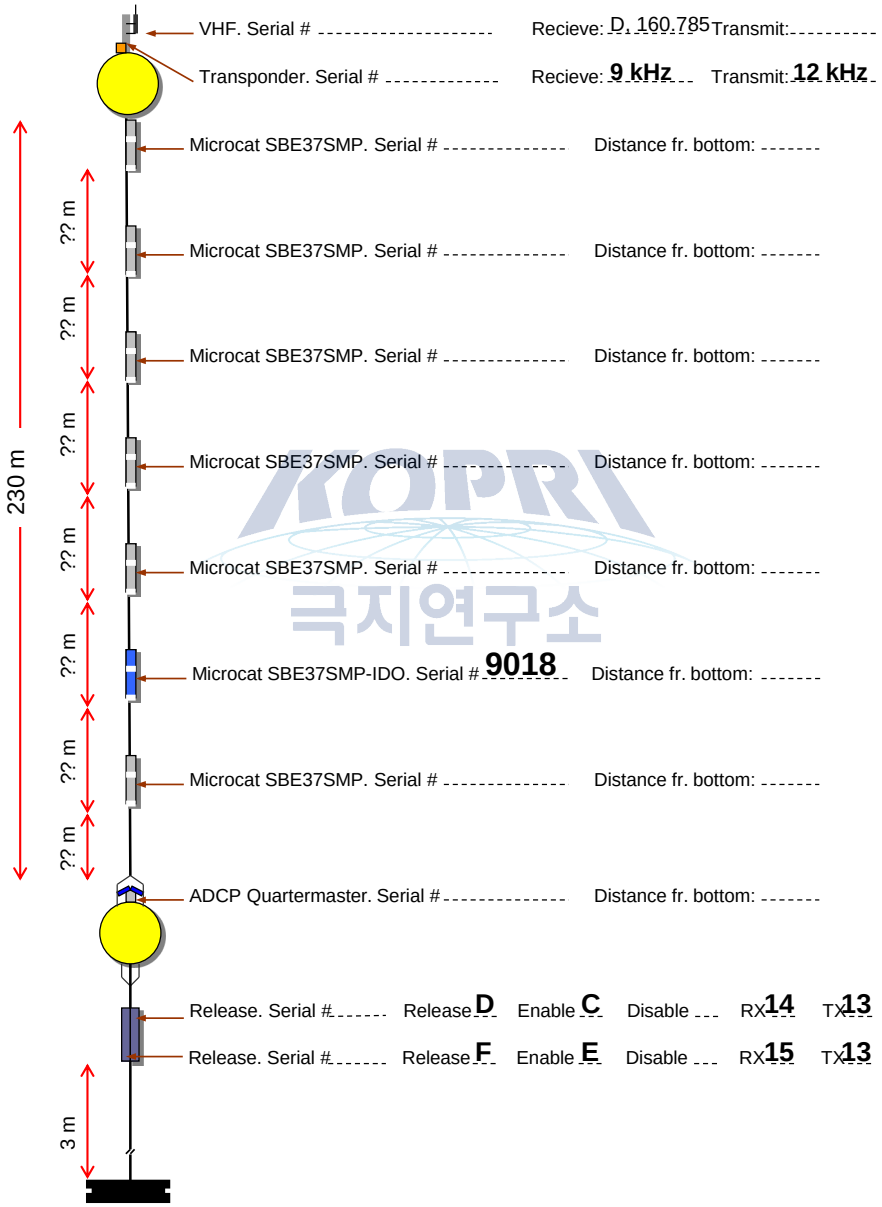

Mooring S2 OLD **Lat:** -73.0165N **Lon:** -117.249E **Depth:** 614 m

Depl. date/time: ---------- **Recov. date/time:** ----------

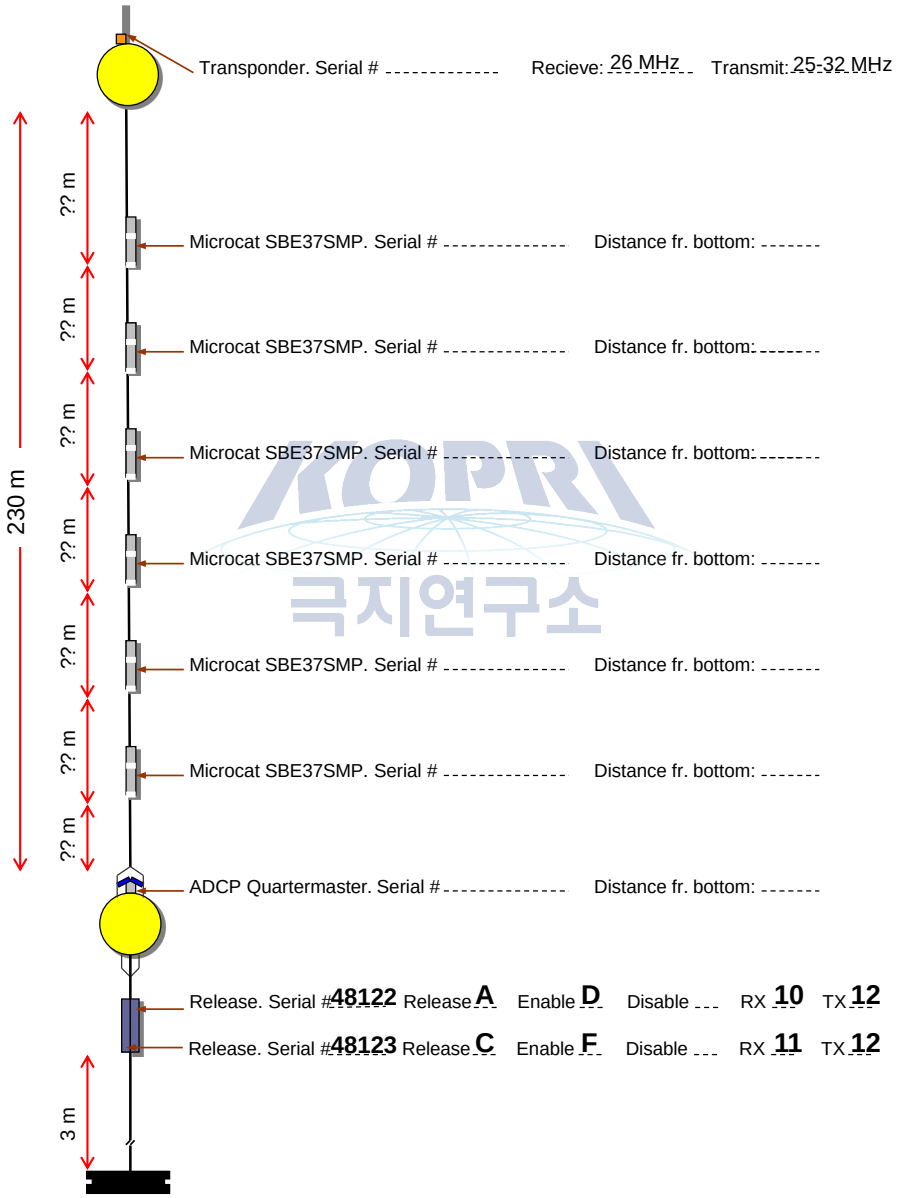

Mooring S1 NEW **Lat:** ---------- **Lon:** ---------- **Depth:** 561 m

Depl. date/time: ---------- **Recov. date/time:** ----------

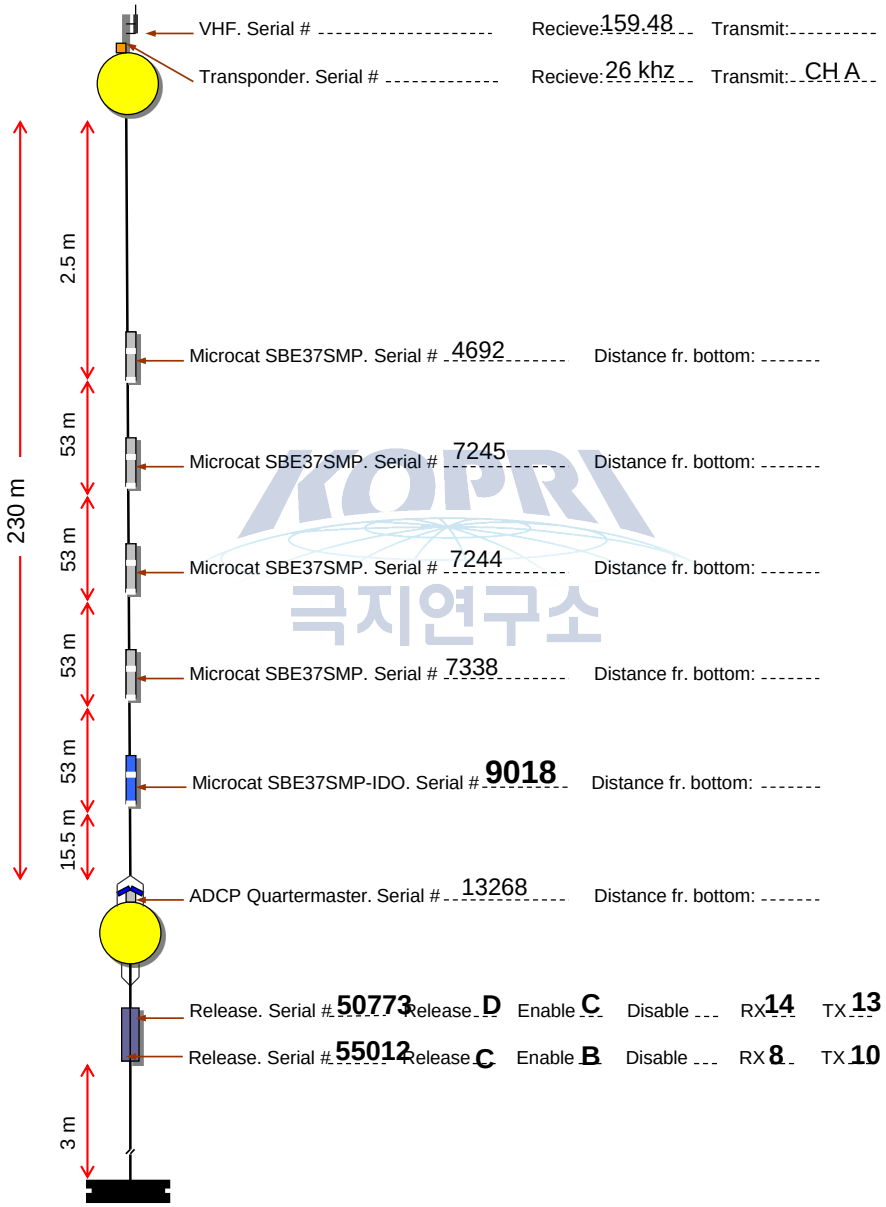

Mooring S2 NEW Lat: 71° 57.061' S Lon: 118° 27.093' W Depth: 620 m

Depl. date/time: 120304/122800 **Recov. date/time:** ----------

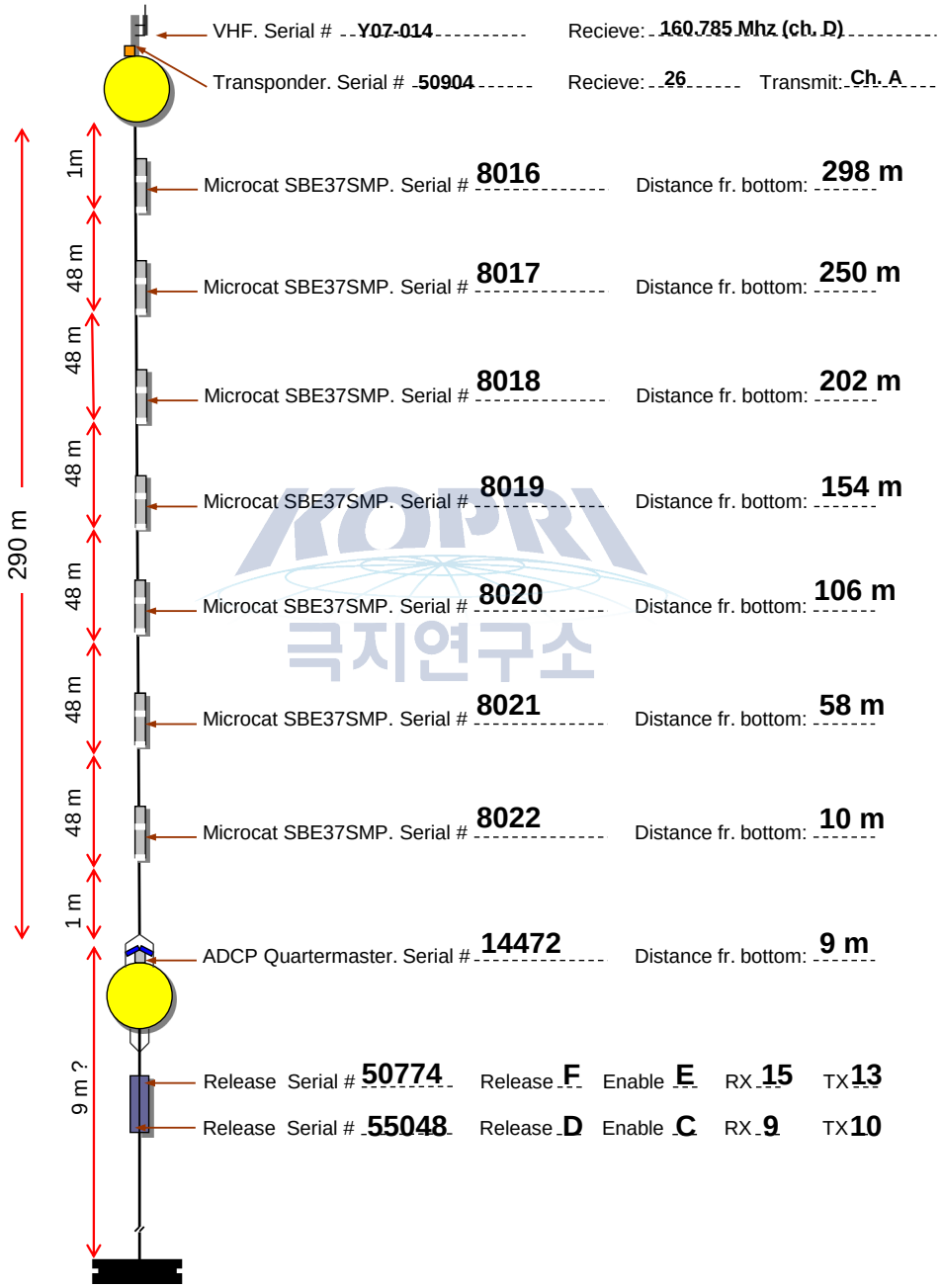

Mooring S3 **Lat:** 72° 55.5796' S **Lon:** 117° 34.8842' W **Depth:** 548 m

Depl. date/time: 1/3/2012 08:36:10 (drop mooring top)

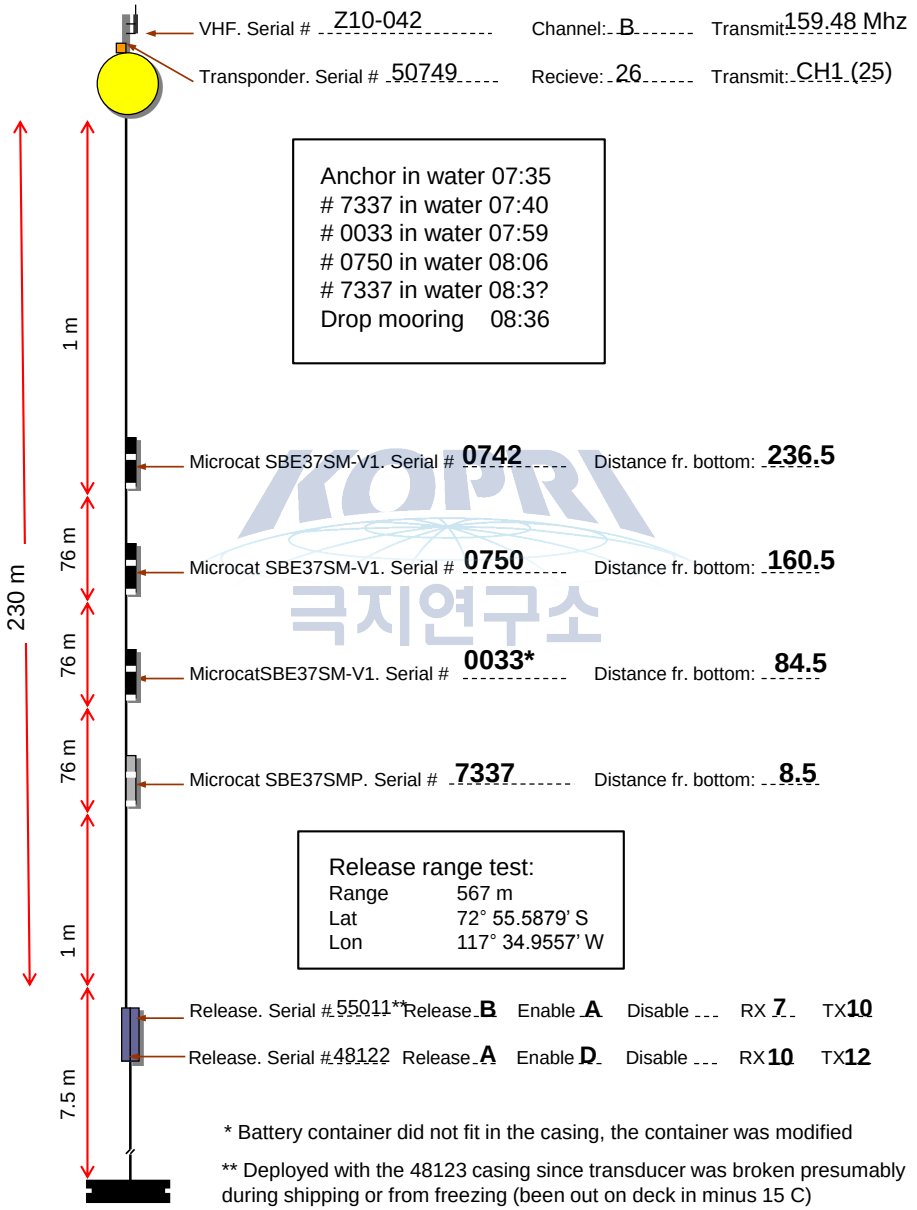

* Battery container did not fit in the casing, the container was modified

** Deployed with the 48123 casing since transducer was broken presumably during shipping or from freezing (been out on deck in minus 15 C)

1.5 Appendix III. Triangulation results of K1, K2 and K3.

See the following pages.

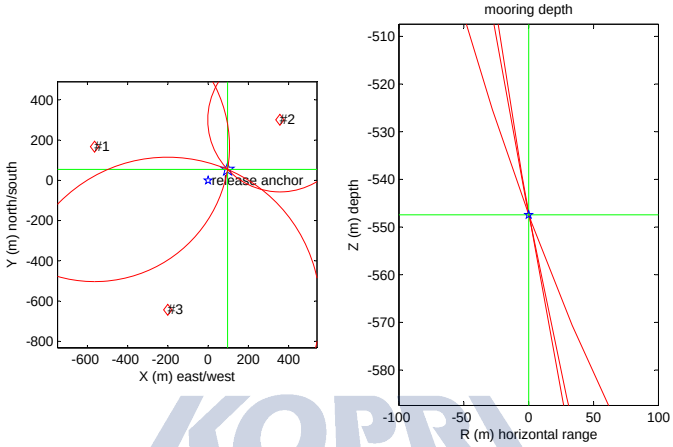

anchor release position: 72°S 23.237' 117°W 42.821'; depth: 525 m
3D mooring position: 72°S 23.208' 117°W 42.649'
drift: 111 m; direction: 61°
mooring depth: 547 m; slant error: 0 m
2D mooring position: 72°S 23.210' 117°W 42.634'
drift: 116 m; direction: 64°
horizontal error: 12 m
sound speed at site: 1500 m/s

#1 pos: 72°S 23.147' 117°W 43.829' range: 826 m range soundspeed 1500
#2 pos: 72°S 23.075' 117°W 42.185' range: 601 m range soundspeed 1500
#3 pos: 72°S 23.585' 117°W 43.180' range: 899 m range soundspeed 1500

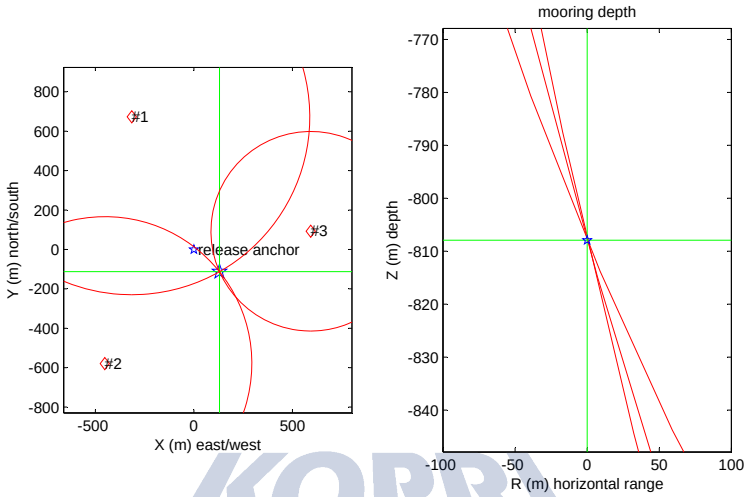

anchor release position: 73°S 16.826' 114°W 57.227'; depth: 830 m
3D mooring position: 73°S 16.887' 114°W 56.984'
drift: 172 m; direction: 131°
mooring depth: 808 m; slant error: 0 m
2D mooring position: 73°S 16.882' 114°W 56.999'
drift: 159 m; direction: 130°
horizontal error: 14 m
sound speed at site: 1460 m/s

#1 pos: 73°S 16.463' 114°W 57.819' range: 1186 m range soundspeed 1500
#2 pos: 73°S 17.139' 114°W 58.076' range: 1071 m range soundspeed 1500
#3 pos: 73°S 16.777' 114°W 56.115' range: 920 m range soundspeed 1500

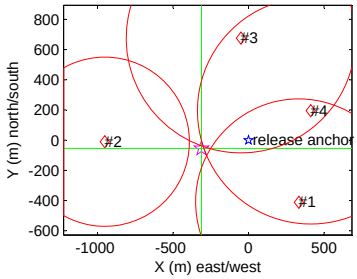

anchor release position: 74°S 11.202' 112°W 31.782'; depth: 1057 m
2D mooring position: 74°S 11.231' 112°W 32.399'
drift: 316 m; direction: 260°
horizontal error: 24 m
sound speed at site: 1445 m/s

#1 pos: 74°S 11.424' 112°W 31.120' range: 1148 m range soundspeed 1500
#2 pos: 74°S 11.207' 112°W 33.668' range: 1079 m range soundspeed 1500
#3 pos: 74°S 10.837' 112°W 31.881' range: 1195 m range soundspeed 1500
#4 pos: 74°S 11.097' 112°W 30.965' range: 1189 m range soundspeed 1500

Chapter 2

Chemical Oceanography

2.1 Survey of Inorganic Carbon System and Dissolved Trace Gases

2.1.1 Inorganic carbon system observation

Rhee, Tae Siek; Jeon, Hyun-Duck; Park, Kyung-Ah
Korea Polar Research Institute, Korea

요약문

2011년에 이어 아문젠해 무기탄소 시스템 관측을 수행하였다. 총용존무기탄소 (Dissolved Inorganic Carbon; DIC), 총알칼리도 (Total Alkalinity; TA), pH, 용존이산화탄소 (pCO_2) 농도를 50개 정점의 수층에서 채수한 600여개 시료에서 분석하였다. DIC는 인산을 이용하여 모두 이산화탄소로 산화시킨 후 이들 이산화탄소를 적정하는 쿨로메트릭 방법을 이용하였으며 TA는 알고 있는 농도의 염산을 해수에 적정하여 적정점을 찾아 농도를 계산하였다. pH는 전위법을 이용하여 분석하였으며 용존 이산화탄소는 니켈 촉매를 이용하여 메탄으로 환원시킨후 FID로 분석하는 가스크로마토그래프를 이용하였다. 아문젠해에서 이제까지 이들 네 개의 무기탄소 인자를 분석하여 보고한 바는 없으며 작년과 금년 아문젠해 탐사에서 처음으로 수행하였다. 이들 자료를 이용하여 아문젠해 폴리냐와 해빙역, 외양을 중심으로한 무탄소 시스템의 차이를 알아보고자 한다.

Objectives

The Amundsen Sea is located in the West Antarctica renowned as a region of rapid melting ice sheets (Rignot et al., 2008). A number of papers evidenced that inflow of the circumpolar deep water to the shelf should drives melting of the ice sheets. The rapid melting of ice sheets will influence ecosystem in the Amundsen Sea which will change in the inorganic and organic carbon storage. To understand the impact of melting ice sheets to the carbon flux in the water column of the Amundsen Sea, we investigated a complete set of inorganic carbon system in the polynyas of Dotson, Getz, and Pine Island Glacies, sea-ice zone, and the open ocean.

Work at sea and preliminary results

Hydrographic survey was conducted in the Amundsen Sea by casting CTD/Rosette at 50 stations (Figure 2.1). The area covers Dotson and Getz polynya and PIB (Pine Island Bay) polynya, sea-ice zone, and the open ocean. Inorganic carbon system was investigated by measuring dissolved CO_2 (pCO_2), pH, dissolved inorganic carbon (DIC), and total alkalinity (TA) in two dimensions, horizontal monitoring along the ship track and vertical profiling at the hydro-casting stations. pCO_2 was measured using two different instruments: a non-dispersive infrared (NDIR) detecting system and a gas chromatographic system. The former was dedicated for measuring pCO_2 underway whereas the latter was both for underway measurement and for analyzing discrete samples collected at the hydro-casting stations. A brand-new NDIR detecting system (Model 8050, General Oceanics) was mounted in the Analytical Chemistry Laboratory in July, 2011. Underway measurement of pCO_2 was carried out by supplying uncontaminated seawater to a small Weiss-type equilibrator from which headspace air was delivered to the analytical system. To determine DIC and TA underway, uncontaminated seawater samples were collected at 1.5 – 2 hours interval along the ship track. For analyzing pCO_2 in the seawater samples collected at the station, a specially designed glass bottle was used to avoid any contamination from the air during sampling and storage. Atmospheric CO_2 in the marine boundary layer was also analyzed in a regular interval using the same instruments by pumping the ambient air. The pCO_2 analyzing systems were calibrated using a series of standard gases and zero air. Dissolved inorganic carbon (DIC) was analyzed by coulometric titration using a system similar to SOMMA analyzer (Johnson et al., 1993). Total alkalinity (TA) was measured by potentiometric titration with HCl in an open cell. DIC and TA analyzer are combined in one analytical system, which saves seawater samples and analytical duration. We developed a pH meter which determines pH by potentiometry using a glass/reference electrode. This consists of thermostatic water bath, voltage follower, glass/reference electrode, and voltmeter with high impedence (DOE, 1994). The analytical systems for DIC, TA, and pH were calibrated using a certified reference material (CRM) provided by Andrew Dickson (Scripps Institution of Oceanography). The inventory of samples collected and analyzed at the hydro-casting stations is listed in Table 2.1.

The NDIR detecting system for pCO_2 equips a streamline of software that provides the values in situ, while the gas chromatographic technique requires computation to determine pCO_2 based on the calibration runs which were carried out between sample runs. We use preliminary data logged in the NDIR detecting system. In Figure 2.1, pCO_2 in seawater drawn by uncontaminated seawater supply system is shown along the ship track. pCO_2 in seawater was supersaturated in the open ocean while that was undersaturated in the sea-ice zone and in the polynya. This pattern is similar to what was observed last year although the degree of saturation seems to be larger this year. pCO_2 concentration in the PIB polynya was in general higher than in the Dotson and Getz polynya. This might be due to different phase of ecosystem in both polynya; While biological activity in the PIB polynya is in the phase of oldness while in the Dotson and Getz polynya ecosystems are still in the healthy condition. Like the last year, seawaters in Dotson and Getz ice sheet are divided in view of not only pCO_2 but also of other chemical items. Most of the sea-ice zone

Table 2.1: Number of samples collected at the station for analyses of inorganic carbon system parameters

Station No.	Cast No.	Date	pCO_2	DIC & TA	pH
1	1	02-10-2012	11	11	11
2	1	02-10-2012	11	11	11
7	1	02-11-2012	12	12	4
62	1	02-11-2012	11	11	11
8	1	02-11-2012	9	9	9
9	1	02-11-2012	11	11	11
10	1	02-12-2012	10	10	10
11	1	02-12-2012	11	11	11
12	1	02-13-2012	11	11	11
13	1	02-13-2012	10	10	10
14	1	02-13-2012	12	12	12
15	1	02-14-2012	12	12	12
16	1	02-14-2012	11	11	11
17	1	02-14-2012	13	13	13
18	1	02-15-2012	16	16	16
71	1	02-16-2012	12	12	12
19	1	02-16-2012	14	14	14
20	1	02-16-2012	14	14	14
28	1	02-17-2012	15	15	15
27	1	02-17-2012	14	14	14
26	1	02-17-2012	15	15	15
25	1	02-18-2012	14	14	14
24	1	02-18-2012	15	15	15
23	1	02-18-2012	13	13	13
22	1	02-18-2012	13	13	13
21	1	02-18-2012	13	13	13
29	1	02-20-2012	11	11	11
30	1	02-22-2012	11	11	11
30	2(seaice)	02-21-2012	5	5	5
87	1	02-22-2012	12	12	12
88	1	02-23-2012	13	13	13
89	1	02-24-2012	17	17	17
31	1	02-24-2012	15	15	15
32	1	02-24-2012	16	19	19
33	1	02-24-2012	13	13	13
34	1	02-25-2012	15	15	15
86	1	02-27-2012	13	13	13
17	2	02-29-2012	2	8	8
63	1	03-01-2012	12	12	12
61	1	03-01-2012	12	12	12
6	1	03-03-2012	11	11	11
3	1	03-04-2012	11	11	11
85	1	03-05-2012	16	16	16
84	1	03-05-2012	10	10	10
83	1	03-05-2012	12	12	12
82	1	03-06-2012	12	12	12
81	1	03-06-2012	12	12	12
90	1	03-06-2012	13	13	13
39	1	03-09-2012	12	12	12
40	1	03-10-2012	17	17	17

Table 2.2: Number of samples collected at the stations to analyze CH_4, N_2O, CO and H_2

Station No.	Cast No.	Sampling date	CH_4/N_2O	CO/H_2
1	1	02-10-2012	11	11
2	1	02-10-2012	11	11
7	1	02-11-2012	12	11
62	1	02-11-2012	11	11
8	1	02-11-2012	9	9
9	1	02-11-2012	11	11
10	1	02-12-2012	10	10
11	1	02-12-2012	11	11
12	1	02-13-2012	11	11
13	1	02-13-2012	10	10
14	1	02-13-2012	12	12
15	1	02-14-2012	12	12
16	1	02-14-2012	11	11
17	1	02-14-2012	13	13
18	1	02-15-2012	16	11
71	1	02-16-2012	12	12
19	1	02-16-2012	14	9
20	1	02-16-2012	14	12
28	1	02-17-2012	15	12
27	1	02-17-2012	14	11
26	1	02-17-2012	15	12
25	1	02-18-2012	14	14
24	1	02-18-2012	15	12
23	1	02-18-2012	13	12
22	1	02-18-2012	13	11
21	1	02-18-2012	13	11
29	1	02-20-2012	11	15
30	1	02-22-2012	11	9
30	2(seaice)	02-21-2012	5	5
87	1	02-22-2012	12	11
88	1	02-23-2012	13	13
89	1	02-24-2012	17	12
31	1	02-24-2012	15	15
32	1	02-24-2012	16	17
33	1	02-24-2012	13	11
34	1	02-25-2012	15	15
86	1	02-27-2012	13	12
17	2	02-29-2012	2	0
63	1	03-01-2012	12	11
61	1	03-01-2012	12	13
6	1	03-03-2012	11	10
3	1	03-04-2012	11	11
85	1	03-05-2012	16	14
84	1	03-05-2012	10	6
83	1	03-05-2012	12	10
82	1	03-06-2012	12	11
81	1	03-06-2012	12	11
90	1	03-06-2012	13	11
39	1	03-09-2012	12	12
40	1	03-10-2012	17	14

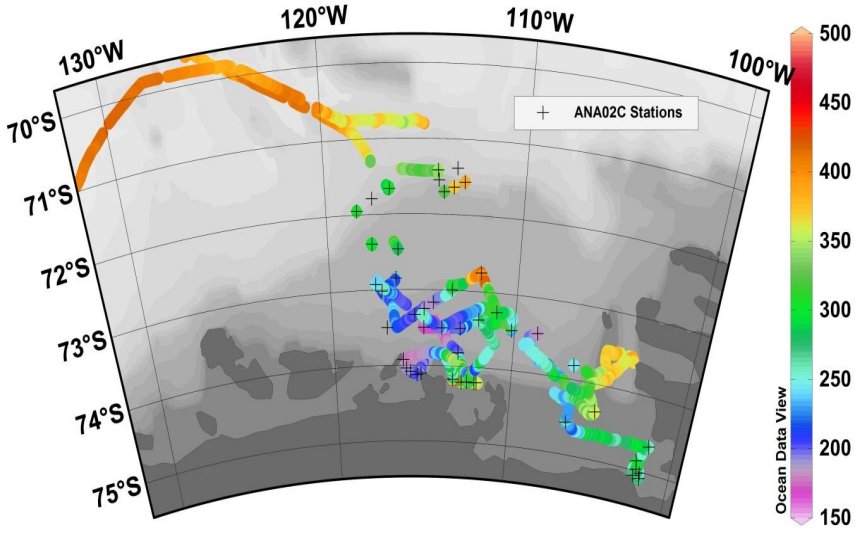

Figure 2.1: Dissolved pCO_2 at the surface waters along ship track.

visited was undersaturated with respect to the atmospheric CO_2. This might be due to strong and high frequent drift of sea-ice which does not allow a unique ecosystem of sea-ice to be formed.

References

Johnson, K. M., Wills, K. D., Butler, D. B., Johnson, W. K., Wong, C. S., 1993, Coulometric total carbon dioxide analysis for marine studies: maximizing the performance of an automated continuous gas extraction system and coulometric detector, Mar. Chem. 44, 167-187.

Rignot, E., Bamber, J.L., Van den Broeke, M.R., Davis, C., Li, Y., Van de Berg, W.J., and Van Meijgaard, E., 2008, Recent Antarctic ice mass loss from radar interferometery and regional climate modeling, Nature Geosci. 1, 106-110

2.1.2 Observation of Non-CO_2 greenhouse gases

Rhee, Tae Siek; Park, Kyung-Ah; Kwon, Young-Shin
1. Korea Polar Research Institute, Korea

요약문

이산화탄소 이외에 메탄과 아산화질소는 지구 기후 변화의 주요 원인으로 지목되는 온실기체이다. 일산화탄소와 수소는 직접적인 온실효과를 가져오지 않지만 대기에서 화학반응에 의해 간접적으로 온실효과를 가져온다. 아문젠해

탐사기간 동안 이들 기체의 해수표층과 해양경계층, 해양 내부의 수직구조 분포를 관측하였으며 일산화탄소와 수소의 광화학 반응과 생물활동으로 인한 농도변화 실험을 26개 정점에서 실행하였다. 이들 용존기체들은 가스크로마토그래프를 이용하여 분석하였으며 표준기체를 이용하여 기기를 보정하였다. 모든 기체 분석 결과를 최종 농도값으로 정량화하는 작업은 탐사후 연구소에 돌아가서 수행할 계획이며 탐사기간 동안에는 자료의 수집에 주력하였다.

Objectives

The ocean acts as a source of CH_4, N_2O, H_2, and CO (e.g., Bates et al., 1995; Rhee et al, 2009). Microbes produce CH_4 and N_2O in water column while photochemical degradation of organic matters is a major source of CO and likely for H_2 in the ocean. However, oceanic source strengths of these gases to the atmospheric budget are not well quantified due mainly to insufficient observations in the ocean. In particular, sea-ice region and continental shelf of the Amundsen Sea is a void of these data. Following the expedition last year, we aim to quantify the emission rates of these gases in the southern ocean and in the Amundsen Sea.

Work at sea and preliminary results

Non-CO_2 greenhouse gases (N_2O, CH_4, H_2, and CO) were monitored along the cruise track in the marine boundary layer and in the surface seawater at 1 hour interval. An air sampling inlet was mounted on the top of formast, 15 m above the sea surface. The air sampling inlet was positioned to avoid the flow of contaminated air from ship's exhaust. Air samples were withdrawn through the polyethylene inner-coated aluminum tubing (Dekabon) using a pump. The total length of tubing was 60 m. The inlet was capped with a funnel to prevent rainwater or sea spray from entering the tubing and a filter pack was mounted at the tip of the inlet to protect the tubing and analyzing system from inhaling solidified sea salts. Uncontaminated surface seawater was supplied at a depth of 10 m into two Weiss-type equilibrators in which the headspace air equilibrates with dissolved gases in seawater. The headspace air was introduced to gas chromatographic analyzers every hour to determine the dissolved gas concentrations. To keep the analyzing system from being wet, sample and calibration gases were forced to flow through a drying agent (P_2O_5).

To investigate the distribution of these gases in the water column, aliquots of seawater samples were drawn into a specially designed glass containers from the Niskin bottles mounted on CTD/Rosette. In the laboratory a precisely known volume of pure N_2 (99.9999%) was injected into the glass containers to make headspace. After equilibration with dissolved gases, the headspace air was taken using a syringe and injected into sample loops equipped in the gas chromatographs. CH_4 and N_2O were separated in packed columns, detected by flame ionization detector (FID) and electron capture detector (ECD), respectively, and quantified by calibrating the gas chromatographic system using a series of calibration gases. CO and H_2 were separated in a molecular sieve packed column and detected by Hg vapour which was quantitatively produced by the reaction of CO and H_2 with HgO in a hot bed at 250°C. Gas chromatograph for CO and H_2 measurements was calibrated for every sample from the equilibrator or from the marine boundary layer. Total 616 samples were ana-

Table 2.3: Stations and the number of samples collect for analysis of ^{14}C in dissolved inorganic carbon

Station	No. of samples	Latitude	Longitude
2	6	71°53.24	117°30.81
7	7	72°50.77	116°29.78
8	5	73°29.91	116°30.77
K2	11	73°15.02	114°59.87
12	6	72°59.39	113°29.33
13	4	72°44.80	112°00.33
17	8	73°29.98	114°0.203
A1	8	73°49.25	113°03.99
K3	10	74°12.12	112°30.66
27	6	74°10.67	113°18.35
24	6	74°04.79	115°43.48
31	6	75°05.24	101°45.55
K1	7	72°23.15	117°43.21
3	5	71°56.98	118°26.84
OS1	8	71°34.84	133°59.29
total	103		

lyzed for CH_4 and N_2O and 562 samples for CO and H_2 in the water columns during the expedition (Table 2.2). These results are under process to obtain the final concentrations.

References

Bates, T., Kelly, K. C., Johnson, J.E., Gammon, R.H., 1995, Regional and seasonal variations of in the flux of oceanic carbon monoxide to the atmosphere, J. Geophysic. Res. 100, 23093-23101.

Rhee, T.S., Kettle, A.J., Andreae, M.O., 2009, Methane and nitrous oxide emissions from the ocean: A reassessment using basin-wide observations in the Atlantic, J. Geophysic. Res. 114, D12304.

2.2 Estimation of POC Export Flux Using $^{234}Th/^{238}U$ Disequilibrium in the Amundsen Sea

Kim, Miseon[1]; Choi, Mansik[1]
[1] Div. Oceanography, Chungnam National University

요약문

남극 아문젠 해에서 탄소 순환을 이해하는데 중요한 지표인 export production (EP)을 알아보기 위해 $^{234}Th/^{238}U$ 비평형법을 이용하여 총 ^{234}Th 을 측정하였다. 이와함께 유광대 입자의 화학 조성에 따른 EP의 지역적 변화를 검토해 보고자 해역별 15개의 정점에서 수층에 따라 3 L씩 채수하여 여과된 해수를 현장에서 Mn 공침 후 β-spectrometer로 ^{234}Th 를 측정하였다. 이는 6개월 후 다시 측정할 예정이다. 3 L의 해수에서 GF/F와 nuclepore에 여과된 입자상 물질은실험실에서 분석할 예정이다. 또한 미량금속(Mn, Cd, Ni)의 수직 농도 분포를 알아보기 위해 각 정점의 7 – 14개 수층에서 0.5 L의 해수를 채수하여 냉동보관하였다. 이는 실험실에서 분석할 예정이다.

Objectives

The export fluxes of particulate organic carbon (POC) play an important role in the transfer of carbon between the atmosphere and the ocean. Accurate estimates of POC export fluxes are critical for constraining models of the global carbon cycle. Over the past few decades, the radioisotope pair ^{238}U and ^{234}Th has been increasingly used to estimate POC export fluxes from the euphotic zone. This method is based on the uptake of ^{234}Th onto biogenic particles in the euphotic zone and the subsequent sinking of particles into deep water. The POC export flux is determined by multiplying the depth-integrated ^{234}Th flux by the $POC/^{234}Th$ ratio on sinking particles. This study aims to estimate the POC export fluxes in the Amundsen Sea using $^{234}Th/^{238}U$ disequilibrium method, and to discuss the variability of export ratio (export flux/primary production) in several regions.

Work at sea

A given amount of seawater samples were collected at water depths of 16 stations (Table 2.1) following analytical procedure shown in Figure 2.2:

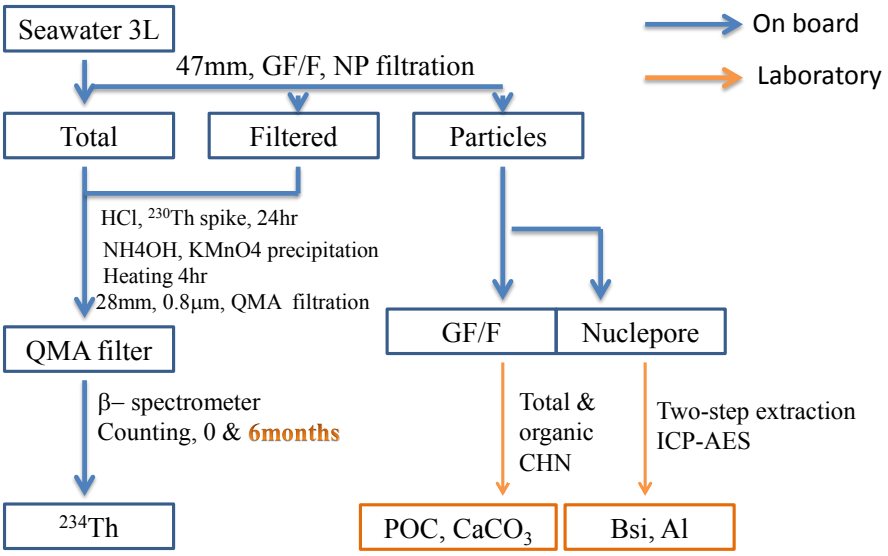

Figure 2.2: Analytical procedure to measure total, particulate, and dissolved ^{234}Th

1. 3 L of seawater is require for analysis of total ^{234}Th
2. 6 L of seawater for particulate V, POC, biogenic silicate, and Al analyses
3. 0.5 L of seawater for trace metal (Mn, Cd, Ni) analysis

Total and dissolved ^{234}Th activities were analyzed for bulk and filtered seawaters, respectively, using a gas-flow proportional β-spectrometer manufactured by Risø National Laboratories (Roskilde, Denmark) following methods described in Buesseler et al. (2001). 3 L of seawater was acidified using 3 ml of concentric nitric acid immediately after collection, and was then spiked with 1 g of 230Th (IRMM-061, 12 pg/g) solution. After equilibration for 8–12 hours, the pH of seawater was adjusted to 8.0 ± 0.15 using ammonia solution. Manganese precipitates were created by adding $KMnO_4$ (7.5 g $KMnO_4$/L) 100 μL and $MnCl_2$ (33.3 g $MnCl_2 \cdot 5H_2O$/L) 100 μL. The precipitates were aged by heating the seawater at 80°C in a water bath for 2–3 hours and filtered using QMA filter paper with 25-mm diameter and 1.2-μm pore size. After drying the precipitates, the QMA filter papers were directly counted by spectrometer five times every 24 days. The background counts were about 0.2 cpm using only filter paper, and each sample was counted for 12 hrs. Initial ^{234}Th activities were acquired after best fitting of the radioactive decay equation for ^{234}Th.

2.3 Noble gases in the seawater

2.3.1 Water sampling for the measurement of noble gases

Doshik Hahm
Korea Polar Research Institute, Korea

Table 2.4: The number of samples collected for analysis of trace metals and ^{234}Th

Station	Latitude	Longitude		No. of trace metal sample	No. of ^{234}Th sample
1	71°39.65	116°46.68		9	10
7	72°49.53	116°31.21		11	10
10	73°15.02	114°59.87		13	10
16	73°29.96	113°00.01		11	10
19	74°12.12	112°30.66		14	10
27	74°03.21	113°23.93		10	-
24	74°04.79	115°43.48		7	-
22	73°55.46	116°08.21		-	10
sea-ice				2	5
87	74°21.98	104°59.93		-	8
31	75°05.24	101°45.55		7	10
86	73°48.69	106°32.14		-	9
17-1	73°29.93	114°01.98		-	9
63	72°55.60	117°35.10		-	10
06	72°23.26	117°43.18		-	9
03	71°56.97	118°26.85		-	9
39	71°34.84	133°59.29		12	9

Objectives

The noble gases, especially helium isotopes (^{3}He and ^{4}He) in conjunction with tritium (^{3}H), have been widely used to trace water mass movement due to their conservative behavior in the environment and to give time constraints (i.e., ^{3}H-^{3}He age) on physical and biological processes in the ocean (e.g., Jenkins, 2008). Another interesting application is to detect ice-related processes using their different partitioning behavior in water, sea-ice and glacier (e.g., Huhn et al., 2008). The hydrography of the Amundsen Sea is supposed to be in substantial change due to rapid loss of glacier ice sheet and sea-ice, occurring around the west Antarctica. Given the high resolving power of noble gases for ice-related processes, they will provide invaluable information on the influence of glacier and sea-ice loss of this area on the changes of its hydrography and, in turn, biological processes.

Work at sea

Water samples for noble gases were collected at 28 selected stations (bull's eyes in Fig. 2.3) among the 52 CTD stations covered during the cruise. The sampling locations were selected with the following two aims in mind: (1) to illustrate and quantify the input of glacial and sea-ice meltwater to the Amundsen Sea, with emphasis on the across the trough variation (from Station 8 to 12) and (2) to compare the magnitudes of galcial meltwater input and the degrees of interaction with Circumpolar Deep Water with ice shelves among the three ice shelves (i.e., Getz, Dotson, and Pine Island Bay ice shelves). The preliminary results of CTD castings suggest that the western and eastern sides have constrasting physical and chemical (e.g., lower dissolved oxygen and nutirents in the western sides) characteristics.

2.3.2 Continuous O_2/Ar measurement as a proxy of net community production

Doshik Hahm
Korea Polar Research Institute, Korea

Objectives

Net community production (NCP), defined as the difference between autotrophic photosynthesis and (autrophic and heterotrophic) respiration, produces O_2 proportional to the amount of net carbon. By measuring chemically and biologically inert Ar together with O_2, it is possible to remove O_2 variation by physical processes (e.g., air temperature and pressure change and mixing of water masses) and deduce O_2 variation by biological processes.

To determine the net community (oxygen) production underway, we adopted a continuous O_2/Ar measurement system developed by Cassar et al. (2009). The so called 'equilibrator inlet mass spectrometer (EIMS)' is centered around a quadrupole mass spectrometer that measures dissolved gas molecules equilibrated with air in and supplied by an equilibrator. Unlike Cassar et al. (2009) who used a membrane contactor, we took advantage of a pre-installed Weiss-type equilibrator for the measurements of other dissolved gases (CH_4 and N_2O).

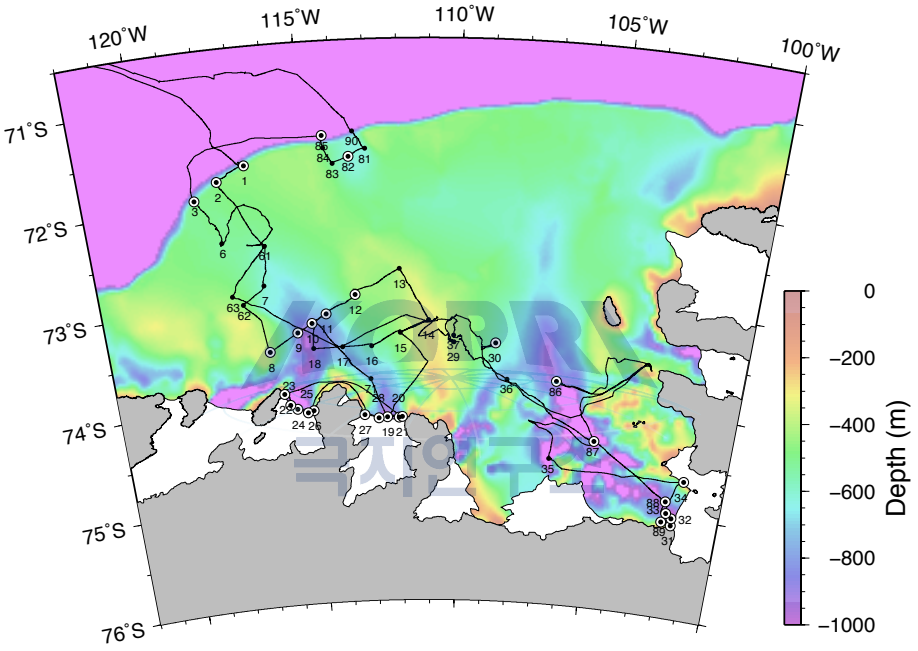

Figure 2.3: Map showing the stations where water samples for noble gases were collected (bull's eyes). Shown together is the cruise track along which underway measurements were performed. The measured parameters are temperature, salinity, fluorescence, pCO_2 and $\Delta O_2/Ar$ (See section 2.3.2).

Water temperature, salinity, oxygen and fluorescence were also obtained to help the interpretation of temporal and spatial variation of O_2/Ar.

Preliminary results

The preliminary results were summarized in Fig. 2.4 and 2.5. $\Delta O_2/Ar$ (the excess of biological O_2) were close to zero in open water before entering the continental shelf (until February 9, 2012) and were increased up to 10% in the center of the Amundsen Sea Polynya. An exception was the waters close to the Doton ice shelf (Sation 27 to 21) where $\Delta O_2/Ar$ were as low as -15%. Another place which showed minus values of $\Delta O_2/Ar$ was the vicinity of Station 13. This place was exceptionally colder and saltier than the other areas of the polynya, possibly one of the first places experiencing the formation of sea-ice and thus brine rejection. The Pine Island Bay (PIB) polynya showed much lower $\Delta O_2/Ar$ than the other polynya. Given that the magnitudes of primary production in the polynyas of the Amundsen Sea decrease abruptly and become less than half of the peak in a few weeks (Arrigo et al., 2003), it is not clear whether the difference is persistent geographical feature or simply reflects the different observation periods (early vs. late February). An observation favoring the latter explanation is the fact that $\Delta O_2/Ar$ of Station 17 became close to zero when revisited on 29th after the survey in the PIB from near 10% on 15th of February.

Overall, the magnitudes of $\Delta O_2/Ar$ in the Amundsen Sea polynya was much lower than those in the year of 2011. For example, the maximum of fluorescence and $\Delta O_2/Ar$ were two third and one third of of the values in 2011; they were 30 and 30%, respectively.

References

Cassar, N., Barnett, B. A., Bender, M. L. , Kaiser, J. , Hamme, R. C. and Tilbrook, B. (2009). Continuous high-frequency dissolved O2/Ar measurements by equilibrator inlet mass spectrometry. Analytical Chemistry, 81, 1855–1864.

Huhn, O., Hellmer, H. H. , Rhein, M., Rodehacke, C., Roether, W. , Schodlok, M. P. and Schroeder, M. (2008). Evidence of deep- and bottom-water formation in the western weddell sea. Deep-Sea Research Part I, 55, 1098–1116.

Jenkins, W. J. , 2008. The biogeochemical consequences of changing ventilation in the Japan/East Sea. MarineChemistry, 108, 137–147.

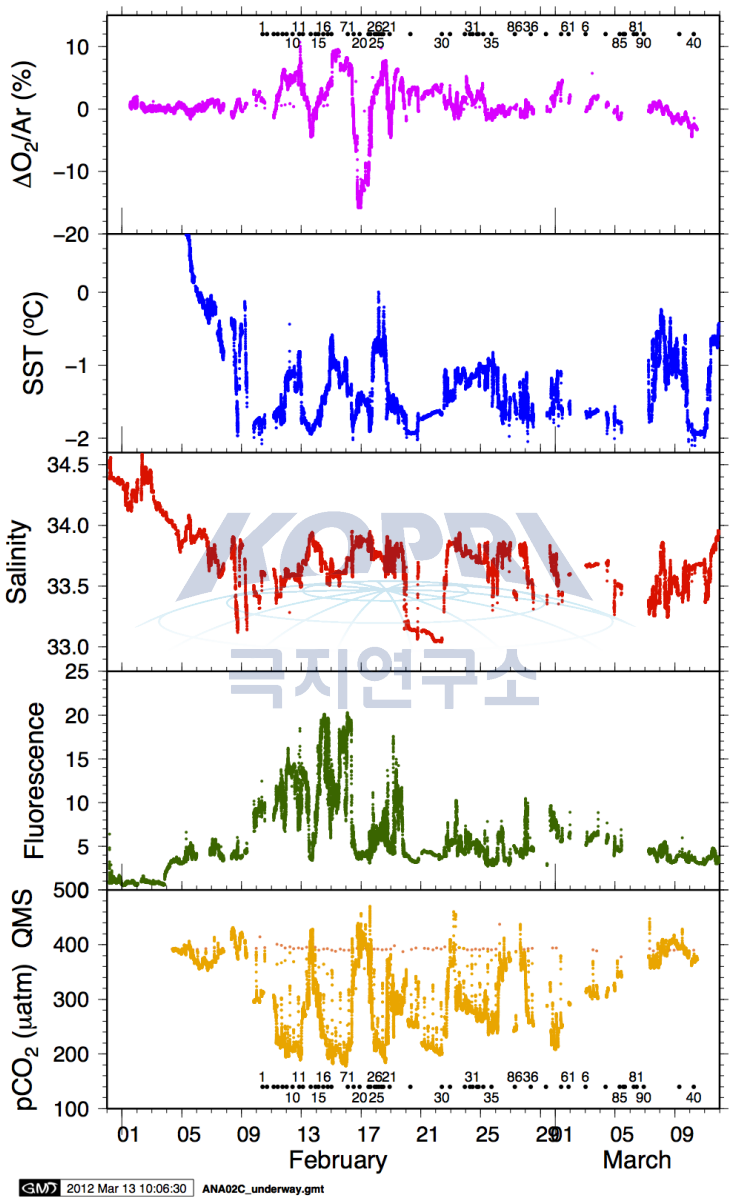

Figure 2.4: The preliminary results of $\Delta O_2/Ar$, temperature, salinity, fluorescence and pCO_2.

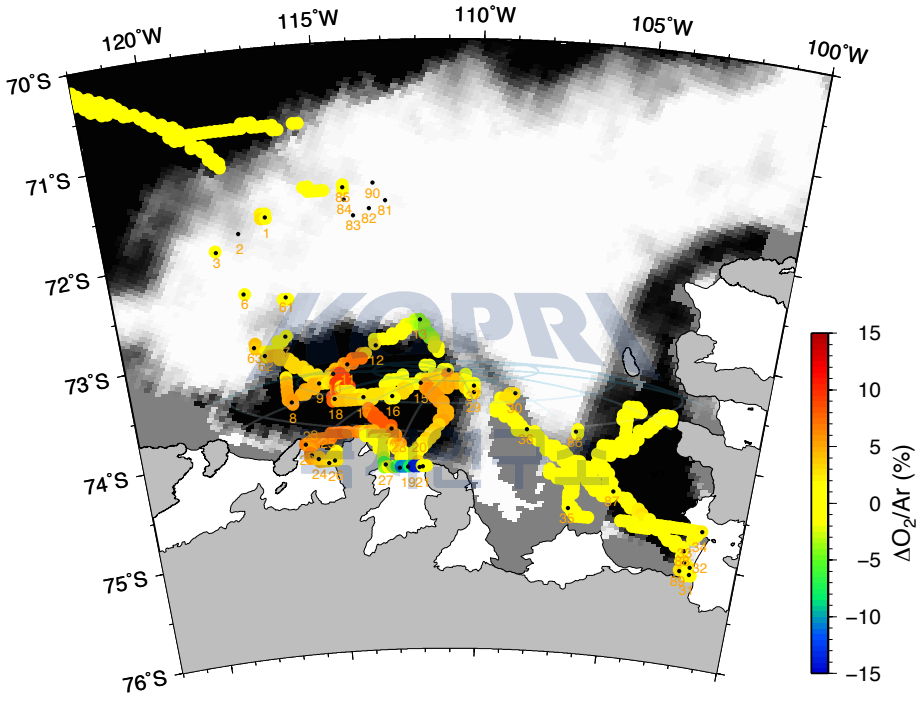

Figure 2.5: Spatial variation of $\Delta O_2/Ar$ superimposed on the ice concentration map on February 19, 2012.

2.4 Dissolved oxygen and nutirents

2.4.1 Determination of dissolved oxygen by spectrophotometric Winkler method

Doshik Hahm
Korea Polar Research Institute, Korea

Objectives

Due to its central role in biological redox reactions and the availability of reliable sensors, oxygen is one of the most common parameters in a sea-going observation. In the cruise, along with the oxygen sensor (SBE-43) attached to the CTD-rosette system, we determined oxygen concentration by spectrophotometric method (Labasque et al., 2004). The bottle oxygen measurements will be used to calibrate SBE-43 oxygen sensor, Annderra oxygen optode (No. 3835, part of O_2/Ar measurement system) and be paired with other chemical measurements such as nutrients, CH_4, N_2O and noble gases.

Work at sea

Our spectrophotometric measurement is a replication of Labasque et al. (2004) with the reagents prepared according to the WHP Reference Manual (Dickson, 1995). However, we reduced the volume of pickling reagents ($MnCl_2$ and NaI/NaOH) to 0.5 mL, respectively because we used smaller volume of sample flask ($\sim$ 63 mL) than commonly used 120 mL bottles. We measured samples collected at the 46 CTD stations out of 52. The repeat measurement of the samples taken from multiple Niskin bottles fired at the same water depth suggest that the precision of the measurement within the same batch (typically 2 to 3 hours) is less than 0.3%. The sensitivity (slope of calibration curves) of the spectrophotometer (UV 1800, Shimadzu) was around 1.529 mAU/μM. However, the sensitivity were slightly variable; the standard deviation of the slopes of 22 calibration curves was 0.75%. This is close to the reproducibility of Labasque et al. (2004) of 0.73% and may indicate the ultimate accuracy which can be obtained with the spectrophotometric Winkler method. WOCE standards call for analyses to have accuracy better than 0.5% of the highest concentration that will be measured in the ocean ($\sim$2 μmol/kg). To meet this requirement it may be considered to adopt alternative approach such as amperometric end-point determination of thiosulfate titration (Langdon, 2010).

Shown in Fig. 2.6 are example profiles of dissolved oxygen. Station 1 and 90 was the first and last CTD cast in the Amundsen Sea, respectively. The flask ('Bottle' in the figure) measurements closely follow the up cast rather than down cast. The difference between the vaues from O_2 sensor on the CTD (a SBE43) and flask measuremets became larger where strong vertical O_2 gradient existed (e.g., around 300 m at Station 1). The difference between SBE43 and flask measurements at relatively stable depths (>600 m, mean of flask measurements: 195$\pm$9 μmol/kg) were 4.2 μmol/kg.

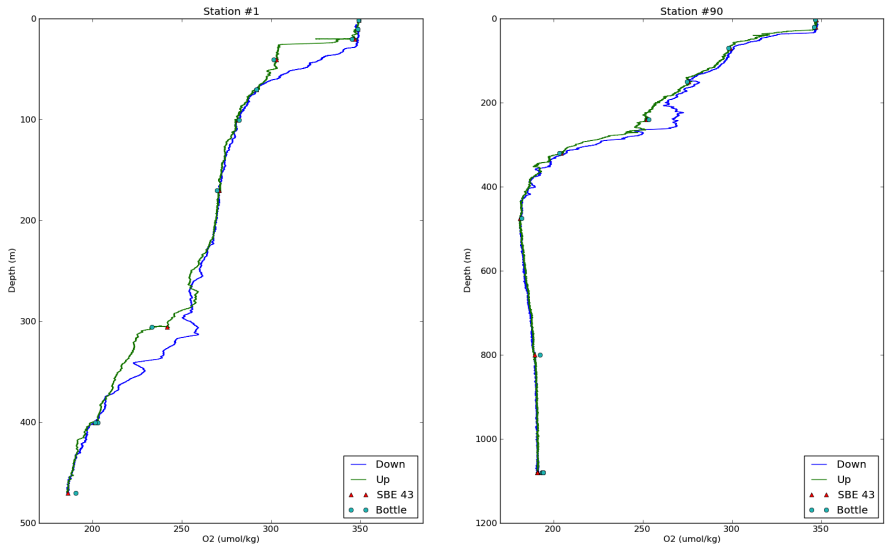

Figure 2.6: Example profiles of dissolved oxygen. Station 1 and 90 was the first and last CTD cast in the Amundsen Sea, respectively. The flask ('Bottle') measurements closely follow the up cast rather than down cast.

2.4.2 Nutrients measurements

Doshik Hahm, Kyung A Park and Tae Siek Rhee
Korea Polar Research Institute, Korea

Objectives

To provide the basis of understanding of biological processes such as primary production, phytoplankton physiology, phytoplankton distribution and taxonomy, we investigate the spatial and temporal variations of the nutrients (phosphate, nitrate+nitrite, ammonium, and silicate) through the contrasting oceanic regions in the Amundsen Sea. These results will also be use to understand interaction between water masses and water circulation in general in conjunction with other physical and chemical data.

Work at sea and preliminary results

Equipment and techniques

The nutrients analyses were performed on a gas-segmented continuous flow analyzer (QuAAtro, Seal Analytical). It has four separate channels each dedicated to phosphate, nitrate+nitrite, ammomium, and silicate. The channel configurations and reagents were prepared according to the 'QuAAtro Applications'. Additionally, many guidelines of Hydes et al. (2010) were followed. Notably, we used reference materials for nutrients in seawater (RMNS) produced by 'KANSO Technos' (Lot. No. 'BF') along with in-house standards at every batch of run to ensure accurate and inter-comparable measurements.

Sampling and storage

Sampling of nutrients followed that for noble gases, oxygen, dissolved inorganic carbon, pH, and oxygen isotope. Samples were drawn into sterilized 50 mL conical tubes (Falcon). These were rinsed three times before filling. Samples were then stored in the refrigerator at 2°C until analysis. Most of the samples stored in the refrigerator were analyzed within three days. However, tests carried out on the cruise showed that samples from all depths stored in the refrigerator were stable up to 9 days; the difference between the samples analyzed immediately and the stored was less than 2% except ammonium. Ammonium concentrations appeared to have been changed more than 20% after 5 days.

Sample analysis and calibration

Artificial seawater made of NaCl and deionized water have been used as wash solution which was injected between samples and as mixing solution which was used to prepare in-house calibration standards. A full set of calibrants were analyzed both at the start and end of a run to check sensitivity drift during the analysis which was typically lasted 3 – 4 hours. Additionally, a high concentration calibrant was added in a regular interval to check the short-term sensitivity change. The slopes of the calibration cruves at the start and end of each run did not differ more than 2% for phosphate, nitrate+nitrite, and silicate. Another set of calibrant was prepared by diluting the RMNS to the concentrations of 1/3, 1/2, 2/3 and 1 of Lot 'BF'. All the concentrations of samples were calibrated against the calibration curves dervied from the RMNS measurements. The in-house standard solutions have been used only to calibrate the samples for ammonium and to check inter-run consistency and sensitivity drift during a run. Ammonium measurements appeared to be suffered from cotamination from room air. The contamination became severe when samples were exposured for a long time. Tests on the cruise showed that the concentration of a blank (i.e., 0 μmol/L) have risen up to 0.4 μmol/L after 2 hours.

An example of preliminary results

Shown in Fig. 2.7 is the section map of silicate from the northern end of the trough to in front of the Dotson ice shelf. The variability of the silicate concentration by biological activity on surface layer was less pronounced than the other nutrients. This compound may be more adequate to the identification of CDW and its gradually modification along the trough.

References

Dickson, A. G. (1995) Determination of dissolved oxygen in seawater by Winkler titration. WOCE Operations Manual. WHP Office Report WHPO 91-1, 1995.

Hydes, D. J., M. Aoyama, A. Aminot, K. Bakker, S. Becker, S. Coverly, A. Daniel, A. G. Dickson, O. Grosso, R. Kerouel, J. van Ooijen, K. Sato, T. Tanhua, E. M. S. Woodward, J. Z. Zhang (2010) Determination of dissolved nutrients (N, P, Si) in seawater with high precision and inter-comparability using gas-segmented continuous flow analysers. GO-SHIP Repeat Hydrography Manual. IOCCP Report No. 14, ICPO Publication Series No. 134.

Labasque, T., Chaumery, C., Aminot, A. and Kergoat, G. (2004). Spectrophotometric Winkler determination of dissolved oxygen: re-examination of critical factors and reliability. Marine Chemistry, 88, 53– 60.

Langdon, C. (2010) Determination of dissolved oxygen in seawater by Winkler titration using the amperometric technique. GO-SHIP Repeat Hydrography Manual. IOCCP Report No. 14, ICPO Publication Series No. 134.

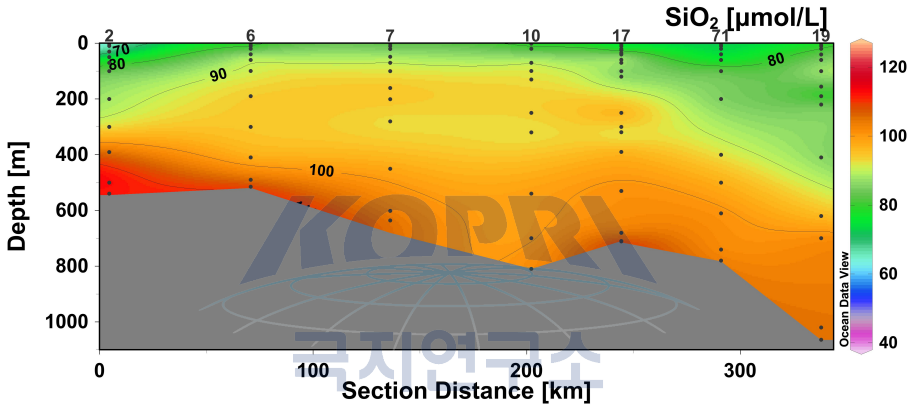

Figure 2.7: Section map of silicate along the trough. The numbers on top of the map are station numbers. Refer to Fig. 2.3 for the locations. The variability of the silicate concentration by biological activity on surface layer was less pronounced than the other nutrients. This compound may be more adequate to the identification of CDW and its gradually modification.

Chapter 3

Biological Oceanography

3.1 Phytoplankton and Primary production

Jeon MiSa[1] , Joo HuiTae[2]
[1]Korea Polar Research Institute, Korea,
[2]Department of Oceanography, Pusan National University, Korea

요약문

2012년 아문젠 하계 연구기간 동안 각기 다른 수괴환경에 따른 식물플랑크톤 생물량과 크기별 군집구조에 대하여 조사하였다. 조사해역은 아문젠해의 외해역, 외해 폴리니아, 대륙사면 및 연안 폴리니아로 구성되어 있다. 조사 정점은 총 33개 정점이었으며 한 정점 당 표준 수심 및 Sub-surface chlorophyll a maximum dept에서 시료를 채집하였다. 본 연구는 조사기간 동안의 엽록소-a 농도 및 크기별 엽록소-a 농도를 측정하여 조사수역의 식물플랑크톤 생물량 분포 및 군집구조에 대하여 조사하였으며 향후 HPMA (HydroxyPropyl MethAcrylate) Silde를 이용하여 식물플랑크톤의 종조성에 대해 연구 할 계획이다. 승선기간 중 정점마다 총 3개의 깊이 (100%, 30%, 1%의 광량의 깊이)에서 탄소와 질산염, 암모늄의 흡수량과 광합성에 의한 식물플랑크톤의 거대분자조성 (탄수화물, 지방, 단백질, LMWM)에 대한 연구를 실시하였다. 탄소와 질산염, 암모늄 의 흡수량은 총 19개의 정점에서 실험을 하였으며 거대분자조성에 대한 실험은 총 14 곳에서 실시 하였다.

Introduction or Objective

The Amundsen Sea, Which is historically known as a region of heavy ice, is undergoing sea ice recession within the last decades (Jacobs and Comiso, 1993), and extensive phytoplankton blooms near the coast have been observed (Smith and Comiso, 2008). Change of ocean and sea ice Condition in this area will profoundly alter ecosystem structure by changing pathways of energy flow and the spatial distribution and species composition of plankton. The aim of the present study was to characterize the systematic composition of phytoplankton assemblages, their distribution, abundance, and size composition and associate them with varying abiotic factors during a limited period of time in summer 2012 in the Amundsen Sea. The Southern Ocean plays an important role in the global carbon cycle, accounting for 20% of global ocean CO_2 uptake (Takahashi

et al. 2009). The marine carbon cycle in the Southern Ocean is very sensitive to climatic fluctuation (Sarmiento et al. 2004). The Southern Ocean is the largest high-nutrient and low-chlorophyll (HNLC) region. Phytoplankton growth is limited mainly by light during the austral spring (Smith et al. 2000) and by biologically available iron during the summer (Sedwick and DiTullio 1997), or both (Tremblay and Smith 2007). In general, the regions of highest productivity are coastal polynyas and other coastal zones in the Southern Ocean (Arrigo and van Dijken 2003; Smith and Comiso 2008). Among the polynyas, the Amundsen Sea is a region of particularly high productivity in the Southern Ocean, with annual primary production reaching up to 160 g C m^{-2}, based on satellite-based estimations of interannual changes in areal extent, phytoplankton abundance, and primary productivity (Arrigo and van Dijken 2003). During this cruise, we measured in situ carbon and nitrogen uptake rates to precisely estimate primary and new production of phytoplankton and to compare differences between polynyas and non-polynya areas of the Amundsen Sea.

Work at sea

The data were collected in the Amundsen Sea from January 30 to March 20 in 2012. A total of 33 stations were visited. Water samples were collected at 6 depths (Surface, 10m, 20m, 40m, 60m, 100m)with a rosette sampler equipped with 20 L Niskin-type bottles, an in situ fluorometer, and a high-precision Sea-Bird plus CTD probe. To analysis phytoplankton community composition, water samples were obtained with a CTD/rosette unit in 20 L PVC Niskin bottles during the 'up' casts. Aliquots of 125 mL were preserved with glutaraldehyde (final concentration 1%). Sample volumes of 20 to 100 mL were filtered through Gelman GN-6 Metricel filters (0.45 µm pore size, 25 mm diameter). The filters were mounted on microscopic slides in a water-soluble embedding medium (HPMA, 2-hydroxypropyl methacrylate) on board. The HPMA slides were used for identification and estimation of cell concentration and biovolume. The HPMA-mounting technique has some advantages over the classical Utermöhl sedimentation method. Samples were also collected via phytoplankton net tows (20 µm mesh) and preserved with glutaraldehyde (final concentration 2%); these samples were used only for identification of small species in the phytoplankton assemblage. Since the results from this can be biased towards larger specimens, these data were not used for statistical analysis, but only for morphological and systematic analysis. Based on the HPMA slide method, the total 198 slides were made for identifying species compositions of phytoplankton later at the laboratory in KOPRI. To identify small sizes plankton (nano-pico size), phytoplankton net samples were cultured by F/2 media (14 stations). Samples for the determination of total chlorophyll- a were filtered onto Whatman GF/F glass fiber filters (24 mm). Size-fractionated chlorophyll-a was determined on samples passed sequentially through 20 µm and 3 µm Nucleopore filters (47 mm) and 0.7 µm Whatman GF/F filters (47 mm). Concentrations of chlorophyll-a were measured on the board using a Turner Designs (Triology), which had been calibrated with commercially purified chlorophyll-a preparations. To estimate carbon and nitrogen uptake of phytoplankton at different locations, productivity experiments were executed by incubating phytoplankton in the incubators on the deck for 3-4 hours after stable isotopes (^{13}C, $^{15}NO_3$, and $^{15}NH_4$) as tracers were inoculated into each bottle. Total 19 productivity experiments were

completed during this cruise. At every CTD station, the productivity waters were collected by CTD rosette water samplers at 3 different light depths (100, 30, and 1%). In addition, Along with the small (1 L) productivity bottle experiments, 14 large volume (8.8 L) productivity experiments for three depths (100, 30, and 1% light depths) were executed to study the physiological status and nutritional conditions of phytoplankton at the productivity stations. These filtered (GF/F, π = 47 m) samples will be chemically analyzed for the macromolecular level end products (such as lipids, proteins, polycarbonates and LMWM) of photosynthesis.

Reference & Acknowledgement

Arrigo, K.R., G.L. van Dijken, 2004. Annual changes in sea-ice, chlorophyll a, and primary production in the Ross Sea, Antarctica Deep-Sea Research Part II: Topical Studies in Oceanography, 51 (1-3), pp. 117-138.

Kang, S.-H., D.-Y. Kim, J.-S. Kang, M.-Y. Lee and S.H. Lee, 1995. Antarcticphytoplankton in the eastern Bransfield Strait region and in the northwestern Weddell Sea marginal ice zone during austral summer. Korea J. of Pol. Res., 6: 1-30.

Kang, S.-H., J.-S. Kang, S. Lee, K. H. Chung, D. Kim and M. G. Park. 2001. Antarctic phytoplankton assemblates in the marginal ice zone of the northwestern Weddell Sea. J. Plank. Res., in press.

Smith Jr., W.O., J.C. Comiso, 2008. Influence of sea ice on primary production in the Southern Ocean: A satellite perspective Journal of Geophysical Research C: Oceans, 113 (5), art. no. C05S93.

Yang, S.R., S.-H. Kang and S. Lee, 1998. Carbon and nitrogen productivities in the Weddell Sea and the Bransfield Strait, Antarctica, The 5th International symposium on Antarctic Science. Korean J. Polar Res., 9(1): 55-62.

3.2 Pytoplankton physiological study

3.2.1 Photoinhibition and recovery, nutrient limitation

Park, Jisoo
Korea Polar Research Institute, Korea

요약문

식물플랑크톤 광합성과 관련된 생리활성도 측정을 위해 Fluorescence Induction and Relaxation (FIRe 2)를 이용하였다. 총 21개 정점의 5개 수층에서 채수한 해수를 이용하였으며, 대륙사면과 해빙에 둘러싸인 해역 7개, 아문젠해 폴리니아 안의 9개 정점, 그리고 파인아일랜드베이 폴리니아 안의 5개 정점으로 이루어졌다. 이들 광합성시스템 II 에서의 생리활성도 측정을 통하여 관측해역 식물플랑크톤의 광저해 효과 및 영양염 결핍에 대한 정보를 유추할 수 있다.

Objectives

To investigate the impact of physico-chemical conditions on photosynthesis, we measured photosynthetic characteristics of phytoplankton at 21 stations using a

Fluorescence Induction and Relaxation (FIRe 2) system (Fig. 3.1). These measurements provide an express diagnostics of the effects of environmental factors on photosynthetic processes such as photoinhibition, recovery of photoinhibition as well as nutrient limitation.

Work at sea

Active (and fast) fluorometry is a non-destructive and rapid method, and it has been used to monitor variations in the photochemistry (Kolber and Falkowski 1993; Falkowski and Kolber 1995). The total stations were 21 which include ice margin, Amundsen polynya, Pine Island Bay polynya, and offshore (Fig. 3.2). After collection from Niskin bottles at five depths, samples were kept under in situ temperature in light and amber bottles. Light bottle samples were measured once immediately, and we measured repetition at every 30 minutes and one hour after low light adaptation. Amber bottle samples were dark adapted for one hour for recovery from non-photochemical quenching. Photosystem II (PSII) parameters such as the minimal fluorescence yield (F0; when all reaction centers are open), the maximal fluorescence yield (Fm; all reaction centers are closed), the quantum efficiency of PSII (Fv/Fm), the functional (or effective) absorption cross-section of PSII (σPSII) were measured as describe in Kolber et al. (1998). Quantum efficiency of photochemistry in PSII (Fv/Fm) was calculated as a ratio of variable fluorescence (Fv=Fm-F0) to the maximum one (Fm). The fluorescence measurements were corrected for the blank signal recorded from filtered seawater. I also acquired 100 ml seawater samples in the pre-cleaned LDPE bottles by deployment of Go-Flo sampler at the subsurface (ca. 15 m) for the measurement of ambient iron concentration (total 15 stations). Samples were frozen and were kept in the deep-freezer. Moreover, I also observed photosynthetic parameters using pumped seawater through a flow-through cuvette in a fluorometer on deck laboratory of a ship during the cruise and ARAON transit from Incheon to the Antarctic.

Preliminary results

The quantum efficiency of PSII (Fv/Fm) was relatively high at the Pine Island Bay Polynya and two stations in the sea-ice zone (Fig. 3.3, 3.4). This values somewhat correlated with the functional absorption cross-section of PSII (σPSII). However, I can't find any relationship between ambient light intensity and photoinhition. The quantum efficiencies in the Pine Island Bay Polynya and also in the some stations showed vertically homogeneous, so it seems that phytoplankton in the regions was not limited by nutrient including iron. But in the most stations in the Amundsen Polynya, the quantum efficiency at the surface was significantly lower than that in the subsurface.

References

Falkowski, P. G. and Z. Kolber (1995). "Variations in chlorophyll fluorescence yields in phytoplankton in the world oceans." Aust. J. Plant Physiol. 22(2): 341-355.

Kolber, Z. and P. G. Falkowski (1993). "Use of active fluorescence to estimate phytoplankton photosynthesis in situ." Limnol. Oceanogr. 38(8): 1646-1665.

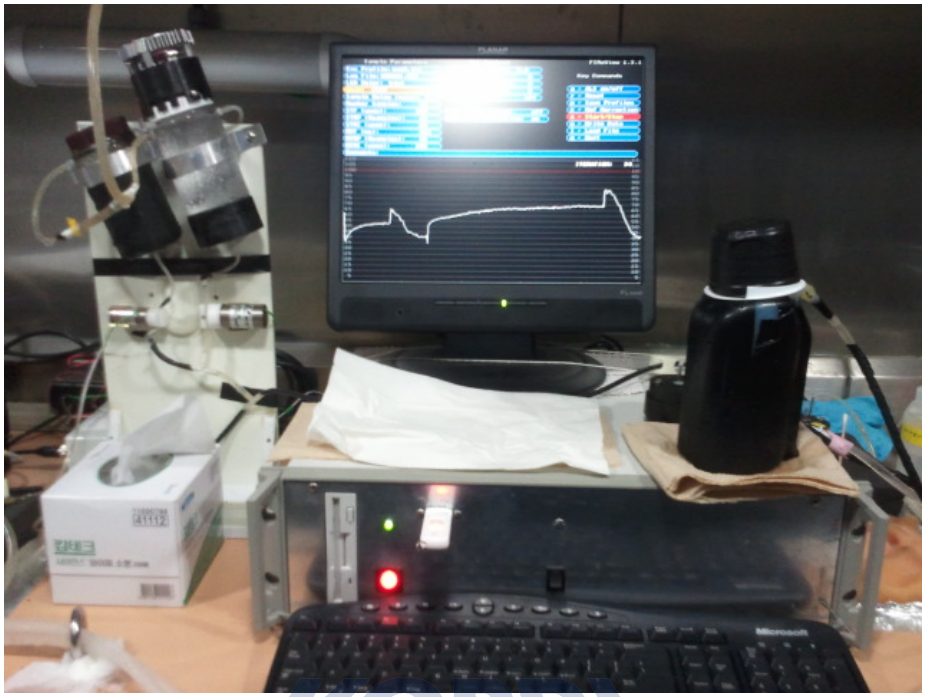

Figure 3.1: A Fluorescence Induction and Relaxation (FIRe 2) system which was installed on the ARAON.

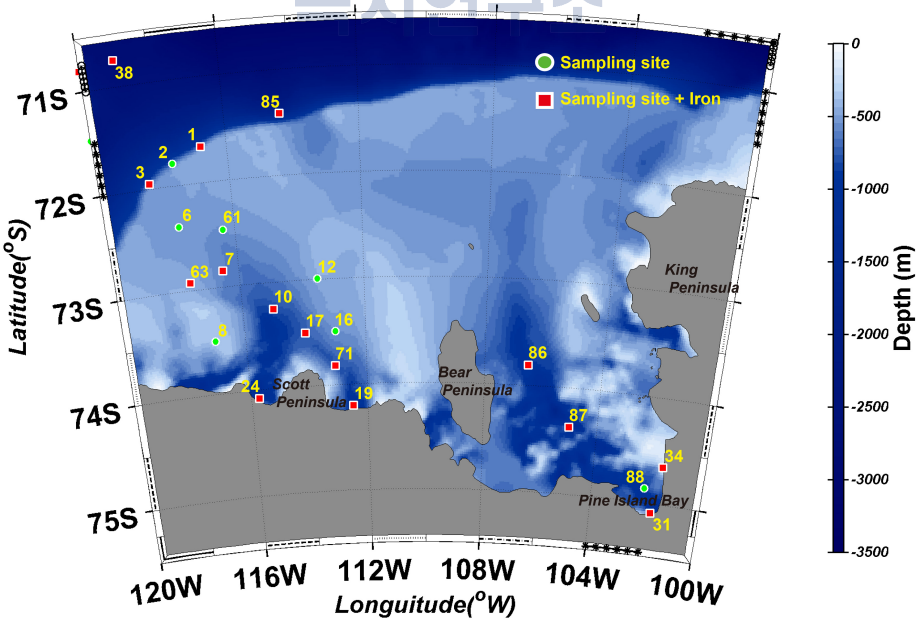

Figure 3.2: Station map during the 2012 Amundsen cruise. Blue colors represent bottom topography.

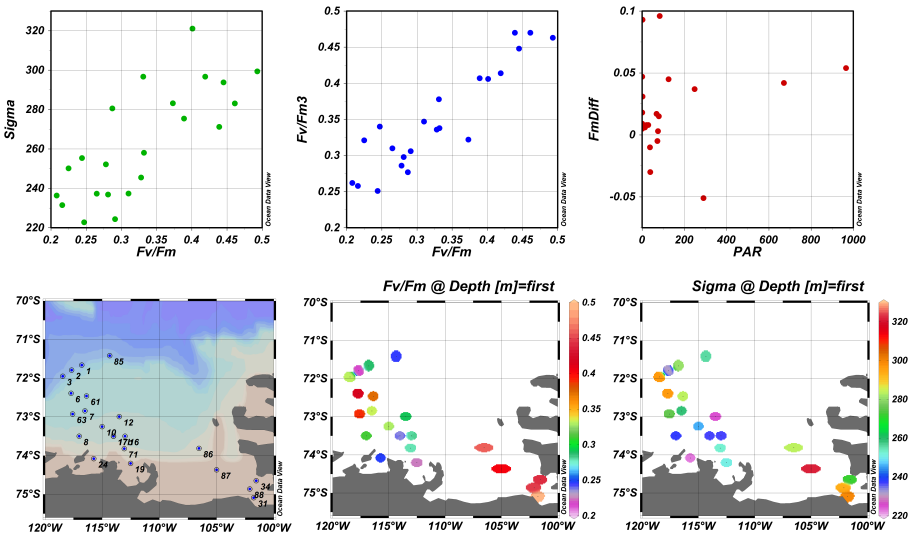

Figure 3.3: Photosynthetic parameters (Fv/Fm and σPSII) at the surface and relationships among the variables.

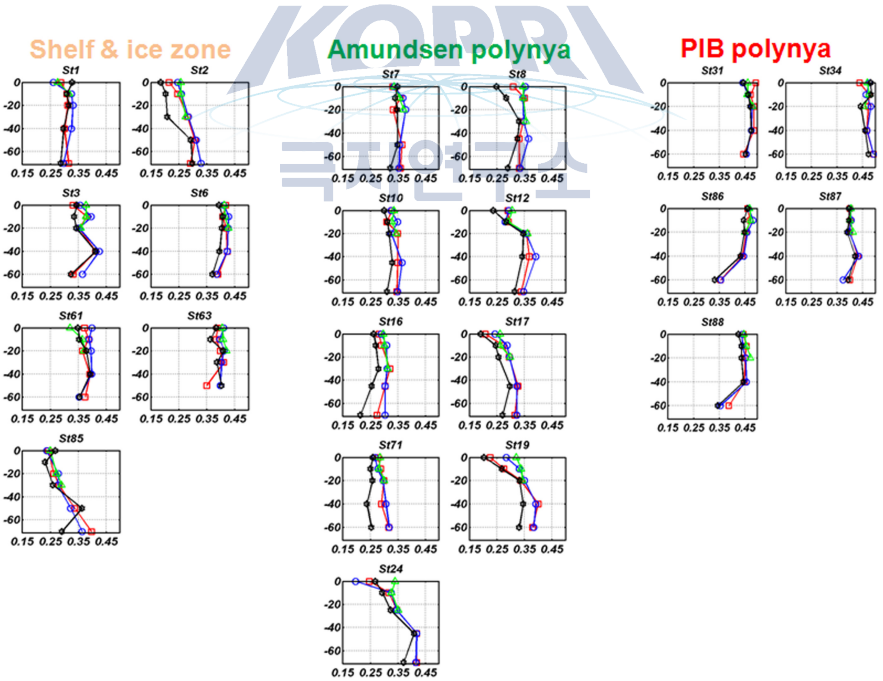

Figure 3.4: Vertical distributions of quantum efficiency (Fv/Fm) in the Amundsen Sea during the 2012 cruise. Red rectangles represent immediately measured values, blue circles represent 30 minutes low light adapted samples, green triangles represent 1 hour low light adapted samples, and black diamond represent 1 hour dark adapted samples, respectively.

Kolber, Z. S., O. Prasil, et al. (1998). "Measurements of variable chlorophyll fluorescence using fast repetition rate techniques: defining methodology and experimental protocols." Biochimica et Biophysica Acta-Bioenergetics 1367(1-3): 88-106.

3.2.2 Light dependencies of photosynthesis and respiration in large phytoplankton in Amundsen sea

Bailleul, Benjamin
Rutgers University

Abstract

The bioenergetic performances of large phytoplankton, in terms of photosynthesis and respiration, were measured in 20 stations in Amundsen polynya, Pine Island Bay polynya, as well as in sea-ice and coastal regions. Photosynthetic and respiratory rates were probed under a wide range of light irradiances, from 0 to 800 $\mu E/m^2/s$, i.e mimicking the range of light intensities experienced by phytoplankton from the bottom of the eutrophic zone to the ocean surface on a sunny day. Preliminary results suggest that the light optimum for photosynthesis is in the 5-15 $\mu E/m^2/s$ range, and that photo-inhibition occurs mainly above 100-200 $\mu E/m^2/s$. A very clear and reproducible direct light regulation of respiration was observed in all samples, leading to a 3 to 5-fold increase of its rate at full sunlight, compared to dark conditions.

Objectives

To investigate the bioenergetic performances of phytoplankton during the Amundsen cruise of Araon 2012, Membrane Inlet Mass Spectrometry (MIMS, BB-fig-1) associated to oxygen labeling (O18) techniques were used. MIMS allows the measurement of the concentration of several dissolved gases, including O216 and O218, as well as biologically "inert" ones (N_2, Argon) with high kinetic resolution, which allows the measurements of photosynthetic and respiratory rates (Beckman et al, 2009). The first objective of this project was to provide a proof of methods for MIMS in polar environment. The second was to get insights into the light dependencies of photosynthesis and respiration in large phytoplankton, and the relationship between those two bioenergetic processes.

Work at sea

After collection from Niskin bottles at one or two depth (surface, middle or bottom of the upper mixed layer), samples were kept under in situ temperature under low light ambient intensity (2-5 $\mu E/m^2/s$) in 10 or 20L carboys, during concentration to obtain 2.5 mL of 2 mg/L chl a sample. The filtration- resuspension process was a critical step, as an increase in temperature or excessively strong pipeting or filtration proved to be harmless for phytoplankton physiology. 250mL was filtered on 3 µm Millipore filter under very low pressure difference (3 mbar), and then gently resupended in 2.5mL of the initial water sample. This procedure was repeated as many times as necessary to reach a ∼4 µg chl a final sample, and Fv/Fm was then measured in the initial and concentrated samples,

Figure 3.5: A Membrane Inlet Mass Spectrometer (MIMS) system was installed in the 10 degrees room of ARAON.

as a diagnostic of phytoplankton physiology. Only samples for which Fv/Fm was not decreased by the procedure were kept for further stages. 0.5 mL of the final sample was used for chlorophyll concentration for later normalization and 2 mL were transfered to a cuvette with magnetic stirring, temperature (0.5 degree) and light regulations, connected to the MIMS, prealably equilibrated for 5-10 hours with water sample and calibrated for Argon, N_2, O216 and O218 masses.

During continuous measurement of dissolved gases concentrations, light intensity was increased from 0 to 800 μE/m^2/s, by 5 to 10 steps of 15-30 minutes each, in order to mimick the upward displacement of phytoplankton from bottom to top of the eutrophic layer in a relevant characteristic time (2-4 hours). O216 and O218 signals were normalized to Argon signal to correct for pressure changes, and slopes of the normalized signals under the different light regimes were eventually analyzed, normalized to chlorophyll concentration to get respiratory and photosynthetic rates.

Preliminary results

Fig. 3.6 shows an experiment used as a proof of methods for this project. 30L of water sample from 20m depth at station 3 were kept for 30 hours under low light, in situ temperature. Although the conditions of this experiment is somehow artificial and despite a very incomplete analysis of the other stations results, this experiment can be considered as representative of some reproducible trends, observed in all samples:

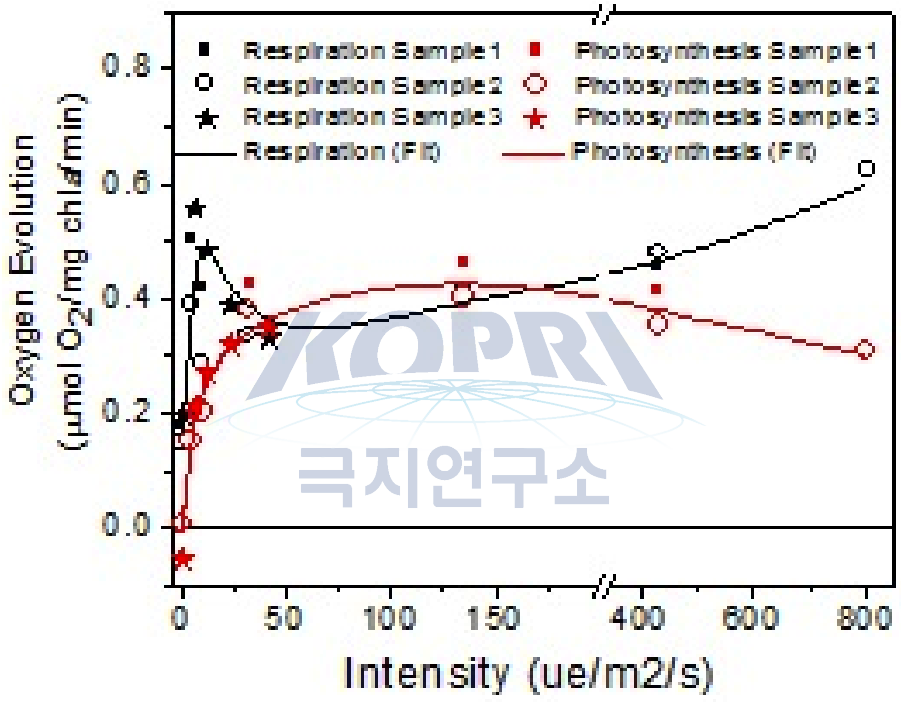

Figure 3.6: Photosynthetic and respiratory rates as a function of light irradiance. 3 triplicates of a water sample from 20m depth at Station 3 were measured 30-40h after sampling.

1. Light optimum for photosynthesis was always low, in the 5-15 $\mu E/m^2/s$ range.

2. Above 100-200 $\mu E/m^2/s$, photoinhibition occurs, reflected by a decrease in photosynthetic rate.

3. Respiratory rate is highly dependant on light intensity. The respiratory rate at the highest light intensity was typically 3 to 5-fold higher than the dark respiration rate. Some further experiments showed that that light regulation was unaffected by the addition of photosynthetic inhibitors (Photosystem II inhibitor DCMU or cytochrom b6f inhibitor DBMIB), which suggests that that it consists in a direct light regulation, and not a photosynthesis-respiration coupling.

References

Beckmann K, Messinger J, Badger MR, Wydrzynski T, Hillier W (2009) On-line mass spectrometry: membrane inlet sampling. Photosynth Res.102(2-3):511-22.

3.3 Phytoplankton pigment analysis

SunA Hwang
Pu-Kyung national univ.

Introduction

Rapid sea ice retreat and the melting of the glacier is expected to affect the primary production in the Southern Ocean. Therefore, we are trying to figure it out the composition of phytoplankton community trough the pigment analysis and look into the environmental feature of the open sea and coastal polynya to understand the principal factors which can influence the phytoplankton community.

Dissolved Organic Carbon play an important role as a major carbon supplyment in marine carbon cycle. The DOC formation is affected by the composition of community of phytoplankton and the DOC concentration is decided according to the physical mixing of water column and the activities of microorganism.

In this research, the vertical distribution of DOC is observed to investigate the pattern of carbon cycle and the relationships between DOC and Chl.a in the Southern Ocean. This research would contribute toward a more comprehensive understanding of marine carbon cycle of the Southern Ocean.

Method

Dissolved Organic Matter (DOC)

Seawater samples for analysis of DOC were filtered under a gentle vacuum (<5 in /Hg) through precombusted (6 hr at 450℃) Whatman GF/F glass fiber filters (diameter:25mm) and collected directly into pre-cleaned and precombusted sample glass bottles (125ml Clear narrow neck bottle). After filtration, 1N HCl were added for removal to impact of inorganic carbon. Until analysis, sample bottles were stored in a freezer (-20℃) after covered with foil. A Shimadzu

Table 3.1: Station No. and number of samples

Station No.	HPLC	DOC	Station No.	HPCL	DOC
ANA02C C1	7	10	ANA02C ST88	8	
ANA02C C2	7		ANA02C ST31	7	18
ANA02C C7	7	14	ANA02C ST35	7	18
ANA02C C8	7		ANA02C ST87	7	
ANA02C C10	7	13	ANA02C ST86	7	
ANA02C C12	8		ANA02C ST17-1	6	
ANA02C C16	7	13	ANA02C ST63	8	
ANA02C C17	7		ANA02C ST61	7	
ANA02C A1	8		ANA02C ST06	7	13
ANA02C ST19	7	17	ANA02C ST03	7	13
ANA02C ST27	7		ANA02C ST85	7	
ANA02C ST24	7	17	ANA02C ST39	8	14
ANA02C ST22	7		ANA02C ST40	7	
ANA02C Sea Ice	5				

TOC analyzer (TOC-V model) was used for high-temperature combustion oxidation (HTCO) analysis of DOC. The HTCO method is based on the method described by Sugimura and Suzuki (1998), and was modified by Dittmar et al. (2006). Milli-Q water was used as a blank sample and for accurate measurement. Milli-Q water was added to every 10 samples. DOC measurement was conducted using 40 ml tube. Before measuring the samples, calibration curve need to be adjusted by making the concentration of TC and TN into 1, 2, 4M.

HPLC (Wright et al)

2L water sample was filtered in situ and put it in the freezer to analyze Chl.a. Photosynthesis pigment of phytoplankton was extracted with 100% Acetone 5㎖ and Canthaxanthin 50 μl as a standard was added do compensate for sample loss. Cells were broken up with supersonic wave grinder for 5 minutes and put it in the cold dark place for 24 hours. Then, fitter paper was grinded and centrifuged for 10 minutes at 2000rpm. 1㎖ upper water with 300μl HPLC water was injected to HPLC for analyzing. Concentration is calculated with following equation.

C = Area × Rf × (AIS / SIS) × Vi / Vs.

C: concentration [ng/l]

Area: area of the peak [area]

Rf: standard response factor [ng l-1 area-1]

AIS: peak area of the internal standard (IS) when 1 ml IS was mixed with 300 µl of H2O

SIS: peak area of IS added to sample
Vi: volume of IS added to sample [l]
Vs: volume of filtered water sample

3.4 Bacteria

Hyun, Jung-Ho; Kim, Sung-Han; Choi, A-Yeon
Department of Environmental Marine Sciences, Hanyang University, Korea

요약문

남극 아문젠해의 아문젠 polynya(AP)와 Pine Island Bay(PIB)의 outer-shelf, polynya 및 ice-shelf에 위치한 연구정점들에서, 수층의 물리-화학-생물 요인의 변화에 따른 박테리아의 생체량 및 미생물 호흡율 변화양상을 규명하기 위한 연구를 실시하였다. 호흡율은 polynya(51–138 mmol m^{-3} d^{-1})가 outer shelf(27–72 mmol m^{-3} d^{-1}), ice-shelf(14–42 mmol m^{-3} d^{-1}) 및 외양역(16–18 mmol m^{-3} d^{-1})에 비해 높은 값을 나타냈다. 호흡율의 분포는 클로로필의 분포와 높은 양의 상관관계 (r2 =0.5753; n = 26; P < 0.0001)를 보였는데, 이는 아문젠해에서의 호흡율이 수층의 유기탄소의 공급과 밀접한 관계가 있음을 나타내는 것이다. 한편, 미생물 생체량 분포 및 미생물 생장조절 요인을 파악하기 위한 다양한 실험들(UV 효과, 생장제한 영양요인 등)을 선택된 연구 정점들에서 추가적으로 실시하였으며, 추후 연구실에서의 분석을 위해 확보된 시료들을 냉장 또는 냉동상태로 보관하였다.

Background

Respiration represents the transfer of carbon from organic pool to inorganic pool, and reflects the rate of organic matter supply that is available to the biota within the system (Jahnke and Craven, 1995). Long-term shifts in respiration have a potential to provide the best warning system for global change (del Giorgio and Williams, 2005). Therefore, it is particularly important to measure the respiration in polar ocean to better understand any shifts in biogeochemical carbon cycles.

Work at sea

During this cruise, we measured the planktonic respiration rates at 4 different sites, polynya, outer shelf, ice-shelf and offshore. Water samples were collected using a Sea-bird Electronics CTD system equipped with specific sensors such as photosynthetically active radiation (PAR) sensor, fluorometer, transmissometer and dissolved oxygen meter. Water samples for bacterial abundance were fixed with glutaraldehyde (final concentration, 1%) and kept in the freezer for cell enumeration in the lab. Respiraton rates were measured onboard from the decrease of dissolved oxygen concentration during incubation using a spectrophotometeric-Winkler method (Labasque et al. 2004). Briefly, water samples were taken using 20-l Niskin bottles at 3 – 5 different water depth in the surface layer, and were then transferred into six 300-ml BOD bottles (Wheaton Co.) that were washed and rinsed with acid (10% HCl) and distilled water, respectively. The BOD bottles were wrapped with aluminum foil, and then were

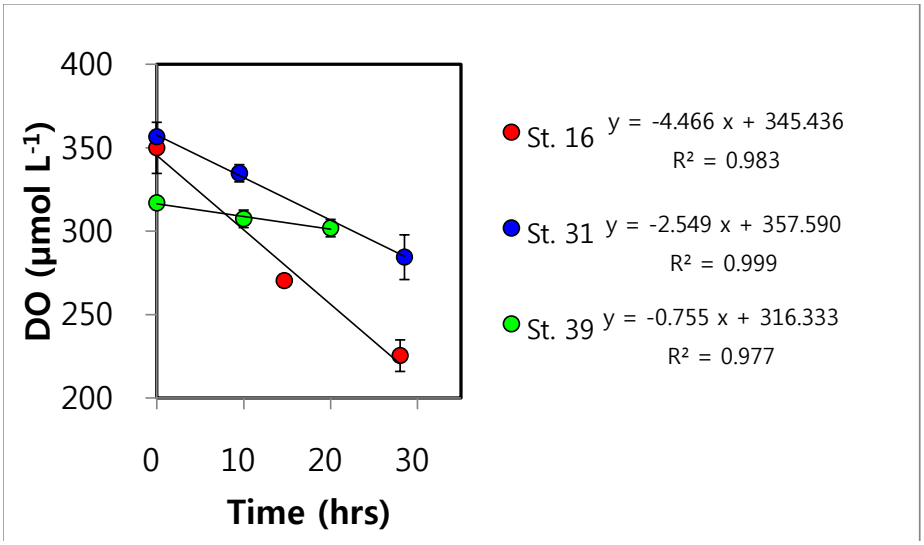

Figure 3.7: An example of the respiration rates measured at polynya (St. 16), outer shelf (St. 31) and offshore (St. 39) sites. Note that respiration rates were highest at polynya.

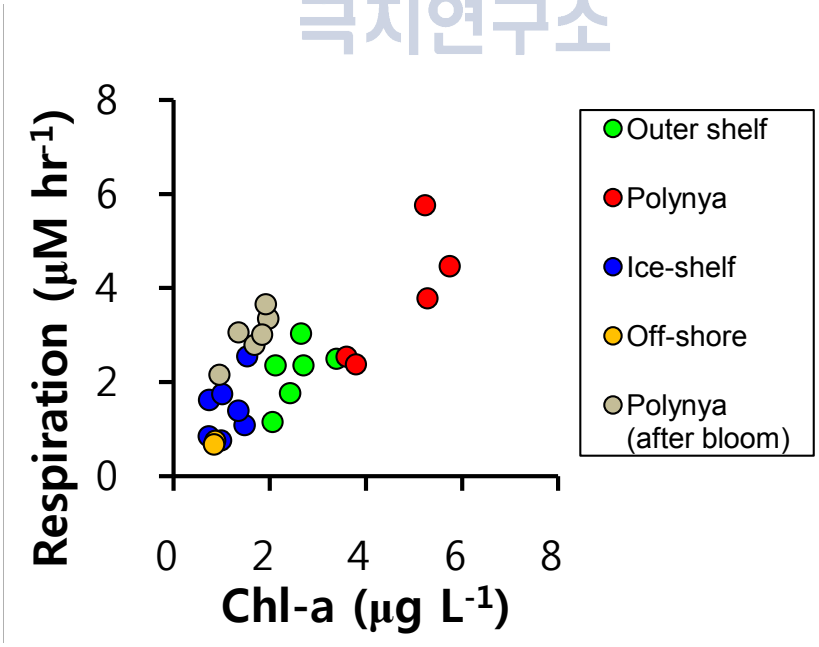

Figure 3.8: Relationship between chlorophyll-a and respiration rates

incubated for 20 – 25 hours in the dark in incubator through which in situ seawater continuously flowed. At the end of incubation, BOD bottles were immediately fixed by adding 2 ml of manganese chloride and 2 ml of alkaline iodide reagents. After being vigorously shaken for about 1 min, the BOD bottles were stored in the dark. When most of the flocculation had settled, the bottles were reopened and 2 ml of sulfuric acid solution was added. The mixture was then gently stirred with a magnetic stirrer until all the precipitate had dissolved. Absorbance was measured onboard within 3 min using a Shimadzu UV-1700 spectrophotometer. The spectrophotometric Winkler method has a precision of 0.1% for the onboard measurement. Respiration rates were calculated from the linear regression of time-course measurement of dissolved oxygen concentration with time.

Preliminary results

- An example of respiration measured at polynya, ice shelf and offshore sites is presented in Fig. 3.7. Respiration rates at polynya (51–138 mmol m^{-3} d^{-1}) were higher than those measured at outer shelf (27–72 mmol m^{-3} d^{-1}), ice-shelf (14–42 mmol m^{-3} d^{-1}) and offshore sites (16–18 mmol m^{-3} d^{-1}).

- Strong positive relationship between respiration rates and Chl-a concentration (r2 =0.5753; n = 26; P < 0.0001) indicated that the respiration rates at the Amundsen Sea was mainly controlled by the supply of organic carbon (Fig. 3.8).

Reference

del Giorgio, P. A. and Williams, P. J. le B., 2005. The global significance of respiration in aquatic ecosystems: from single cells to the biosphere. In: P.A. del Giorgio and P. J. le B. Williams (eds) respiration in aquatic ecosystems. Oxford University Press, New York, pp. 267-303.

Jahnke, R. A. and Craven, D. B., 1995. Quantifying the role of heterotrophic bacteria in the carbon cycle: a need for respiration rate measurements. Limnology and Oceanography. 40: 436-441.

Labasque, T., Chaumery, C., Aminot, A., and Kergoat, G., 2004. Spectrophotometric Winkler determination of dissolved oxygen:re-examination of critical factors and reliability, Marine Chemistry, 88, 53-60.

3.5 Grazing impacts and community structure of heterotrophic protists

Yang Eun Jin, Lee Dong Jin
Korea Polar Research Institute

요약문

2012년 2월 - 3월에 아문젠 폴리니아와 파인아일랜드 폴리니아에서 원생동물의 생물량, 군집구조, 식물플랑크톤 및 박테리아에 대한 섭식률 실험을 수행하였다. 원생동물의 생물량 분포 및 군집구조 분석은 현장에서 고정하여 랩으로

가져간 후 분석 되어질 예정이다. 또한 해수 희석법을 이용하여 측정한 식물플랑크톤과 박테리아에 대한 섭식률 측정은 2011년 자료와 비교하여 분석되어질 예정이다.

Background study

Heterotrophic protists ingest a broad size spectrum of prey, from bacteria to microphytoplankton, and are themselves important prey items for mesozooplankton. Many researches suggest that heterotrophic protists contribute to the trophic linkage between phytoplankton and mesozooplankton and are important in the pelagic food webs of many oceanic waters. The importance of heterotrophic protists in pelagic ecosystems has become increasingly evident in the past two decades, and trophic interaction between heterotrophic protists and phytoplankton has been reported in various marine. Studies of protozooplankton in the Southern Ocean have emphasized the importance of protozooplankton in microbial communities and their role as major consumers of phytoplankton (Burkill et al., 1995; Froneman and Perissinotto, 1996; Landry et al., 2001; Pearce et al., 2011; Safi et al., 2007; Selph et al., 2001). Overall, previous research has suggested that knowledge of the structure of the microbial community and protozoan grazing impacts, is central to developing an understanding of carbon flux in the Southern Ocean. However, comprehensive studies on protozooplankton assemblages have been generally limited to the Weddell Sea, Bellingshausen Sea, and the Atlantic and Indian sectors of the Southern Ocean, particularly the marginal ice-edge zone (Froneman et al., 2004; Klass, 1997; Safi et al., 2007). There is no information on the relative importance of heterotrophic protists in the pelagic ecosystem of the Amundsen Sea. The Amundsen Sea, which is historically known as a region of heavy ice, is undergoing sea ice recession within the last decades (Jacobs and Comiso, 1993), and extensive phytoplankton blooms near the coast have been observed (Smith and Comiso, 2008). In this study area, we investigated the meso-scale variations and structure of heterotrophic protist communities and grazing rates on phytoplankton in the various environmental conditions such as sea ice zone and polynya. During this cruise, we investigated protozoa abundance, biomass and grazing rate in total 30 stations

Work at Sea

Abundance and community composition of heterotrophic protists

To determine the abundance of heterotrophic protists, a CTD-Niskin rosette sampler was used to take water samples from the following 6 depths. For ciliates and sarcodina, 1,000 ml water from the vertical profiles was preserved with 1% acid Lugol's iodine solution these samples were then stored in darkness. For heterotrophic nanoflagellates and heterotrophic dinoflagellates smaller than 20 µm, 500 ml of water was preserved with glutaraldehyde (0.5% final concentration) and stored at 4°C.

Grazing experiments

Grazing rates of heterotrophic protists were determined by the dilution method (Landry and Hassett 1982). Water for grazing experiments was collected from 3 depth (surface, SCM, 1% light depth) of each station, and gently filtered through a 200-μm mesh. At each station, 30L seawater were collected in a Niskin bottle and transferred to a polycarbonate carboy. Part of this water

was filtered through the 0.22-μm filtration system. Dilution series were set up in ten 1.3-l PC bottles. Ten bottles were used to establish a nutrient-enriched dilution series consisting of replicate bottles with 11, 28, 50, 75, and 100% natural seawater. The bottles were incubated on deck for 24 – 48 h at ambient sea surface temperatures and screened to the ambient light level with neutral density screening. Subsamples were collected from replicate bottles at 0 and 24-48h to determine chlorophyll-a concentrations and bacterial abundance.

Reference

Jacobs, S. S., Comiso, J. C. 1993. A recent sea-ice retreat west of the Antarctic Peninsula. Geophysical Research Letters 20: 1171-1174.

Smith, W. O. Jr., Comiso, J. C. 2008. Influence of sea ice on primary production in the Southern Ocean: a satellite perspective. Journal of Geophysical Research 113 doi:10.1029/2007JC004251.

Pearce, I., Davidson, A.T., Thomson, P.G., Wright, S., van den Enden, R., 2011. Marine microbial ecology in the sub-Antarctic Zone: Rate of bacterial and phytoplankton growth and grazing by heterotrophic protists. Deep-Sea Res. Part II. 58, 2248-2259.

Safi, K.A., Griffiths, F.B., Hall, J.A., 2007. Microzooplankton composition, biomass and grazing rates along the WOCE SR3 line between Tasmania and Antarctica. Deep-Sea Res. Part I. 54, 1025-1041.

Selph, K.E., Landry, M.R., Allen, C.B., Calbet, A., Christiansen, S., Bidigare, R.R., 2001. Microbial community composition and growth dynamics in the Antarctic Polar Front and seasonal ice zone during late spring 1997. Deep-Sea Res. Part II. 48, 4059-4080.

Landry, M.R., Brown, S.L., Selph, K.E., Abbott, M.R., Letelier, R.M., Christensen, S., Bidigare, R.R., Casciotti, K., 2001. Initiation of the spring phytoplankton increase in the Antarctic Polar Front Zone at 170°W. J. Geophys. Res. 106(C7), 13,903-13,915.

Froneman, P.W., 2004. Protozooplankton community structure and grazing impact in the eastern Atlantic sector of the Southern Ocean in austral summer 1998. Deep-Sea Res. Part II. 51, 2633-2643.

Landry, M.R., Hassett, R.P., 1982. Estimating the grazing impact of marine microzooplankton. Mar. Biol. 67, 283-288.

Froneman, P.W., Perissinotto, R., 1996. Structure and grazing of the microzooplankton communities of the subtropical convergence and a warm core eddy in the Atlantic sector of the Southern Ocean. Mar. Ecol. Prog. Ser. 135, 237-245.

Burkill, P.H., Edwards, E.S., Sleigh, M.A., 1995. Microzooplankton and their role in controlling phytoplankton growth in the marginal ice zone of the Bellingshausen Sea. Deep-Sea Res. Part II. 42, 1277-1299.

3.6 Assessment of mesozooplankton community and feeding rate

Lee, Doo Byoul
Korea Polar Research Institute, Korea

요약문

중형동물플랑크톤은 아문젠 해역을 포함한 남극 해역의 해양 생태계 내에서 하위 영양 단계와 상위 영양 단계를 연결해 주는 연결 고리 역할을 한다. 이에 이들의 분포를 정량적으로 파악하고 이들의 섭식량을 정량적으로 파악하는 것은 아문젠 해역의 하위 영양 생태계를 이해하는데 필수적인 요인이 된다. 이에 본 연구에서는 중형동물플랑크톤 분포 및 우점 요각류와 크릴의 섭식량을 파악하기 위해 18개 정점에서 Bongo net를 이용하여 채집하였다. 또한, 아문젠 해역에 우점하는 동물플랑크톤의 호흡률을 micro respiration system을 이용하여 미세 단위로 측정하였다. 동물플랑크톤의 광역 분포는 개체수와 biomass를 측정하였으며, 우점 요각류와 크릴의 섭식량은 gut pigment contents를 분석을 통해 파악하였다.

Introduction

Polynya, an area of open water surrounded by sea ice, is an important part of the Antarctic ice system occurred seasonally at the same time and place each year. Mesoscale patches of high chlorophyll concentration and productivity for extended period often occur in frontal regions, coastal/neritic waters, the Marginal Ice Zone and polynyas (Smith and Gordon 1997; Arrigo and van Dijken 2003), which supports zooplankton processes (Deibel and Daly 2007). Because animals can adapt their life strategies to this regularity, these types of polynyas are of special ecological research significance. In spring, the thin or absent ice cover allows light in, through the surface layer as soon as the winter night ends, which triggers the early blooming of microalgae that are at the basis of the marine food chain. So, polynyas are suspected to be places where intense and early production of the planktonic herbivores ensure the transfer of solar energy (food chain) fixed by planktonic microalgae to minke, killer whales, leopard seals and emperor and Adélie penguins.

The Amundsen Seas is one of the most productive areas of the Southern Ocean (Fragoso and Smith 2012), with annual primary production reaching up to 160 g C m-2 and chlorophyll concentrations exceeding >10 µg l-1 (Arrigo and van Djiken 2003). The Amundsen Sea has received much attention in recent years because of the observation of a rapid sea ice retreat and the noticeable melting of the Pine Island Glacier (PIG) located east of the Amundsen Sea.

Zooplankton is an important element of Southern Ocean ecosystems including the Amundsen Sea and plays a major role in Antarctic biogeochemistry (Atkinson 1988). Little is known about the abundance and community of zooplankton throughout the Amundsen Sea, because most biological investigations have focused on other trophic levels. Also, despite the numerical importance of copepods within the zooplankton community, no studies have been conducted on their feeding ecology in the Amundsen Sea.

Feeding behavior plays an important role in the adaptive strategies of marine organisms. Feeding is also the main route for the transfer of energy and material from lower to higher trophic organisms within communities and, as such, its quantification is a key factor in understanding trophic interactions. Grazing impact by zooplankton, especially copepods and Euphausiids, is a key factor in controlling composition and dynamics of phytoplankton communities in the Southern Ocean (Pasternak and Schnack-Schiel 2001). It has been suggested that zooplankton grazing may at times control phytoplankton composi-

Table 3.2: Latitude and longitude at sampling site and sampling depth of Bongo net from 10 February to 8 March 2012.

Latitude	Longitude	Station	Date/Time	Depth (m)
71.39.97	116.47.53	ANA02C01	2012-02-10	150
72.51.44	116.31.11	ANA02C07	2012-02-11	170
73.01.65	117.24.91	ANA02C62	2012-02-11	120
73.29.88	116.30.90	ANA02C08	2012-02-12	170
73.15.02	114.59.87	ANA02C10	2012-02-13	150
72.59.33	113.29.316	ANA02C12	2012-02-13	190
73.29.96	113.00.01	ANA02C16	2012-02-14	170
73.49.25	113.03.99	ANA02C71	2012-02-16	190
74.12.12	112.30.66	ANA02C19	2012-02-17	190
74.04.80	115.43.47	ANA02C24	2012-02-18	190
74.52.02	102.06.49	ANA02C88	2012-02-24	150
75.05.24	101.45.55	ANA02C31	2012-02-24	165
74.38.82	101.31.97	ANA02C34	2012-02-25	170
74.21.98	104.59.93	ANA02C87	2012-02-26	170
73.48.64	106.32.15	ANA02C86	2012-02-27	170
72.27.41	116.20.78	ANA02C61	2012-03-02	180
72.24.16	117.43.34	ANA02C06	2012-03-03	170
71.56.94	118.26.90	ANA02C03	2012-03-03	170

tion and the development of such phytoplankton blooms (Dubischar and Bathmann 1997).

The primary objectives are (1) to quantify the mesozooplankton community, (2) to understand interactions among the environmental factors (i.e. seawater temperature, salinity and chlorophyll a concentration), protozoa and mesozooplankton community in the polynya and non-polynya area according to different water masses. Furthermore, we evaluated the grazing impact of major copepods and Euphausia crystallorophias on the phytoplankton biomass in the polynya and non-polynya areas. In the additional study, the mesozooplankton respiration rate was measured by new method.

Material and methods

Field sampling for mesozooplankton

Zooplankton samples were collected with a Bongo net (333 and 505 μm

Figure 3.9: Micro respiration system.

mesh) at 18 selected stations (Table 3.2). The net was towed twice vertically or obliquely within the upper 200 m of water column. Tow speed and duration were about 1.5-2 knots and 15-20 minutes, respectively. Samples from the first tows were immediately fixed and preserved with buffered formaldehyde (pH 8, final concentration ca. 5%) for quantitative analyses. From the second-towed samples, healthy individuals were transferred to 10 l polycarbonate carboys filled with natural seawater. The animals were transferred into 20 ml vials containing filtered seawater. These vials were frozen at -80°C defreezer for the gut content analyses.

Mesozooplankton respiration rate

Freshly caught healthy individuals were immediately sorted out and transferred to 2.4 L polycarbonate bottles on the site. Undamaged healthy adult females of the animals from the 2.4 L bottles were transferred into 300 ml polycarbonate bottles filled with a 0.45 µm filtered seawater. Animals for experiments were starved for 12 h by placing the bottles in a container filled with filtered seawater at in situ temperatures. Starved animals transferred into 2 ml micro-chambers filled with 0.45 µm filtered seawater (0 oC, 33.2 psu) in the dark room. Controls were made by 0.45 µm filtered seawater without animals. All chambers are dark incubated in a water bath at 0±0.5oC. The dissoloved oxygen (DO) concentrations in the micro-chambers were monitored by an oxygen sensor probe (Unisense A/S Modular micro-respiration system). The electrode was calibrated at anoxic condition and full saturation condition (Fig. 3.9).

References

Arrigo KR, van Dijken GL (2003) Phytoplankton dynamics within 37 Antarctic coastal polynyas. J Geophy Res 108: doi:10.1029/2002JC001739 .
Atkinson A (1998) Life cycles strategies of epipelagic copepods in the Southern Ocean. J Mar Syst 15:289-311.
Deibel D, Daly KL (2007) Zooplankton processes in Arctic and Antarctic polynyas. In: Smith WO Jr, Barber DG (eds) Polynyas, windows to the world. Elsevier, Oxford, UK, pp 271-322.
Dubischar CD, Bathmann UV (1997) Grazing impact of copepods and salps on phytoplankton in Atlantic sector of the Southern Ocean. Deep Sea Res II 44:415-433.
Fragoso GM, Smith WO (2012) Influence of hydrography on phytoplankton distribution in the Amundsen and Ross Seas, Antarctica. J Mar Syst 89:19-29.
Pasternak AF, Schnack-Schiel SB (2001) Feeding patterns of dominant Antarctic copepods: an interplay of diapause, selectivity, and availability of food. Hydrobiol 453/454:25-36.
Smith WO, Gordon LI (1997) Hyperproductivity of the Ross Sea (Antarctica) polynya during austral spring. Geophys Res Lett 24:233-236.

3.7 Diversity and function analysis of microbial community in Amundsen sea: Sample collection

Kim, Jong Geol
Chungbuk National University

요약문

작년 아문젠 크루즈를 통하여 남극의 아문젠해(Polynya)에서의 Prokaryotes (세균 및 고세균)의 다양성을 알아 볼 수 있었다. 이러한 결과를 토대로 남극의 특정환경인 Polynya에서 일반 open ocean 과는 다른 특이한 점을 발견할 수 있었다. 이에 이번 크루즈를 통하여 남극의 아문젠해에서의 Polynya의 발달에 대해 추가적인 연구를 하고자 하였으며, 관련하여 대양으로부터 해빙해양, polynya로 이어지는 극지해양환경에서의 Procaryotes의 다양성과 기능성을 연구하고자 한다. 나아가, 분자생태기술(ex, Metagenome)을 이용하여 온난화가스(N_2O, CH_4)의 생성과 분해에 관련된 미생물의 활성과 분포 및 다양성을 연구하고자 하며, 배양을 통하여 이러한 과정에 중요한 기능을 하는 미생물 자원을 확보하고자 한다. 크루즈기간동안 구체적으로 수행한 일은 1) 중요한 정점에 대하여 깊이별로 해수 샘플링 후 필터를 통하여 바이오매스를 확보하였다. 바이오매스를 함유하고 있는 필터는 DNA/RNA가 분해되지 않게 보존할 수 있는 용액에 담군 후 바로 동결시켰다. 2) 배양을 통한 활성 측정 및 신규 미생물의 확보을 위하여 해수샘플도 확보하여 냉장보관하였다. 3) 메타지놈 분석을 위한 해수 샘플링은 기존에 하였던 깊이별 해수 샘플링보다 훨씬 많은 대용량 해수를 filter 함으로써 실험에 필요한 바이오 매스를 확보하였다.앞으로, 확보한 시료로부터 DNA/RNA를 추출하여 Procaryotes의 rRNA 및 그 유전자의 다양성 및 기능성 분석을 실시하고자 한다. 나아가, 이를 토대로 신규 생물자원의 존재와 확보를 시도하고자 한다.

Objectives

Global biogeochemical cycles are essentially mediated by diverse prokaryotic microorganisms. The antarctica has been focused as an important region in the aspect of global climate change. In this cruise, we collected seawater samples in the Amundsen sea area which includes polynya and their surrounding seaice environments. Polynya is annual melt area with large bloom event. There aer various procaryotes involved in nitrogen cycles: nitrogen fixation and nitrification which might be tightly related with polynya bloom. We are going to study key players of the nitrogen cycle in the polynya region. Further, we are interested in the diversity, activity, and abundance of procaryotes involved in the generation and consumption of non-CO_2 greenhouse gas, i.e., nitrous oxide and methane. Nitrous oxide is known to be produced by nitrification process which is mediated proteobacteria and archaea. Methane consumption is mediated by aerobic methanotrophs in water column. For this purpose, first, we are going to take a census of procaryotes using sequencing of rRNA or its gene in the Amundsen area (sea ice area, polynya, ice margin, open ocean). Second, diversity and expression of functional genes involved in nitrogen cycles (such as nifH and amoA) and the transformation of greenhouse gases (such as nirK, and pmoA) will be studied in representative stations. Third, candidate microorganisms of essential and abundant biogeochemical function in the Amundsen sea suggested from the studies above molecular survey will be cultivated in the laboratory. The results obtained from these studies will be crucial for understanding the biogeochemical cycles involved in the polynya bloom and concurring greenhouse gas dynamics, which will give insight into climate change in the antarctic area.

Work at sea and preliminary results

Water samples were collected at discrete depths using a 24-bottle conductivity-temperature-depth rosette sampler. Samples for nucleic acid extraction were collected from the rosette in 2–4 l sterile plastic bottles. Cells were harvested by vacuum filtration onto 47 mm filters housed in Millipore filter holders; first through a 20 µm pore size polyester pre-filter (Whatman) and then a 0.2 µm Supor filter (Pall). For simultaneous DNA/RNA extraction, 2–4 l volumes were filtered and frozen with the addition of 1 ml RNA Later solution prior to freezing. About 20 40 liters of surface seawaters were filtered at the ice stations for comprehensive analysis of the prokaryotic community by pyrosequencing of the metagenomic DNA. Further, microorganisms in ice core were collected from melt water of sectioned ice core layers showing algal bloom which was indicated by yellow pigment in the corresponding layers.

Reference

1. Rohit Ghai, Ana-Beléen Martin-Cuadrado, Aitor Gonzaga Molto, Inmaculada Garcíia Heredia, Raúul Cabrera, Javier Martin, Miguel Verdúu, Philippe Deschamps, David Moreira, Purificacióon Lóopez-Garcíia, Alex Mira, Rodriguez-Valera, F. Metagenome of the Mediterranean deep chlorophyll maximum studied by direct and fosmid library 454 pyrosequencing. ISME Journal, 4(9):1154-1166

2. Comeau AM, Li WK, Tremblay JE, Carmack EC, Lovejoy C (2011). Arctic Ocean microbial community structure before and after the 2007 record sea ice minimum. PLoS One 6: e27492.

3. Collins RE, Rocap G, Deming JW (2010). Persistence of bacterial and archaeal communities in sea ice through an Arctic winter. Environ Microbiol 12: 1828-1841.

Chapter 4

Antarctic krill acoustics

4.1 Distribution of Euphausia crystallorophias in Amundsen Sea coastal polynyas

La, Hyoung Sul1; Lee, Hyung Been2
Korea Polar Research Institute1 (KOPRI)
Korea Ocean Research Development Institute2 (KORDI)

요약문

남극 아문젠 해역 연안 폴리냐에서 음향 조사를 통한 아이스 크릴 (Ice krill, Euphausia crystallorophias)의 밀도를 추정하고 지역적 특성을 조사하였다. 지역별 크릴 밀도 및 분포 특성을 파악하기 위하여 외해, 폴리냐, 빙벽 부근에서 총 4개의 정선 조사를 실시하였다. 음향시스템은 아라온에 설치된 과학어군탐지기 (scientific echo sounder) EK60을 사용하였으며 3개의 주파수 (38, 120, 200 kHz)를 이용하여 표층에서 수심 400 m까지 데이터를 수신하였다. 센서의 보정은 조류가 약한 해빙 지역에서 보정구를 이용하여 실시하였다. 크릴 밀도는 음향자료의 안정성을 고려하여 6-10 노트의 자료만을 사용하여 추정하였으며, 모크니스 (MOCNESS)와 봉고 네트 (Bongo net)를 이용한 타겟 트롤 (target trawl)을 통해 음향 산란층 내의 생물을 채집하였다. 채집된 샘플은 현장에서 길이 (body length/total length) 분포를 측정하였다. 채집된 아이스 크릴은 최소 8 mm 에서 최대 30 mm의 범위에서 bi-modal 분포를 나타냈으며, 평균 길이는 17.11 mm (표준 편차: 4.91) 로 측정되었다. 본 레포트에서는 2개 주파수 (38 kHz와 120 kHz)를 사용하여 분석된 평균후방산란강도 차 (MVBS120-38)를 이용하여 아이스 크릴의 지역별 분포 특성을 확인하였다. 분석 결과 전반적으로 pack ice와 coastal polynya 의 경계면과 Getz 빙붕 주위에서 높은 MVBS120-38가 나타났으며, 외해에서 가장 낮은 MVBS120-38 값을 보였다. 향후 각 정선에서 우점종별 분포 밀도를 계산할 예정이며 이들 분포 밀도와 수온, 염분, 용존산소량, 식물플랑크톤 그리고 해빙 분포와 같은 환경 자료와의 상관성을 비교 분석할 예정이다. 또한 정점에서 2시간 이상 연속 관측한 음향 데이터로부터 아이스 크릴의 수직 분포를 확인하고 수직 분포에 영향을 미치는 환경 요인을 파악하고자 한다.

Table 4.1: Acoustics EK60 settings.

Parameter	38 kHz	120 kHz	200 kHz
Mode	Active	Active	Active
Transducer type	Split	Split	Split
Power (W)	2000	500	300
Transducer depth (m)	7.5	7.5	7.5
Pulse length (μs)	1024	1024	1024
Collection range (m)	400	400	400
2-way beam angle (dB)	-20.60	-21.00	-20.70
Receiver Bandwidth (kHz)	2.43	3.03	5.97
Transducer gain (dB)	21.35	26.17	23.61
Sa correction (dB)	-0.44	-0.35	-0.35
Angle sensitivity along	21.90	23.00	23.00
Angle sensitivity athwart	21.90	23.00	23.00
3 dB Beam along (deg)	7.06	6.67	6.59
3 dB Beam athwart (deg)	6.99	6.57	6.54
Along offset (deg)	-0.01	0.01	0.04
Athwart offset (deg)	0.00	0.03	-0.04
Absorption Coefficient (db/km)	9.899	24.844	38.940
Temperature (ºC)	-0.5	-0.5	-0.5
Salinity (psu)	34.0	34.0	34.0
Sound Velocity (m/s)	1449.39	1449.39	1449.39

Introduction

In recent, attention has focused on processes associated with structural features unique to areas of reduced sea ice cover within the ice pack, the coastal polynyas. The polynya is noted for sustaining enhanced levels of biological production and biogeochemical activity during because they are the first polar marine systems to be exposed to the increasing solar radiation during spring and summer (Arrigo, 2003). The coastal polynya is considered significant regions not only for the primary production but also zooplankton because highly deformed ice with many ridges provides a favorable habitat for zooplankton. The Amundsen Sea coastal polynya is also well known for the rapid sea ice retreat (Jacobs and Comiso, 1997), as well as one of the most productive areas among 37 coastal polynyas in the Southern Ocean. It is responsible for >75% of total production in Antarctica (Arrigo, 2003). While a few biological investigations have conducted, little is known about the abundance and distribution of zooplankton throughout the Amundsen Sea because it is one of the most remote and least known continental shelf regions of the Southern Ocean (Jones, 1982).

In this study, the primary objective is to investigate spatial/vertical distribution and density of Ice krill in the Amundsen Sea coastal polynya through

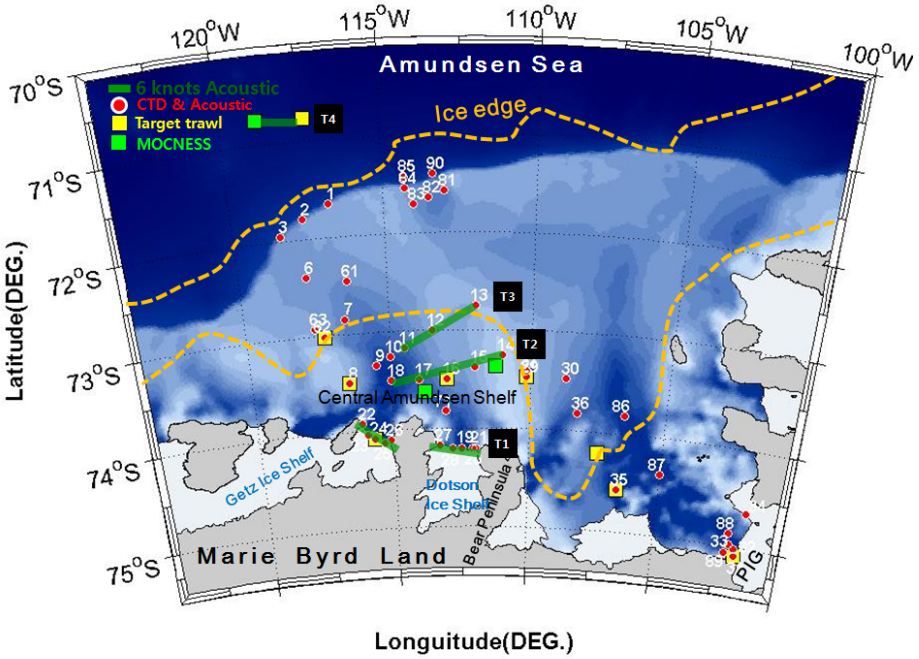

Figure 4.1: Map of the study locations in the Amundsen. CTD stations (close red circles), Net stations (close squares) and transect (A1-A4, green line) were occupied.

hydroacosutic survey which is considered the best approach for estimating the distribution and abundance of ice kill. The MVBS120-38 (Difference of Mean Volume Backscattering Strength between 120 kHz MVBS and 38 kHz MVBS) was used to classify the ice krill from the other organisms such as fish. Additional analysis is to calculate the ice krill density and describe the spatial abundance with each transect at different locations in the coastal polynya. Also, the relationships between ice vertical distribution and environmental variables such as temperature/salinity, phytoplankton, sea-ice distribution and bathymetry will be presented.

Work at sea

Hydroacoustic data were collected using a multi-frequency echo sounder (EK60, Simrad) configured with down-looking 38, 120, and 200 kHz split-beam transducers mounted in the hull of RVIB ARAON. These transducers were calibrated using three standard spheres with each frequency while the ship was stopped at steady station in the sea ice zone. The sea state is very stable and the surface current was not exceeded over 1 knots. During the surveys, acoustic pulses were transmitted with synchronization system, and the pulse duration was 1 ms. Detail echosounder settings are given in Table 4.1. Because of stability of the acoustic data, confined data with ship speed below 6 knots were used. Acoustic surveys were divided into four transects in the Amundsen Sea (Figure 4.1): (1)

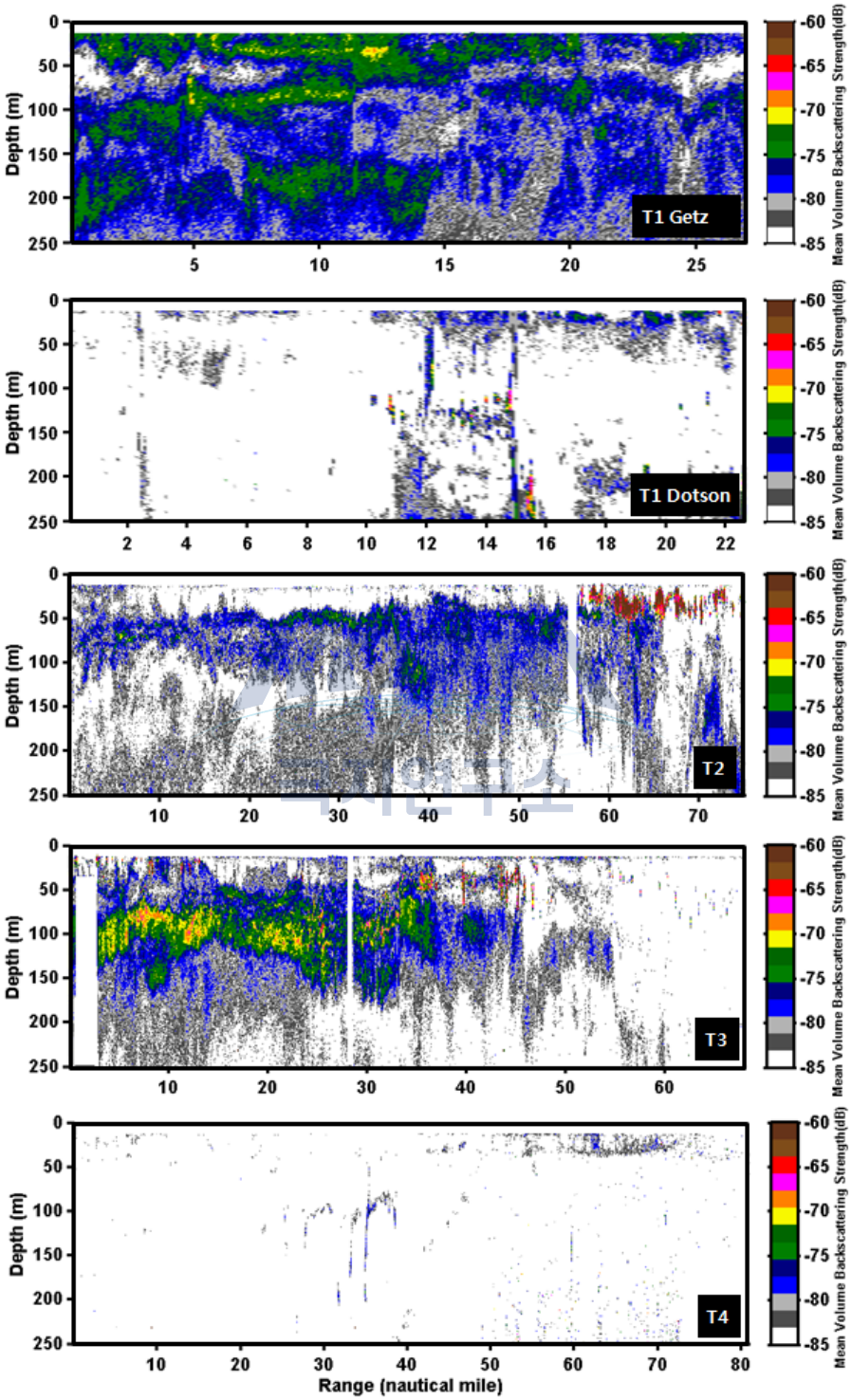

Figure 4.2: Echograms of ice krill MVBS120-38 with each transect, A1-A4.

51 mile near ice shelf (Gets/Dotson) (transect 1); (2) 76 mile in coastal polynya (transect 2); (3) 69 mile in boundary between pack ice and coastal polynya (transect 3); (4) 82 mile off in the open sea (transect 4).

CTD observations were conducted at stations. The temperature and salinity profiles were used to calculate the sound speed and absorption coefficients. MOCNESS and bongo-net target trawl was used to obtain length-frequency distributions of ice krill. The body length was defined as length from the anterior margin of the eye to the tip of the telson without terminal spines. The body lengths of 400 specimens were measured and these length-frequency distributions were used to average the backscattering cross-section All acoustic data sampled with two frequencies (38 and 120 kHz) of the four transects were compressed using virtual echogram technique (Myriax, Echoview software version 4.10). The raw acoustic data were converted to raw volume backscattering strengths (Sv) binned into mean Sv cells with an interval of 0.1 nautical $\cdot$ mile (nmi) horizontal distance and a width of 1 meter depth. In the echo integration processing, the range from the sea surface to a depth of 20 m was not used because of the transducer depth (6-7 m), nearfields, bubble and ice breaking noise.

The ice krill was identified with the difference in the binned mean volume backscattering strengths (MVBS) cells between 120 and 38 kHz. The data were thresholded to -90 dB at both frequencies. The contribution of copepod was negligible because of their low densities and low mean target strength (TS 103 dB for a 2-3 mm long copepod at 120 kHz; Stanton and Chu, 2000). TS was estimated for 17.11 mm long ice krill using a factor based on the simplified, stochastic, distorted-wave, Born-approximation (simplified SDWBA) krill TS model (Conti and Demer, 2006) and is tuned for ice krill assuming constant contrasts g=1.0357, and sound speed contrast h=1.0279, and θ distribution of N (11°, 4°). The conversion factor was computed as the ratio of the ice krill mass and backscattering cross section, each weighted by the ice krill total-length distribution (8-30 mm). The predicted MVBS120-38 distribution from the SDWBA model with θ =N (11°, 4°) was computed for the body krill-length distribution and fell within 12.5–19.4 dB for ice krill.

Preliminary results

High concentrations of Ice krill were found on the coastal polynya (A2), boundary between pack ice and coastal polynya (A3) and Getz ice shelf (A1). In the case of A2 and A3 regions, the strong scattering layer of Ice krill was formed along the whole transect. The main habitat of Ice krill was formed between 50 and 150 m at A3 transect and 50 100 m at A2 transect. Although dense aggregations of ice krill were continuously observed in the coastal polynya (A2 and A3), the maximum MVBS120-38 at A2 was about -65 dB, few Antarctic krill were observed near stations 12 and 14 below 50 m depths. On the contrary, Ice krill patch along the Dotson ice shelf (A1) and open ocean (A4) was shown relatively low strengths than the other transects (Figure 4.2. Specially, in the open ocean (A4) the MVBS120-38 is mainly distributed -85 -80 dB and any distinguishable scattering layer or patch for ice krill wasn't found during transects. In the two ice shelves, Getz and Dotson, MVBS120-38 echograms shows different vertical distribution nevertheless these ice shelves are located closely each other. It can be assumed that these two ice shelf regions have different environmental features

such as water temperature/salinity, dissolved oxygen and phytoplankton, etc. In Getz ice shelf, relatively high MVBS120-38 was observed with -85 -70 dB in whole water depth compared to MVBS120-38 distributions, -80 -75 dB in Dotson ice shelf. Ice krill was distributed whole water column and dense scattering layer was formed between surfaces to 100 m depth in the Getz ice shelf. Along the Dotson ice shelf the ice krill scattering layer was arisen from middle of the shelf (St. 19) to east shelf (St 22). The scattering layer was distributed from surface to 100 m and 200 m bottom.

In general, in the Southern Ocean, E. superba is often dominant among zooplankton abundance and biomass. However, in Amundsen Sea, E. crystallorophias are dominant zooplankton in the ice shelf (A1), coastal polynya (A2) and boundary between pack ice and coastal polynya (A3) while the E. superba and the other zooplankton species such as copepod are scarce. The copepod was major zooplankton in the open ocean (A4). In the nearly future, ice krill density for each transect will be estimated from length-weight relationship with net sampling and volume backscattering strengths data. Simultaneously, the relationships between krill (Ice krill and Antarctic krill) and key environmental variables such as bathymetry, phytoplankton, sea-ice distribution, and temperature/salinity will be described.

Reference

Arrigo, K.R., and van Dijken, G.L., 2003. Phytoplnkton dynamics within 37 Antarctic coastal polynya systems. Journal of Geophysical Research 108: 3271

Conti, S.G., and Demer, D.A. 2006. Improved parameterization of the SDWBA for estimating krill target strength. ICES Journal of Marine Science, 63: 928-935.

Jacobs, S.S., and Comiso, J.C. 1997. A climate anomaly in the Amundsen and Bellingshausen Seas. J. Climate, 10: 697-711.

Jones, A.G.E. 1982. Antarctica Observed. Caedmon of Whitby, Yorkshire, UK. 118 pp.

Stanton, T.K. and Chu, D. 2000. Review and recommendations for the modelling of acoustic scattering by fluid-like elongated zooplankton: euphausiids and copepods. ICES J. Mar. Sci., 57 (4): 793-807.

Chapter 5

Satellite remote sensing

5.1 Calibration/validation of satellite remote sensing ocean color data

Han, Jeong min; Lee, Seung Kyeom

Korea Polar Research Institute, KOPRI

요약문

인공위성을 이용하여 관측한 해색 (ocean color)은 해수 중에 존재하는 유기물 (algal)과 무기물 (non algal) 등의 입자들이 흡광 (absorption)과 산란 (scatter)을 함으로서 나타나는 광스펙트럼의 형태를 경험식을 바탕으로 유추한 chlorophyll-a 의 양이다. 그러나, 해수면 아래에서 일어나는 생물-광 신호의 변화를 인공위성에서 감지하는 데는 여러 가지 해결해야 할 문제가 있다. 특히 극지역의 경우 중위도권에 비해 낮은 태양고도에 의한 해수면 반사도의 특수성과, 현장 검증을 위한 조사를 수행하기 어려운 곳이라는 점 등에 의해 해색 원격탐사 부분에서 해결해야 할 숙제가 많은 곳이다. 이번 아문젠해 조사를 통해 총 34개의 각기 다른 정점(Figure 5.1)에서 수층 별 3개 수심에서 306개의 흡광도, 즉, 식물플랑크톤에 의한 흡광 (aph), 부유물질에 의한 흡광 (ass), 용존유기물에 의한 흡광 (aCDOM)을 측정하였다. 각 흡광의 계수를 계산하기 위해 엽록소 (chlorophyll-a) 농도 및 부유성 입자(suspended sediments; SS)의 농도를 측정하였다. 동시에 수심별 광스펙트럼 변화를 350 800nm 의 스펙트럼에서 측정 가능한 hyper-spectrometer profiler (HPROII, Satlantic inc., Figure 5.3)를 이용해서 관측하였다. 또한, 쇄빙선 아라온호 선수에 장착한 해수면 반사도 측정기 (above water spectro-radiometer, HSAS, Satlantic inc., Figure 5.4)를 이용하여 아라온 항적을 따라 매 15분 마다, 해수면 반사도 (350-800nm) 및 해수면 온도 (Infrared)를 측정하였다.

Objectives

Satellites borne ocean color sensors, such as Sea-viewing Wide Field-of-View Sensor (SeaWiFS), Moderate Resolution Imaging Spectrometer (MODIS), and Medium Resolution Imaging Spectrometer (MERIS), can provide synoptic global-scale observation of the oceanic phytoplankton. However, high latitude oceans, e.g. Amundsen Sea, have not been studied in as much detailed as temperature

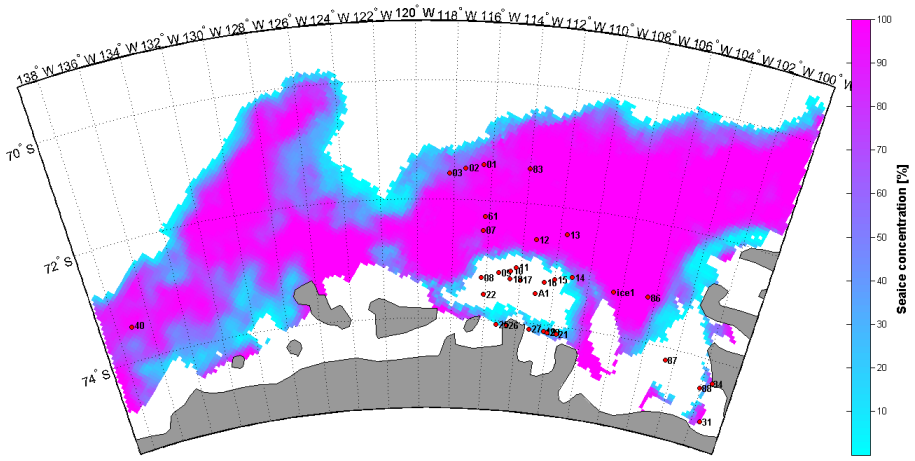

Figure 5.1: Station Map of Remote sensing CAL/VAL data sampled

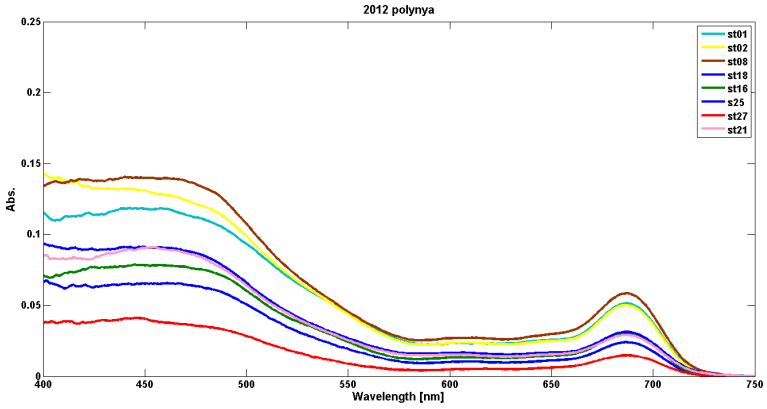

Figure 5.2: Examples of total pigments absorbance (before processing)

or tropical oceans, due to location and cold environment which are not easy to assess. Hence, through Amundsen Sea expedition, we try to get bio-optical relationship to improve ocean color data quality by observing 1) inherent optical properties (IOPs) of water such as absorption by phytoplankton, suspended sediment, and dissolved organic meters, and 2) apparent optical properties (AOPs) of water such as downward irradiances (Ed) and upwelling radiance (Lu) over spectrum range of 350-800nm.

Work at sea

With hydrographic survey, such as CTD/Rosette, we sampled 306 waters at 34 stations (Figure 5.1) with 3 depths of surface, subsurface chlorophyll maximum depth (SCM), and bottom euphotic depth (see below station map). To measure inherent optical properties (IOPs) of water, seawater volumes of 500 ml were filtered on 25 mm glass-fiber filters (Whatman GF/F). For absorption by CDOM, seawater volumes of 50 ml were filtered onto disposable syringe filter unit of Advantec (cellulose acetate 0.45 μm). Optical densities of total particulate matters were measured directly on the wet filters by methods of Truper and Yentch (1967) with a double-beam recording spectroradiometer of Simatsu UV1800 in spectral range 350-900nm (spectrum resolution was 0.5nm) the filter was placed in front of a diffusing windows adjacent to an end-on photomultiplier of large surface area. For a reference blank and baseline variations, an unused wetted filter was taken as were automatically corrected. After the measurement of optical density of total pigments, the spectral absorption by nonalgal material was measured separately with method of Kishino et al.(1985). The filter was placed in absolute methanol for 1 1.5 hr in order to extract pigments. For the measuring of apparent optical properties (AOPs) of water, we deployed hyper-spectroradiometer of Satlantic Inc. (HPRO II, Figure 5.3), which is free-fall type (0.5m per second) with 350-800nm of downward irradiance (Ed) and upwelling radiance (Lu). For reference as ambient irradiance variation, downward irradiance (Es) was measured on deck, where is no shaded place of R/V ARAON. At the same time, through whole expedition we observed above water reflectance every 15 minutes by using 'Above water spectroradiometer of Satlantic Inc.(HyperSAS, Figure 5.4)', mounted on a head of vessel to continuous monitoring of ocean color along the ship's track. This data will be used to calibration/validation currently operated remote sensed ocean color data.

References

Truper, H. G. and C.S. Yentsch, 1967. Use of glass fiber filters for the rapid preparation of in vivo absorption spectra of photosynthetic bacteria. J. Bact.94, 1255-1256.

Kishino, M., N. Okami, M. Takahashi, and S. Ichimura, 1986. Light utilization efficiency and quantum yield of phytoplankton in a thermally stratified sea. Limnol. Oceangr., 31, 557-566.

Figure 5.3: Hyper-spectroradiometer profiler (HPRO II, Satlantic Inc.,right figure) deployed in water(left figure).

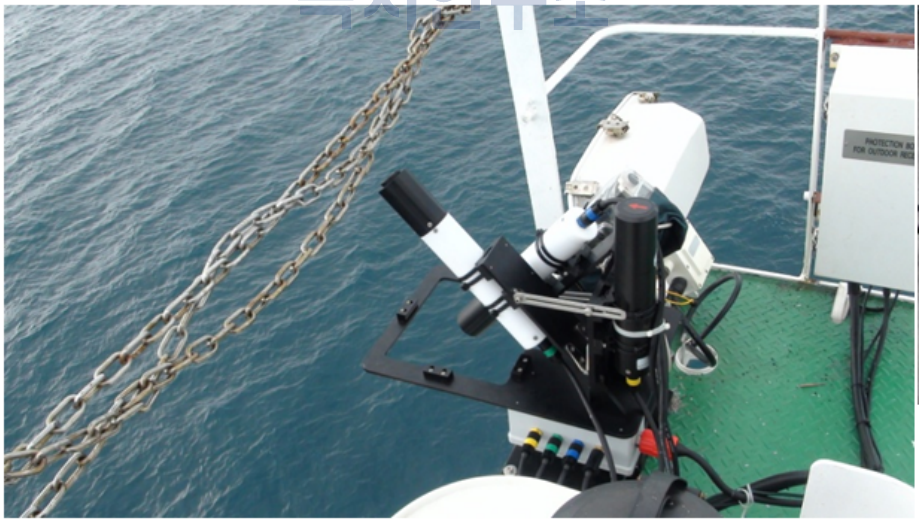

Figure 5.4: Above hyper-spectroradiometer with infrared temperature sensor (HyperSAS, Satlantic Inc.), this is mounted on Ship's head.

5.2 High Resolution Airborne Synthetic Aperture Radar

Kim, Jin-Woo; Kim, Seung Hee
Seoul National University, Korea

요약문

고해상도 Airborne 합성개구레이다를 이용하여 Thwaites Ice Tongue 와 B-22A 빙하의 표면 이미지를 획득하였다. 이미지 보정과 추후 얼음의 이동 추적을 위하여 Corner Reflector를 5군데 설치하였다. 위경도 보정은 보조 GPS 데이터를 이용 하였으며 GoPRO 비디오 장비를 이용하여 SAR 영상과 비교할 수 있는 현장 사진 자료를 획득하였다.

Introduction

Physical phenomenon and properties of ice, such as thinning, retreating and calving, in the Polar Regions are known to effectively infer climate changes. Especially, two biggest outlet glaciers located in the Amundsen Sea in West Antarctica are on a hot plate among the science societies due to their fast and vast responses (Jenkins et al. 2010; Joughin et al. 2011; Rignot 2006). However, the remoteness and extreme weather conditions, especially during the winter season, prevent extensive field surveys over the region. Thus, the remote sensing using satellites is regarded as one of the best useful techniques that can overcome those obstacles.

Numerous researches using various satellites already had been carried out in the Amundsen Sea. Particularly, Synthetic Aperture Radar is a competitive instrument in remote sensing because, unlike other passive satellites which use optical sensors, it uses microwave with which the influence of the atmosphere is insignificant and has an ability to penetrate snow. For example, Rignot et al. (2001, 2002) presented the evidence of the acceleration of Pine Island Glacier and Thwaites Glacier using one of SAR techniques, called Interferometry. Besides, SAR can be used diversely in other purposes.

In this study, High Resolution Airborne SAR sensors are used to monitor the surface of Thwaites Glacier in a sense of a complement to the spaceborne SAR data, which have a limited resolution. Also, for the purposes of reference and calibration, corner reflectors are installed over the surveyed area.

Study Area

Thwaite Glacier is located at about 75°S and between 105°W and 110°W. It has been known from the previous researches that the average flow velocity at the terminus is approximately 3.4 km/year, while the grounded part moves 1.0 km/year slower (Rignot et al. 2001). Acceleration of the flow velocity and widening had also been reported from numerous recent papers. Besides, several calving events were observed and the latest calving is recorded in 2002, which created an iceberg B-22. In 2011, we discovered a possible crack on Thwaites Glacier near the grounding line using Full-Polarimetric Synthetic Aperture Rada. Although the evidence was not enough to convince the complete breakup, the possibility of calving was well proposed.

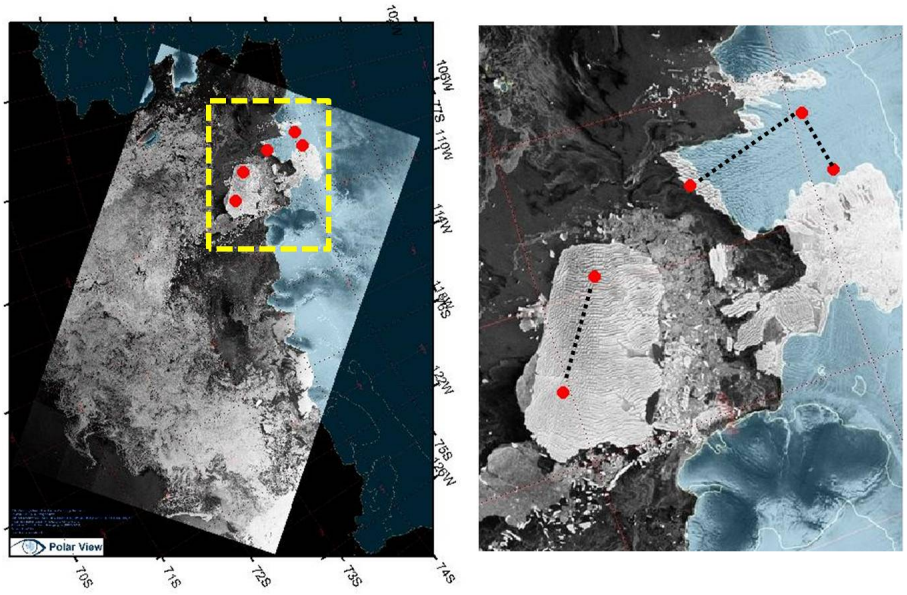

Figure 5.5: Envisat ASAR image on March 3, 2012 provided by Polarview. Red circles indicate the locations of the corner reflectors. Black dots indicate the flight path of the airborne SAR measurements.

Iceberg B-22A is the remaining of B-22 which was calved off from Thwaites Glacier in 2002. According to the satellite images, the iceberg has not moved for 10 years after the calving, probably due to the ridge under the ice. Its current size is approximately 70km by 40km.

Proposed Operations

1) Installations of Corner Reflectors

Main objectives of installations of corner reflectors are to have reference points on the SAR image and to use the backscattered radar signal for calibration of the airborne SAR images. A corner reflector is composed of three right triangles made of aluminum and is designed so that each installation would take the minimum time considering the possible rapid transition of weather conditions (Fig 5.6a).

2) High Resolution Airborne Synthetic Aperture Radar

A portable Synthetic Aperture Radar, called NanoSAR and manufactured by ImSAR in USA, operates at X-band and has the maximum resolution of 0.30m. The radar is mounted on the left lever of the helicopter and a GPS is placed on the dashboard inside for the best view of the sky (Fig 5.6b). A video recorder is also placed next to the radar so that the SAR images can be compared for further analysis.

Results

A total of 5 corner reflectors are installed on Thwaites Glacier and B-22A Iceberg on February 26, 2012. The coordinates of the installations are overlaid on Envisat

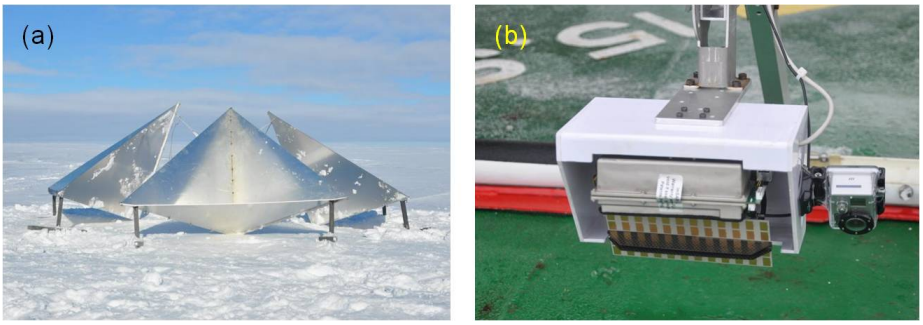

Figure 5.6: (a) Installed corner reflector (b) Airborne SAR sensors, NanoSAR A.

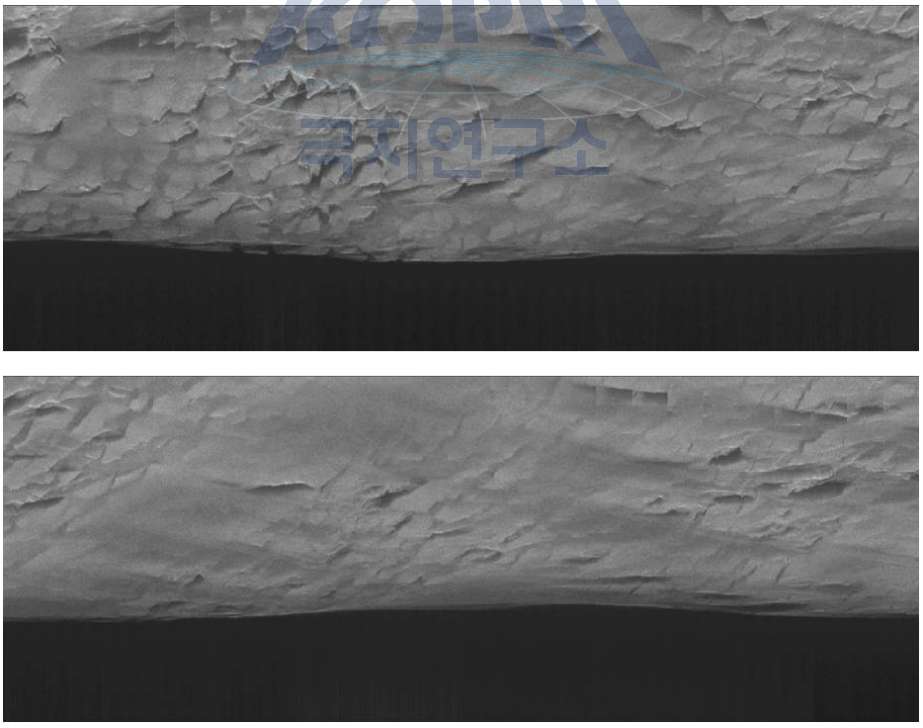

Figure 5.7: High Resolution Airborne SAR images on Thwaites Glacier.

ASAR image which was acquired a week after the installations of the corner reflectors (Fig 5.5). Airborne SAR acquisition was carried out for approximately 2 hours after the installations were completed. Figure 5.7 displays the obtained SAR images and various interesting features are presented in the images. The comparison and analysis of these features will be conducted with the obtained GoPRO images afterwards.

References

Jenkins, A., Dutrieux, P., Jacobs, S.S., McPhail, S.D., Perrett, J.R., Webb, A.T. and White, D., (2010) Observations beneath Pine Island Glacier in West Antarctica and implications for its retreat. Nature Geoscience, 3, 468-472.

Joughin I and Alley R. B., (2011) Stability of the West Antarctic Ice Sheet in a Warming World. Nature Geoscience, 4, 506-513

Rignot, E. (2001), Evidence for rapid retreat and mass loss of Thwaites Glacier, West Antarctica, J. Glaciol., 47, 213–.222.

Rignot, E., D. Vaughan, M. Schmeltz, T. Dupont, and D. MacAyeal (2002), Acceleration of Pine Island and Thwaites Glaciers, West Antarctica, Ann. Glaciol., 34, 189–.194.

Rignot, E. (2006), Changes in Ice Dynamics and Mass Balance of the Antarctic Ice Sheet, Phil. Trans. R. Soc, A 2006 364, 1637-1655

Chapter 6

Activity related with atmospheric research and snow chemistry

6.1 Maintenance of automatic weather stations

Choi, Taejin[1] (Meteorology)/Park, Ha Dong[1] (Safety guard) Haam, Suk Hyun[2] (Engineer)
[1]Korea Polar Research Institute, Korea
[2]Neo-Sea Tech

요약문

서남극 연안 지역 기상 및 기후변화 이해를 위한 실측 자료 획득을 위해 세 지역에 자동기상측정 시스템(AWS)이 운영 중이다. 첫 번째 AWS는 2008년 아문젠 해의 린지 섬(Lindsey Island, 73° 36‘ 4.32“ S/ 103° 01’ 15.18” W)에 설치되었으며, 두 번째 AWS는 2010년 Marie Byrd Land의 Cape Burks(S 74°45.596’, W 136°48.604´)에 설치되었다. 끝으로 세 번째 AWS는 2011년 아문젠 해 Bear Peninsula의 Moore Dome(74°21’45.56" S, 111°22’13.77" W)에 설치되어 운영 중이다. 본 연구 항해 기간에는 이 세 곳을 방문하여 AWS 보수 및 자료 백업, 그리고 Moore Dome 에 에디 공분산 플럭스 시스템을 설치하는 것이다. 2월 17일 19일 무어 돔을 방문하였다. 2011년 설치했던 AWS를 찾을 수 없었으며, GPR 탐사 결과 표면으로부터 약 1.5 3 m 깊이에 묻힌 것으로 나타났다. 에디 공분산 플럭스 시스템을 설치하였으나 이곳의 많은 적설량을 감안하여 약 하루 정도 운영하여 지표 에너지 플럭스 성분들을 측정 후 철수 하였다. 두 번째로, 2월 27일 – 28일 린지 섬에서 AWS 보완 및 지표 에너지 플럭스 시스템을 설치하였다. AWS의 경우 풍향 풍속계 및 온습도계, 기압계를 교체하였으며, 적설 관측은 종료하였다. AWS로부터 약 1 km 남쪽에 Moore Dome에 설치하려 했던 에디 공분산 플럭스 시스템을 설치하여, 린지 섬 주변 바다와 대기 간의 열 에너지 교환을 측정하도록 하였다. 마지막으로 3월 11일 케이프 벅스를 약 1시간 동안 방문하였다. AWS와 영상 촬영 장치는 모두 쓰러져 있었다. 아라온이 위치한 곳과는 달리 강한 바람이 불어 장 시간 체류할 수 없는 관계로 자료 및 주요 측기만을 회수하여 철수하였다.

Objectives

To better understand the atmospheric forcing on the climate process on West Antarctica based on in situ measurements, three automatic weather stations have been operated at Lindsey Island, Amundsen Sea (73° 36' 4.32" S/ 103° 01' 15.18" W), Moore Dome, Bear Peninsula, Amundsen Sea (74°21'45.56" S, 111°22'13.77" W), and Cape Burks, Marie Byrd Land. The objective during ANA02C are to maintain the AWSs and to setup eddy covariance flux system at Moore Dome to understand the energy exchanges between the atmosphere and the glaciated surface in high altitude area.

Work at three AWS sites and preliminary results

1) Moore Dome

Five people including glaciologist visited the Moore Dome site from 17 to 19 in February. The objectives at the Moore Dome were to complement the AWS established in 2011 and to set up eddy covariance flux system to study the interaction between the atmosphere and snow-covered area. The Ice-breaking research vessel, ARAON stopped near the ice shelf of the Bear Peninsula. Two helicopters (AS350) were used to transport researchers and cargo. When we were over the site, we could not find the AWS which had been setup in 2011. After landing and a meeting, we decided to do as planned first, not to spend time to search it. After base camp was set up, eddy covariance flux system was setup 5 m away from the base camp to the north. In the meanwhile, three people worked for snow-pit sample. Later, ground penetrating radar (GPR) was used to figure out the structure of the glaciated area and to find out the AWS. When GPR was near the AWS location coordinate twice, it showed two pronounced signals, different from ones at the other survey area. Based on the rough calculation, the AWS was turned out to be buried 1.5 3 m below the surface. Since the height of the AWS was 2.87 m and the AWS data logging system was put near the surface in 2011, we decided not to withdraw it due to limited time and not-favored weather forecast. Eddy covariance system was operated for one day, concerning heavy snow next one or two years. To measure turbulent fluxes of sensible heat and latent heat, a 3-D sonic anemometer (CSAT3, Campbell Scientific. Inc.) and a krypton hygrometer (KH20, Campbell Scientific. Inc.) were used. For surface radiation budget measurement, a net radiometer (CNR4, Kipp & Zonnen) was installed. Raw data and 30-min. statistics data was recorded on a data logger (CR3000 Campbell Scientific. Inc.). Measurement height of eddy covariance system was 3.7 m above the surface. The sensor separation between the sonic anemometer and the krypton hygrometer was 0.2 m. The eddy covariance system faced west and net radiometer was set up in the direction of north. To measure heat transport into or out of the snow surface, heat flux plates were installed at a depth of 0.05 and 0.1 m. Snow temperature was measured at a depth of 0.025 and 0.075 m. Based on the measurements 100 m away from the flux tower, the snow density was about 350 kgm^{-3} near the surface. The weather was fine and wind blew from the northwest. Based on the half-hourly values, the sonic temperature was in the range of -3.5 - -8 ℃. In the meanwhile the snow temperature at a depth of 0.25 cm ranged from -6.3 - -17.1 ℃. Downward shortwave radiation increased up to 538 Wm^{-2} with a albedo of 0.66. The resultant net radiation changed from -40 to 80 Wm^{-2}(Fig. 6.1). The calculation

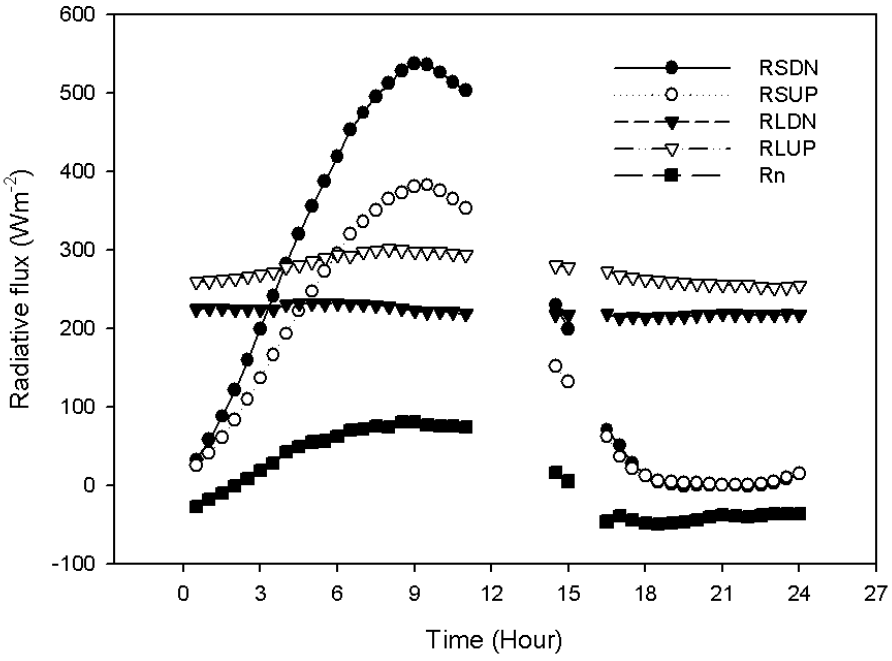

Figure 6.1: Diel variations of radiative energy flux components at Moore Dome on Feb. 18, 2012

of fluxes of latent and sensible heat and heat into or out of the surface will be made later to quantify the energy partitioning at the snow-covered area with a altitude of $>$ 700 m on West Antarctica coast area.

2) Lindsey Island

Five people visited the AWS site at Lindsey Island from 27 to 28 in February. The AWS worked well except for two wind anemometers and a snow accumulation sensor. Wind anemometers were replaced with new ones (05130, R.M. Young) and the snow accumulation sensor was removed. Two temperature/humidity probes (HMT335, Vaisala) and a barometer (PTB100, Vaisala) were also replaced with new temperature/humidity probes (HMP155, Vaisala) and a barometer (PTB110, Vaisala). Two replaced temperature/humidity probes and one barometer were compared with another temperature/humidity probe (HMP155) and barometer (PTB110) at ARAON later. Hourly-averaged AWS data from July of 2008 to March of 2012 was retrieved at the site.

Eddy covariance flux system was installed on a rock (73° 36' 36.6" S, 103° 02'13.2"W) $>$ 1 km away from the AWS to the south (Fig. 6.2). It was $>$ 1 km away from the Canesteo Peninsula where most of wind comes based on the last three-year AWS data. For the measurements of turbulent fluxes of sensible and latent heat, a 3-D sonic anemometer (CSAT3, Campbell Scientific. Inc.) and a krypton hygrometer (KH20, Campbell Scientific. Inc.) were used. For surface radiation measurement, a net radiometer (CNR4, Kipp & Zonne) was installed. Raw data and 30-min. statistics data was recorded on a data logger (CR3000 Campbell Scientific. Inc.). While the radiometer is supposed to be operated

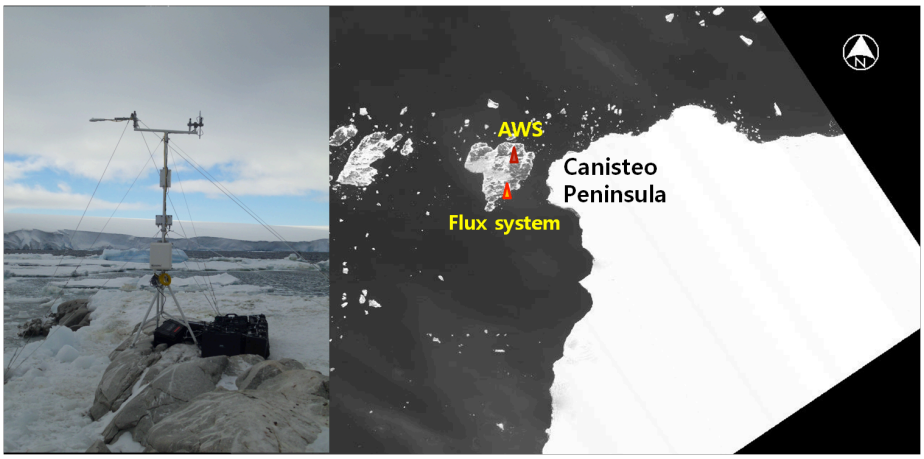

Figure 6.2: The eddy covariance flux system set up on February 27-28, 2012 (left) and its location at Lindsey Island, Anumdsen sea (right)

continuously, eddy covariance system was set to be operated from November to March due to power limit. While turbulent raw data can be recorded about 89 days, 30-min. statistics data can be stored over 1000 days. Recorded data are not overwritten. Total power of1800 Ahr (two 300-Ahr lithium batteries and 12 100-Ahr rechargeable batteries) was available with a solar panel of 30 W for the system. Measurement height of eddy covariance system was 3.7 m above the surface and 5.7 m above the sea surface. The sensor separation between the sonic anemometer and the krypton hygrometer was 0.2 m. The eddy covariance system faced east and net radiometer was set up in the direction of north.

Based on the last four years data retrieved at the site, wind from the east was dominant. Wind speed was stronger in winter with a maximum of 40 ms-1. Air temperature decreased down to -35 ℃ in winter and was above zero ($<$ 4 ℃) in summer.

3) Cape Burks Three people visited the AWS site at Cape Burks, Marie Byrd Land on March 11. Due to sea ice, Araon stopped about 60 miles away from Cape Burks. It was very windy and cloudy at the site. The 5-m AWS as well as two cameras on the 1-m vertical bar have fallen down. Two anemometers, two temperature/humidity probes and a snow accumulation sensor were broken. Due to bad weather at the site, some equipment such as a net radiometer were withdrawn and brought to Araon. Based on the data, the AWS has fallen down on October of 2010.

6.2 On-board measurements

Choi, Taejin
Korea Polar Research Institute, Korea

요약문

ANA02C 연구 항해 현장에서의 기초적인 기상 현상 이해를 위해 쇄빙연구선 아라온에서 기상요소들이 측정되었다. 측정된 요소들은 상대 풍향 및 풍속, 기

온/습도, 기압, 태양 복사이다. 상대 풍향 및 풍속은 쇄빙연구선의 이동 속도 및 방향을 고려하여 교정되었다. 한편, 대기와 해양 간의 교환 작용 연구를 위해 에디 공분산 시스템이 선수 마스트에 설치되었다. 쇄빙연구선의 움직임이 에디 공분산 관측에 미치는 영향을 제거하기 위해 세 축 방향의 가속도와 각 회전율을 측정하는 모션 센서가 설치되었다. 에디 공분산 자료와 동시 측정된 모션 자료를 이용하여 일부 자료에 대한 분석이 이루어졌으며, 발견된 문제점에 근거하여 향후 추가 분석될 예정이다.

Objectives

One of the objectives of the on board measurement is to manage AWS to provide researchers with meteorological variables, which is needed to understand the atmospheric condition during ANA02C. The second one is to measure turbulent fluxes of energy and CO_2 to better understand the interaction between the atmosphere and the sea using eddy covariance flux system set up on the foremast.

Work at sea and preliminary results

Before the Ice-breaking research vessel, Araon, left Korea for Antarctica, some meteorological instruments had been checked or others had been replaced with brand new ones. An eddy covariance flux system was setup on February 12, 2012 during the cruse. Open-path CO_2/H_2O gas analyzer (LI7500, Licor) was zero- and span- calibrated using dew point generator (LI610, Licor) for H_2O and CO_2 standard gas for CO_2. After the cruse it was calibrated again. To remove the effect of ship motion on turbulent flux, motion sensor (MotionPak II, Systron Donner) were attached near the eddy covariance system. For easy comparison of roll and pitch, a commercially available clinometer (DAS) were attached on the top of the motion sensor. When eddy covariance system was operated and connected to a data logger (CR3000, Campbell Scientific Inc.), a anemometer ((05130, R.M. Young) using pulse channel for wind speed measurement were connected to a independent logger (CR1000 or CR200, Campbell Scientific Inc.) powered by 12VDC gel-type battery. While turbulence data were recorded on a PC through automatically, wind data from the anemometer were retrieved manually. After the cruse, eddy covariance system was removed and the propeller type anemometer was connected to CR3000 data logger, again. Sampling rate for flux measurement was 10 Hz. The distance between the 3-D Sonic anemometer (CSAT3, Campbell Scientific Inc.) and motion sensor was 0.87 m and the sensor separation between the sonic anemometer and the open-path gas analyzer was 016 m.

During the cruse, apparent wind speed and direction from the anemometer (05130, R.M. Young) on the foremast were corrected to get true wind speed and wind direction using ship speed and compared with wind data from 2-D sonic anemometer on the radarmast for the cruse. For the correction of flux data, algorithm from Miller et al. (2008) was used. To examine whether the correction is valid, roll and pitch angles from two motion sensors of 1) MotionPak and 2) motion sensor built in the Araon, and 3) the clinometer were compared as the first step. The variation of roll was consistent with each other with different absolute magnitude. This may be due to the different location among motion sensors. In the meanwhile, pitch from the MotionPak shows showed more fluctu-

Table 6.1: The summary of half-hourly meteorological data during the cruise.

Variables	Mean	Maximum	Minimum
Wind speed (ms^{-1})	6.5	20.1	0
Air temperature (^{o}C)	-4.9	-0.2	-16.1
Air pressure (kPa)	98.6	100.7	94.9
Solar radiation (Wm^{-2})	92	518	0

ation than that from ship motion sensor. That is likely due to a vibration of the arm supporting eddy covariance system and the MotionPak. Case study with ship translation speed will be done and to quantify turbulent fluxes of energy and CO_2 between the atmosphere and the sea during the cruise.

Based on the preliminary results during the cruse, wind speed, air temperature, relative humidity, air pressure and solar radiation on half-hourly basis were summarized in Table 6.1.

Due to the late visit to Amundsen sea from mid February to mid March in 2012, it was colder and the solar radiation was smaller than those during ANA01C (late December to mid January). In the meanwhile, air pressure and wind speed were similar except for strong wind up to 20 ms^{-1} during ANA02C. For wind direction, wind from northwest to northeast was dominant (60%), likely due to the low pressure systems coming from the north.

6.3 Evaluation of suitability of shallow ice coring site at the seashore of West Antarctica

Hong, Sangbum[1] (Glaciology)/Choi, Taejin[1] (Meteorology)/Park, Ha Dong[1] (Safety guard)/Kim, Hyungjoon[1] (Assistant) Haam, Suk Hyun[2] (Engineer)
[1]Korea Polar Research Institute, Korea
[2]Neo-Sea Tech

요약문

Southern Annular Mode (SAM)은 남극 대륙의 기후변화에 중요한 역할을 하는 대규모 대기순환으로 남극 기후변화의 원인을 이해하고 예측하기 위해서는 SAM의 변동성을 이해하는 것이 매우 중요하다. 본 연구에서는 과거 200년 동안의 SAM 구성 요소 (강수량, 대기순환 등)의 기록을 복원하기 위해 Amundsen Sea Low (ASL) 세기변화에 민감하게 영향을 받는 서남극 해안 돔 지역의 강수량과 지구물리 탐사 등을 수행하였다. 이를 위해 2012년 2월17-19일에 Bear Peninsula Moore Dome빙하의 두께, 내부구조, 그리고 기저지형을 조사하기 위하여 GPR (ground penetration radar) 조사를 수행하였다. 빙하의 두께와 내부구조의 경우 GPR 측정자료를 통해 깊이가 300 m 이상임을 확인하였으며 내부구조는 비교적 안정적으로 보존 된 것으로 나타났다. Moore Dome 정상부근의 눈 표면에 형성된 Sastrugi특징을 고려할 때 시추 후보지의 주풍은 북서풍으로 판단되었다. 돔 지역의 적설량 (accumulation rate)과 계절별 눈 화학

특징을 조사하기 위해 2.5m 깊이의 눈 시료를 채취하였다. 밀도 측정 결과 표층에서 1m 깊이까지 300 400 kg/m^{3}의 밀도 변화를 보였으며 1-2.5m 깊이에서는 400-450 kg/m^{3}로 거의 일정한 수준으로 나타났다. 온도의 경우 2차례 측정한 결과 최고 온도가 -6℃ 미만으로 나타나 조사기간 동안에 눈층의 용융현상이 발생하지 않을 것으로 조사되었다. 그리고 눈층에서 측정된2차례 측정 기간 동안의 온도 차와 온도변화와 밀도변화와의 관계를 고려할 때 눈층의 공기와 눈표면 대기간의 상호 순환이 반영된 것으로 판단되었다. 향후 채취한 눈시료의 프록시 자료 (수분동위원소, 이온성분, 원소 성분 등)를 추가로 측정하여 프록시 자료의 보존 특성을 조사하고 강수량 추정과 강하 시점의 대기환경 특성을 연구할 예정이다. 마지막으로 Moore dome의 적설량을 2.5m year^{-1}, 빙하의 두께를 600m로 가정하여 과거 200년 동안의 고기후 기록을 복원하기 위해 시추해야 할 빙하의 깊이를 Ice Flow 모델링을 통해 추정해 보았다. 이를 위해 2가지 방법이 사용되었고 상부에서 Firn층까지의 densification과정과 이후 얼음이 형성된 이후에는 Ice Flow-induced 과정을 혼합한 첫번째 방법과 전체 깊이에 대해 Ice Flow-induced 과정을 적용한 두번째 방법을 통해 추정하고 모의 결과를 서로 비교하였다. 연구 결과 Bear Peninsula Moore Dome지역에서 과거 200년 동안 (1800-2000)의 고기후 기록을 복원하기 위해서는 150-190 m의 천부 빙하 시추가 필요한 것으로 나타났다.

Objectives

It has been known that the Southern Annular Mode (SAM), which is the large scale circulation of atmosphere in the Southern Hemisphere, contribute much to the climate change of the Antarctica and the variability of the SAM is closely related with the strength of westerly winds around the Antarctica and thus can sensitively affect on the variability of Amundsen Sea Low (ASL). However, up to date, there have been few researches to identify the natural variability of the SAM before industrial revolution in the past even though it may be critical to understand its variability in the present and future. This is the main driving factor to start the shallow ice coring program on the seashore of West Antarctica and the final goal is to reconstruct the major components of SAM (atmospheric circulation, temperature, mean sea level pressure, and so on) in the past (especially before industrial revolution, spanning the last 200 years) using ice core. As a preliminary study, the objective of 2012 Amundsen Expedition is to evaluate the suitability of shallow ice coring site of Moore Dome in the bear peninsula at the seashore of West Antarctica as the archive of the variability of ASL in the past and, as an important factor of evaluation, the ice thickness, accumulation rate, the possibility of surface melting of snow layer at the top of Moore Dome were investigated.

Experimental

On the 17-19th February 2012, snow pit works and a glaciological survey were performed at a site (74° 21′ 45.6″ S, 111° 20′ 54.0″ W) near the top of Moore Dome in Bear Peninsula. A continuous series of 40 and 50 snow samples for the determination of ionic species, water stable isotopes, and elements from a 250 cm deep snow pit were collected at the upwind site, which is located about 150m to the east from the camping tent. Great precautions were taken in the field to prevent the possibility of snow contamination. The temperature was measured every 10cm with temperature probe and the snow density samples were collected

by 5 × 5cm stainless steel cutter with a sample resolution of 5cm. GPR survey were conducted in detail using Mala ProEX system with RTA 50 MHz antenna. It started at the camping tent to the South and ended at a site with a length of 1.5 km and was conducted once again while the operator went back to the camping tent with an interval of 3m.

Preliminary Result and Discussion

Ground Penetration Radar survey

The ice thickness and infrastructure of glacier at the summit of Moore Dome were measured by GPR survey (Fig. 6.3). The depth section suggested that the glacier was deeper than 300 m and the material of subsurface was relatively homogeneous in the most survey route. However, the bedrock topography and total ice depth were not able to be measured due to the measurement range of system. Fig. 6.3b showed very distinct reflection signal of discrete object which was estimated as Automatic Weather System installed in the 2010/2011 expedition.

The snow surface roughness (Sastrugi) at the Moore Dome The wind driven process has been known to form Sastrugi, which can lead to mixing of layers and mixing of the atmospheric signal. Figure 6.4 indicated the Sastrugi formed at the summit of Moore Dome. The site was characterized by a Sastrugi of roughly 5-10cm height, which might be negligible to the interpretation of proxy data due to high accumulation rate of Dome site. And it was estimated that the prevailing wind direction was mainly north westerly through the type of wind ridge. And this also suggested that ASL usually influenced this area and snow frequently falled down while it moved from AS to main land of West Antarctica.

Snow pit works Figure 6.5 showed field activities of snow sampling and Fig. 6.6 indicated the variations of temperature and density according to the depth. It has been known that the snow deposited in the accumulation area of a glacier or an ice sheet is compressed under the weight of subsequently fallen snow layers. In this study, the snow density rapidly changed in the range of 300-400 kg/m^3 from the surface to the depth of 1m and then constantly maintained at the level of 400-450 kg/m^3. The temperature of snow layer suggested that the occurrence of meltwater formation could be excluded with this relatively low temperature ($<$ -6℃) during the period of snowpit works. And the difference of temperature variations to the depth of snow layer during 1st and 2nd measurement periods might be attributed to the mixing between air above the surface snow layer and interstial air in the sub-snow layer. As a further study, the ionic species, water stable isotope ratios, and elements will be determined in order to investigate their conservation characteristics, the relationship between age and depth, and annual accumulation rate.

Estimated ice coring depth to reconstruct proxy records spanning the last 200 years at Moore Dome

Figure 6.7 indicated the estimated ice coring depth using the density variation of NEEM site in Greenland. The ice thickness and accumulation rate of ice coring site are needed to estimate the age-depth relationship through the simulation of the ice flow modeling. In this study, we assumed that the accumulation rate and ice thickness is 250cm yr^{-1} and 600m, respectively. The age-depth profile was calculated using the two methods. The 1st method was to estimate it using the combination of densification process of snow/firn in the

(Hong 1-a)

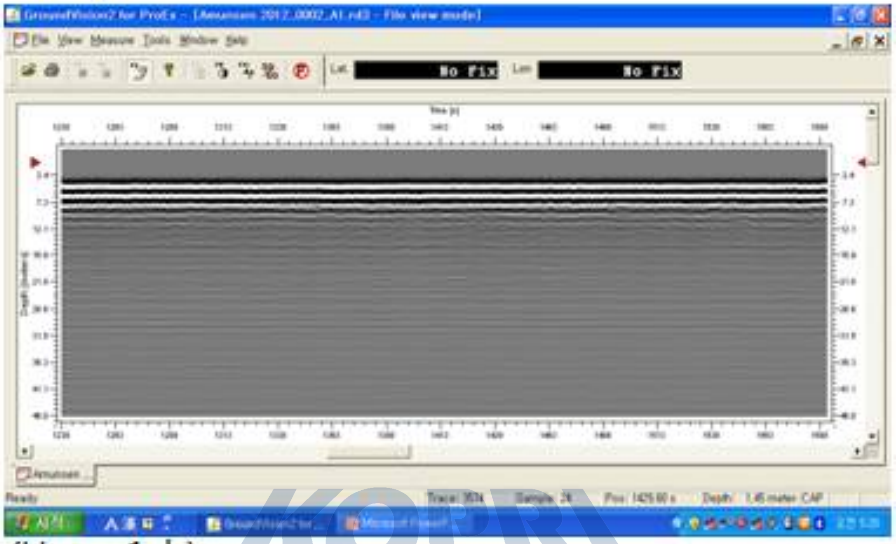

(Hong 1-b)

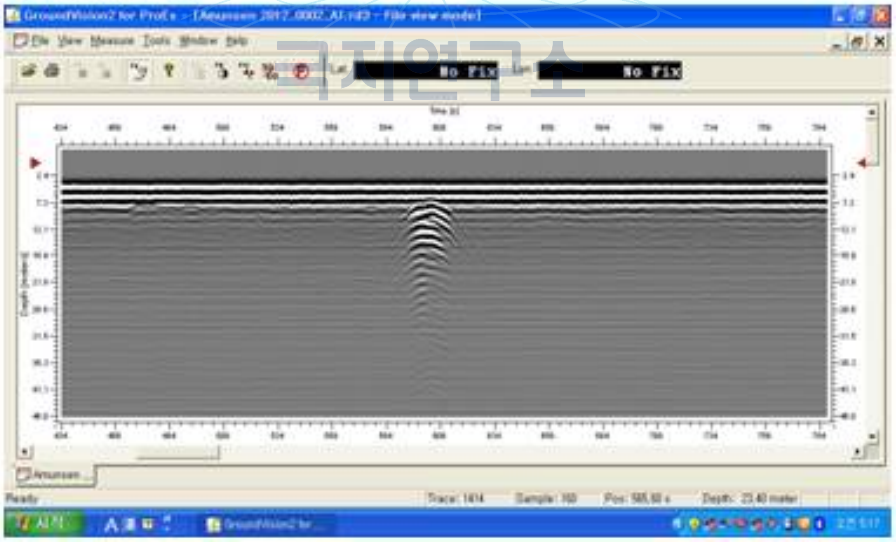

Figure 6.3: Profiles of GPR survey (Fig. Hong 1-a: general profile, Hong 1-b: profile showing "hyperbolic" reflection, appearing as an inverted U, typically associated with discrete object)

Figure 6.4: Sastrugi and wind direction at the top of Moore Dome

Figure 6.5: Field activities of snow sampling at the top of Moore Dome

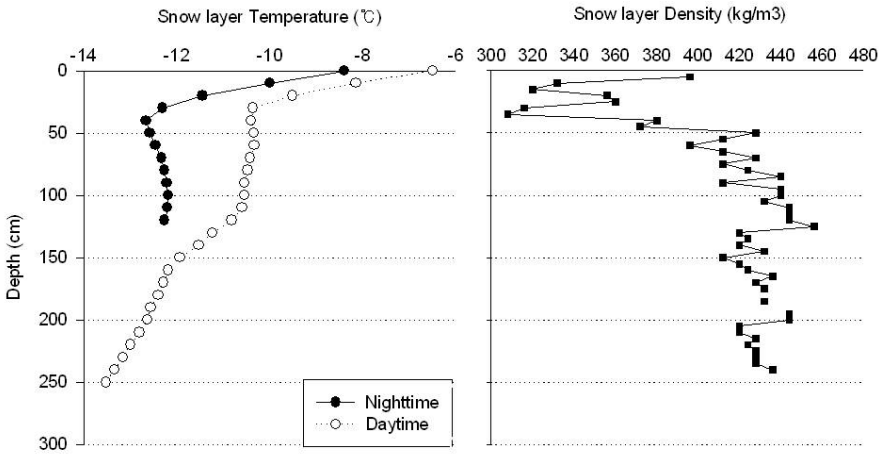

Figure 6.6: The variations of snow layer temperature and density

near surface layer and flow-induced thinning of the ice layer in the glacier. The 2nd method was to assume the flow-induced thinning process for totally thin glacier even before the transformation of firn to ice is completed. The simulation results indicated that the shallow ice coring with the depth of 150-190m might be needed in order to reconstruct the proxy records spanning the last 200 years.

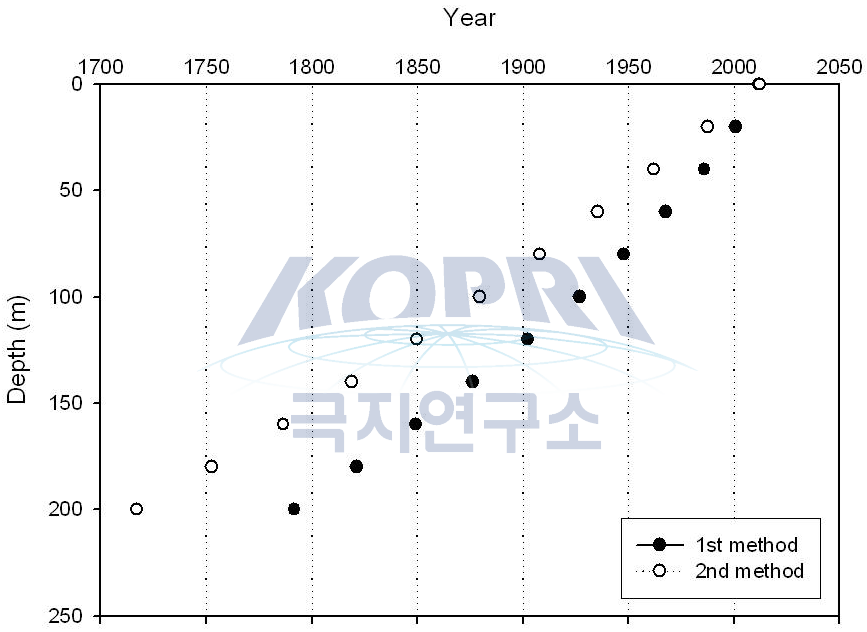

Figure 6.7: Estimated ice coring depth calculated steady state ice modeling

Chapter 7

Multibeam and sediment core

7.1 Multibeam survey

Kim, Hyoung-Jun1
Korea Polar Research Institute, Korea

요약문

다중빔 음향측심기 (MBES, Multi-Beam Echo Sounder)는 일정한 음파각을 가지는 수십 수백개의 빔을 발사하여 음파 (acoustic wave)가 수층 (water column)을 통해 해저면에 반사되어 각각의 수신기에 도달하는 시간을 계산하여 수심을 정확하게 파악할 수 있는 방법이다. 아라온호에 장착되어 있는 다중빔 음향측심기를 이용하여 남극 아문젠 해역의 상세한 해저지형을 획득하였다.

The Multi-Beam Echo Sounder (MBES)

Seafloor topography could be changed from water depths, sediment types or minerals which distributes in the seafloor. To survey the seafloor, geophysical method using the acoustic wave is frequently used.

Multi-Beam Echo Sounder (MBES) known for geophysical survey for seafloor bathymetric survey has the given acoustic wave angle for each beam. These beams discharge acoustic wave which can be reflected from the seafloor, and the water depth can be measured by calculating the delayed time of reflected waves from seafloor to receiver. MBES is more precise and efficient than Single-Beam Echo Sounder (SBES) relatively because it is able to survey a wide area with 3 times or 4 times swath width as much as the depth of water using MBES. Consequently, MBES could be shown in the visualization of seafloor, a wrecked ship and rocks, and survey data can also be shown in color graphic contour map available for other data analyzing.

Bathymetric data collected using a MBES during marine scientific survey is essential for geologic and oceanographic research works. During this cruise, the bathymetry in the Amundsen Sea in West Antarctica is obtained using MBES.

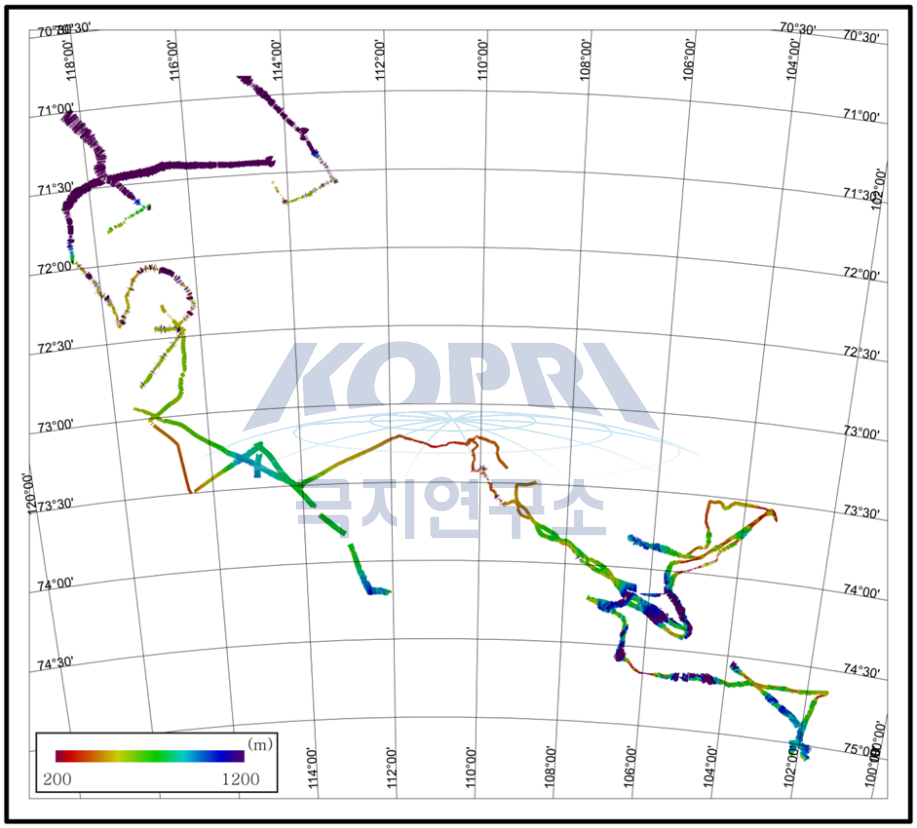

Figure 7.1: he MBES bathymetry in the Amundsen Sea.

7.2 Sediment core

Hyun Jung-Ho[1], Kim Sung-Han[1], Choi A-Yeon[1], Moon Heung-Soo[2]
[1]Dept. of Environmental Marine Sciences, Hanyang University
[2]Korea Polar Research Institute, Korea

요약문

수층의 생산력변화에 따른 저층생태계의 반응을 이해하기 위해, 아문젠 Polynya (AP)내 3정점과 AS의 outer shelf 지역 1 정점에서 박스코어를 이용하여, 퇴적물 내 총산소 소모율 (total oxygen utilization; TOU), 산소투과 깊이 (oxygen penetrate depth) 및 공극수와 퇴적물의 지화학적 특성을 측정하기 위한 시료들을 채집하였다. 퇴적물 내 TOU는 박스코어로부터 sub-core를 취하여, 저온실험실에 설치한 배양기내에서 현장온도 조건하에서 3-5일간 배양하여, 시간에 따른 산소소모율로부터 측정하였다. OPD는 산소 자동측정장치를 이용하여 100 μm 간격으로 표층부터 산소가 완전히 고갈되는 깊이까지 측정하였다. 공극수는 Rhizon을 이용하여 채취한 후 각 항목별로 전 처리를 한 후, 향후 실험실에서의 분석을 위해 냉장 또는 냉동보관을 하였다.

Objectives

Polynyas are open water in ice-covered seas, which in turn implied that more solar radiation penetrates into the water column than ice-covered area and, subsequently, enhanced water column production. Because irradiance in polar regions is the primary control of phytoplankton growth (Smith and Sakshaung, 1990), the growth of phytoplankton in polynya is enhanced relative to the surrounding regions. Especially, the Amundgen Sea polynya exhibits the highest annual primary productivity in the Southern Ocean, with production of 161 g C m^{-2} y^{-1}, which typically supports rich benthic communities through enhanced vertical carbon flux (Arrigo and van Dijken, 2003; Wassman et al., 2004). Several studies have quantified benthic process of carbon and its controls (primary production, water depth, POC export rate, and macrofauna biomass) in various Arctic and Antartic sediments (Ambrose and Renauld, 1995; Bodungen et al. 1995; Cooper et al., 2002; Grant et al., 2002; Hargrave et al., 2002; Barry et al., 2003; Arrigo and van Dijken, 2004). However, despite its high primary production, little has been studied on the benthic process of carbon in Amundgen Sea. Major objective of this study was to quantify total benthic respiration and oxygen penetration depth.

Work at sea

Study location

The oceanographic survey was conducted in the Amundgen Sea, Antartica, from February 10 to March 10, 2012 using the icebreaker ARAON. The TOU (total oxygen uptake), OPD (oxygen penetrate depth) and geochemical properties of sediments were measured at 4 stations (station 10, 17, 19, 83) using multi– and box corer (Table 7.1 and Fig. 7.2). The gravity core samples were collected at all sites except station 17 (Table 7.1, Fig. 7.2).

Table 7.1: Description sampling sites in the Amundgen Sea

Site	Coordinates	Depth	Core Type
10	73° 14.0852 114° 54.5583	802m	Box core 4, Multiple core 1 Gravity Core 1
17	73° 37.4219 113°48.2806	777m	Box core 5
19	74° 12.0009 112° 31.2491	1080m	Box core 4 Gravity Core 1
83	71° 41.8847 114° 02.4136	543m	Box core 4 Gravity Core 1

Figure 7.2: The equipments (box corer, multi corer and gravity corer) for collecting sediment

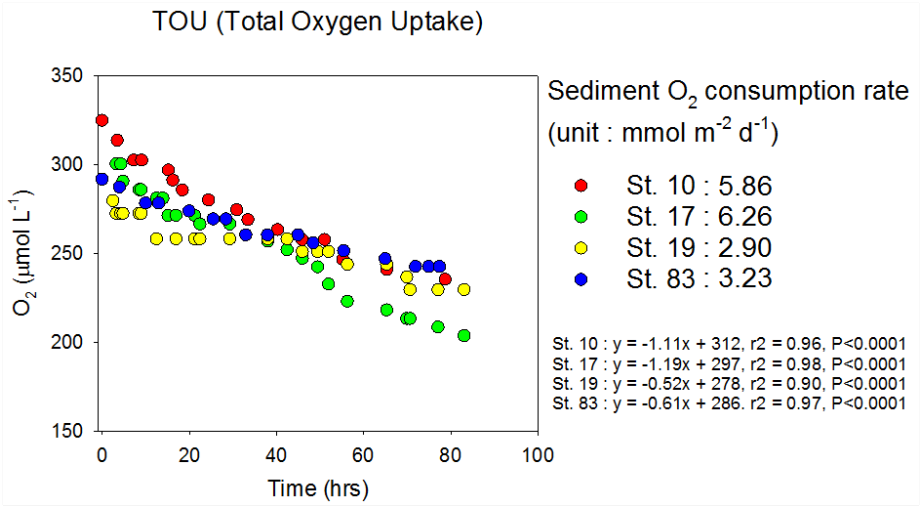

Figure 7.3: Evolution of oxygen concentration with increasing time

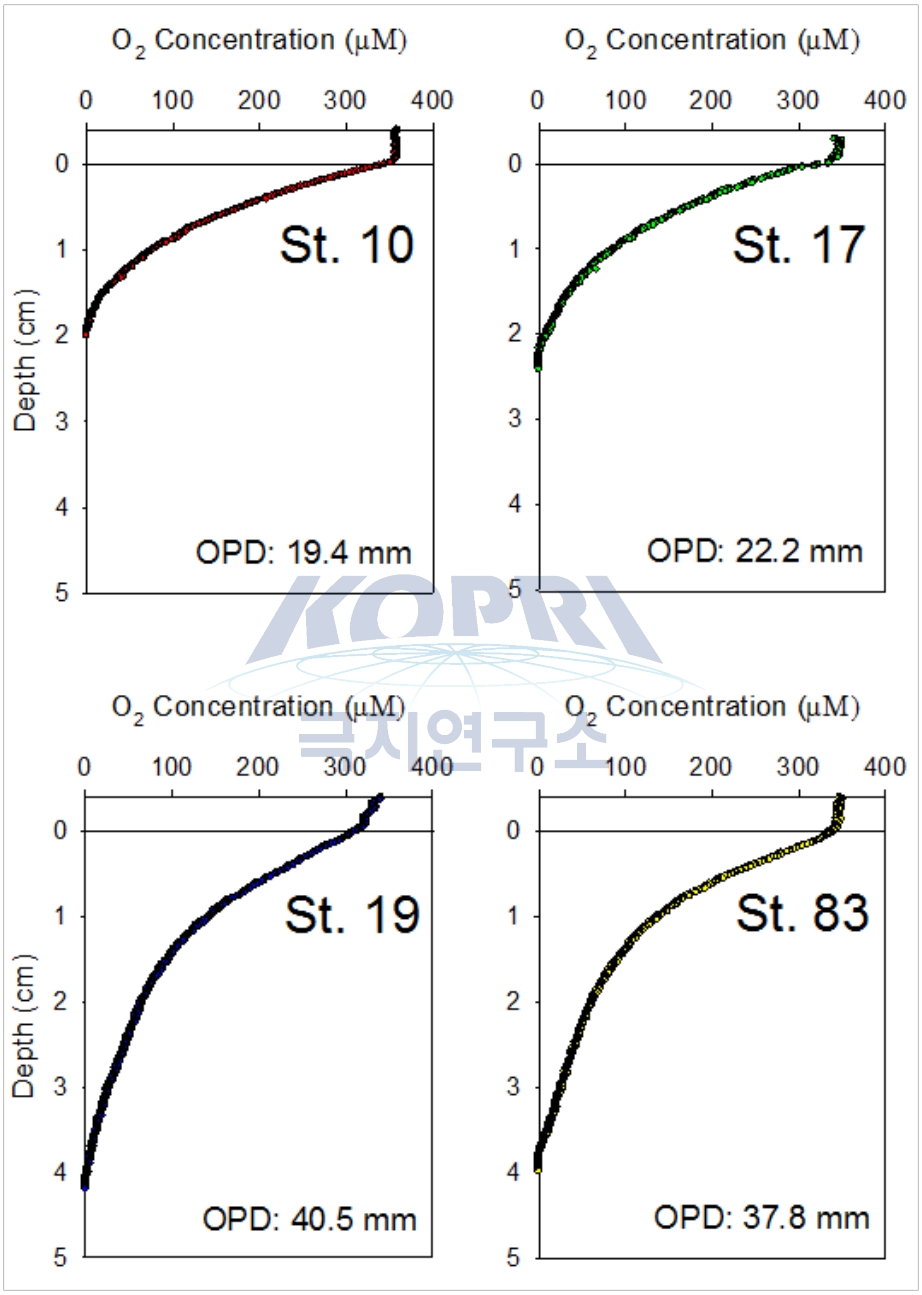

Figure 7.4: Oxygen penetrate depth measured in Amundgen Sea

Preliminary results

Material and methods

Sub-samples were collected using polycarbonate core (10, 4 cm i.d.) for measuring TOU and OPD, respectively in all sites. Duplicate or triplicate sediment samples for geochemical analysis were collected using polycarbonate cores (6 cm i.d.) in all sites, and pore waters were sampled using Rhizon sampler and stored either 4 or -20℃ after pre-treatment according to each item. Sediments for solid-phase analysis were frozen for future analysis.

Measurement of TOU

To estimate TOU, sub-cores for the benthic chamber were collected from the box core and stored at in situ sediment temperature at cold room until the experiments were initiated. To initiate the experiment, overlying water was replaced with bottom water from the Niskin bottle. Chambers were then sealed with lids engineered with o-rings to make the system water-tight. The pump (Greylor Co., PQ-12DC) were used to gently stir the overlying water to minimize oxygen gradients during the experiment. Oxygen sensors (Unisense, OX-50) were fitted on the chamber lid to measure the total oxygen consumption rate (TOU) of the sediment. We measured oxygen concentration every 2-8 hour interval using microelectrode and the experiments were run for 3 – 5 days at in situ temperature. At the end of each experiment, the chambers were sieved through a 1 mm screen to collect the macrofaunal organisms in the sediments of the chamber. Macrofauna were then preserved with formalin (10% in seawater) and stored in 50 ml conical tubes, and kept in refrigerator.

TOU calculation

Benthic oxygen fluxes across the sediment-water interface were calculated as follows: BF = (dC/dt) × (V/A) — (1) where BF is the Oxygen benthic fluxes (mmol m^{-2} d^{-1}), (dC/dt) is the slope of the linear regression line derived from plotting the concentration of relevant species as a function of incubation time (mmol L-1 d^{-1}), V is the chamber volume (m3), and A is the chamber area (m2).

Measurement of Oxygen Penetration Depth (OPD)

To measure OPD, the cores were uncapped and the sensor were positioned by a motor-driven micromanipulator and the sensor current was measured with a picoammter connected to an A-D converter, which transferred the signals to a PC (Revsbech and Jørgensen, 1986).

TOU (total oxygen uptake)

Oxygen concentrations in the benthic chamber gradually decreased over time (Fig. 7.3). Total oxygen uptake rates, calculated by the O2 vs. time slope, were estimated to be 5.86 mmol m^{-2} d^{-1} in station 10 and 6.26 mmol m^{-2} d^{-1} in station 17 at polyna sites. At outer and ice self sites, the OPD was measured 2.90 mmol m^{-2} d^{-1} in station 19 and 3.23 mmol m^{-2} d^{-1} in station 83, respectively. The TOU at polynya sites were about two times higher than at outer and ice shelf sites.

OPD (oxygen penetrate depth)

Oxygen was rapidly decreased in surface-sediment interface at all sites (Fig. 7.4). The OPD was measured 19.4 mm in station 10 and 22.2 mm in station 17 at polynya sites. At outer and ice shelf, OPD was measured 40.5 mm in station 19 and 37.8 mm in station 83 which were about two times higher than those at

polynya sites

Reference & Acknowledgement

Ambrose, W.G., Jr., Renauld, P.E., 1995. enthic response to water column productivity patterns: evidence for benthic-pelagic coupling in the Northeast Water polynya, Journal of Geophysical Research 100, 441-4421.

Arrigo , K.R., van Dijken, G.L., 2003. Phytoplankton dynamics within 37 Antartic coastal polynya systems. Journal of Geophysical Research 108, 1-18.

Arrigo , K.R., van Dijken, G.L., 2004. Annual changes in sea-ice, Chlorophyll a, and primary production in the Ross Sea, Antartica. Deep-Sea Research II 51, 117-138.

Barry, J.P., Gre variatbmeier, J.M., Smith, J., Dunbar, R.B., 2003. Bathmetric versus seafloor habitat control of benthic megafaunal communities in the S.W. Ross Sea, Antartica. In: Ditullio, G.R., Dunbar, R.B. (Eds.), Biogeochemistry of the Ross Sea. American Geophysical Union, Washington, DC, pp. 327-354.

Bodungen, B., et al., 1995. Pelagic processes and vertical flux of particles: an overview of a long term comparative syudy in the Norwegian Sea and Greenland Sea. Geologische Rundschau 84, 11-27.

Cooper, L.W., et al., 2002. Seasonal, variation in sedimentation of organic materials in the St. Lawrence Island Polynya region, Bering Sea. Marine Ecology Progress Series 226, 13-26.

Grant, J., Hargrave, B., Macpherson, P., 2002. Sediment properties and benthic-pelagic coupling in the North Water. Deep-Sea Research II 49, 5259-5275.

Smith, W.O. Jr., Sakshaug, E., 1990. Autotrophic processes in polar regions, In: Smith, W.O. Jr. (Ed.). Polar Oceanography, Part B. Academic Press, San Diego, pp. 477-525.

Revsbech, N.P., Jørgensen, B.B., 1986. Microelectrodes and their use in microbial ecology In: Marshall, K.C. (ed.) Advances in microbial ecology, 198Vol. 9, Plenum Press, New York, pp. 293-352.

Wassman et al., 2004. Particulate organic carbon flux to the arctic sea floor. In: Stein, R., McDonald, R.W.(Eds.), The Organic Carbon Cycle in the Artic Ocean. Springer, Berlin, pp. 101-125.

Chapter 8

Sea Ice Mechanics and Ship Performance in Ice

Choi, Kyungsik[1]; Kim, Hyun Soo[2]; Choi, Gul-Gi[3]; Lee, Jae Man[3]; Ha, Jung Seok[1]
[1]Korea Maritime University;
[2]Inha Technical College;
[3]Korea Ocean Research and Development Institute

요약문

쇄빙선박의 빙해역 쇄빙성능을 파악하기 위하여 ARAON호의 남극 Amundsen Sea Cruise 시 2개 정점에서 쇄빙시험(Icebreaking Test)을 수행하였다. 평탄빙(Level Ice)에서 Auger를 이용한 직접 계측 및 EM31-MK2 장비를 사용하여 해빙의 두께를 계측하였고 7.5cm Corer를 사용하여 추출한 해빙의 코어 시편으로부터 해빙의 재료특성(온도, 염도, 밀도, 압축강도, 굽힘강도)을 조사하였다. ARAON호의 선수부(Bow) 내부 외판(Hull Plating)과 늑골(Frame)에 부착된 총63개의 스트레인게이지(Strain-gage) 채널로부터 선체 구조의 변형을 계측하였고 선체 무게중심에 장착된 2개의 운동계측기(Motion Sensor)로부터는 쇄빙시 선박의 6-DOF 운동가속도를 계측하였다. 평탄빙 쇄빙과 동시에 선박의 속도와 엔진 출력의 변화를 기록하였다. 해빙의 두께(Thickness)/강도(Strength) 특성과 빙판을 깨뜨리며 전진할 때 쇄빙선박이 받는 빙저항(Ice Resistance)/빙하중(Ice Load) 사이의 상관관계를 분석하기 위한 ARAON호의 쇄빙시험 자료는 향후 빙해수조(Model Ice Towing Tank)에서 모형선박에 대한 실험의 정밀도를 향상시키기 위해 사용된다.

8.1 Objectives of the research

Full-scale ice trials of the IBRV ARAON were conducted at two sea ice stations during her Antarctic Sea cruise. Main objective of the full-scale trials is to investigate the ship's capability to move under certain ice conditions, i.e., ice performance and ice-strengthening of the ship's hull. The ice performance of ship is evaluated by means of three interrelated parameters: ship speed, propulsion power and the characteristics of the sea ice cover which include ice/snow

Figure 8.1: Measurement of ice thickness with EM31-MK2 device

thickness and strength. For investigating the ice-strengthening of ship's hull, it is necessary to understand the hull's capability to take ice loads preserving the strength of hull structural elements. The hull strength is determined by the method of strain-gage measurements. The measurement data are used for calculating the response of the structural elements to the ice impacts.

8.2 Research work on sea ice

8.2.1 Measurement of sea ice properties

During the full-scale ice trials of the IBRV ARAON, icebreaking tests on specially selected level ice floes were performed twice. Before each icebreaking test, a straight line, usually longer than 500m, was drawn (at every 100m is marked by a colored flag) along the assumed path of the ship and then various material properties of sea ice were measured from the selected level ice floe for each ice trial.

Ice thickness is the primary parameter among various ice properties. A drill bit connected to an electric motor was used to make 5cm-diameter holes and to measure the thickness of sea ice at every 25/50m. An EM31-MK2 device was used in parallel to measure ice thickness of the ice floe. Snow accumulation and the freeboard of sea ice were also recorded. Core samples were extracted from the sea ice using 7.5cm diameter Kovacs corer and a probe-type thermometer was used in measuring temperatures at every 10cm/20cm distance from the top surface to the bottom.

Ice core was cut into a 19cm long specimen for compression test. Before a compression test, ice density was calculated by measuring the weight and

Figure 8.2: Kovacs 7.5cm ice corer

Figure 8.3: Extracted ice core samples

Figure 8.4: Compressive strength test of ice specimen

the volume of each ice specimen using a portable weight scale. For measuring salinity, the ice samples after compression test were kept to completely melt under room temperature.

Ice strengths are also very important factors in consideration of ice load and ice resistance on a ship's hull. Compressive strength of sea ice was measured using a compression tester onboard the ARAON. Well prepared ice specimens (average 19cm in length and 7.2cm in diameter) were used in the measurement of ice compressive strength. Flexural strength of sea ice were estimated using Timco and O'Brien(1994)'s empirical formula: $\sigma_f = 1.76e^{-5.88\sqrt{\gamma b}}$ where γb is non-dimensional brine volume.

8.2.2 Observation of ship performance in ice

During icebreaking tests, the ship speed and propulsion power were measured onboard the ARAON. The location of ship and ship speed were measured by GPS signal. The engine power of the ship was recorded using a video camera from the dynamic positioning system (DPS) panel of the ship. The wind speed and direction was recorded on the anemometer and air temperature was also measured by thermometer onboard the ship. A gyro compass was used for measuring ship's running course. The pitching/rolling angle was measured by the clinometer. The video recording at several locations onboard the ARAON, such as the front forward/downward view from the bow and starboard side of ship's hull were performed.

Preparing a designated power level of the main engine, then the icebreaking test was carried out. All the digital and analogue signals from the navigational apparatus, such as current location, running course and speed of the ship and torque of the propeller were recorded by video cameras. The load exerted on

Figure 8.5: Marking of an assumed running path with red flags

the front port side hull was also measured by the strain-gage modules (total 63 channels) for stress monitoring system and these results will be analyzed later.

8.3 Preliminary results

Full-scale ice trials of the IBRV ARAON were conducted twice on the selected ice floes in the Amundsen Sea. Preliminary results from the icebreaking test #1 are presented in this section.

The physical-mechanical properties of the sea ice floe on which the first ice trial was performed are summarized in Fig. 8.9 and Table 8.1. The ice floe was a first-year sea ice and the measured ice thickness was almost uniform except one location where a ridge was developed. The compressive/flexural strength of sea ice were a little low compared to a design code generally accepted for classification societies. The season was late summer in Antarctic Sea and the air temperature was close to melting point of sea ice and therefore the structure of ice decayed fast.

Based on measured ice strength and thickness data, the relationship between ship speed and the propulsion power is given in Fig. 8.9–8.10. From this results of icebreaking test #1, diagrams of dependence of the ship motion parameters on the ice cover parameters can be constructed. Significant level of ship motion and strain-gage signals during ice impact events were recorded for the future analysis as shown in Fig. 8.8–8.11 and Fig. 8.8–8.12. Also the data analysis will be utilized for calculation of the safe ship motion speeds under the different ice conditions.

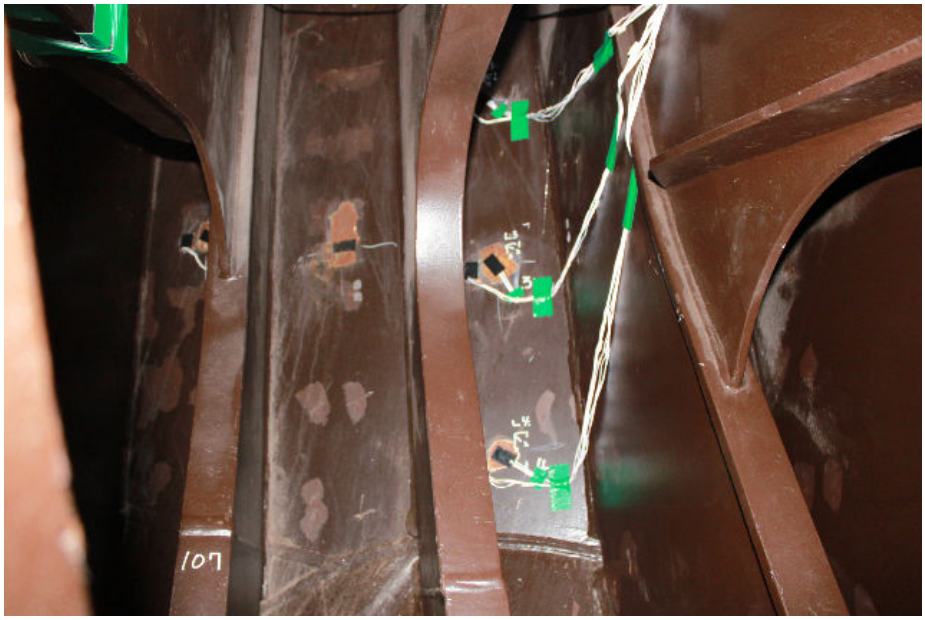

Figure 8.6: Strain-gage modules installed on the inside of ARAON's hull plating and frames

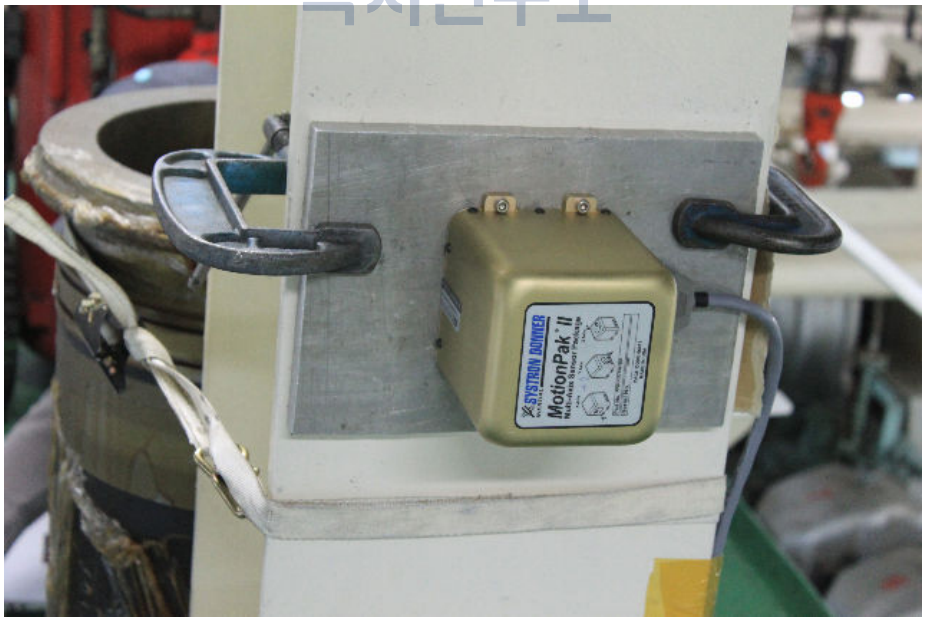

Figure 8.7: Motion sensor installed at the center position of the ARAON

Figure 8.8: Scene from icebreaking test #1 (02/24/2012)

Table 8.1: Physical-mechanical properties of sea ice floe for icebreaking test #1

Coring Position	Temperature [℃]	Density [kg/m^3]	Salinity [‰]	Compressive Strength [MPa]	Flexural Strength [kPa]
100m	-1.45	915.3	3.8	1.30	205
200m	-1.72	843.5	3.8	1.41	292
300m	-1.67	855.8	4.4	1.643	239
400m	-1.68	850.9	4.3	1.247	240
500m	-1.82	824.5	3.8	1.35	302
600m	-1.72	852.1	4.0	1.725	281
700m	-1.77	792.2	4.4	N/A	267
Mean	-1.72	842.6	4.0	1.445	274

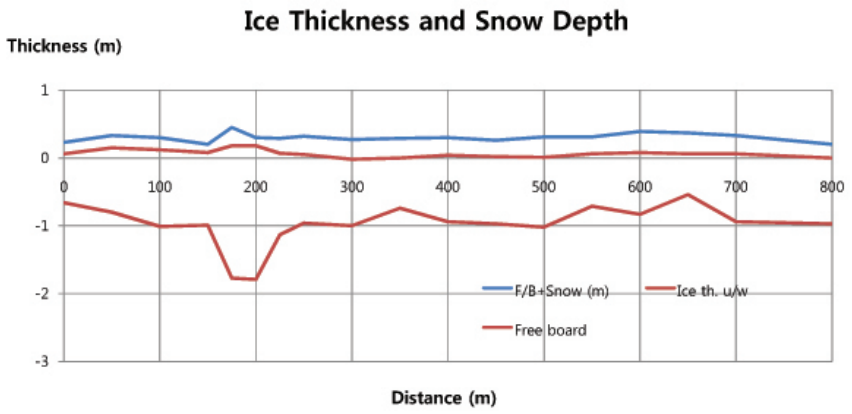

Figure 8.9: Measured thickness profiles of level ice floe for icebreaking test #1

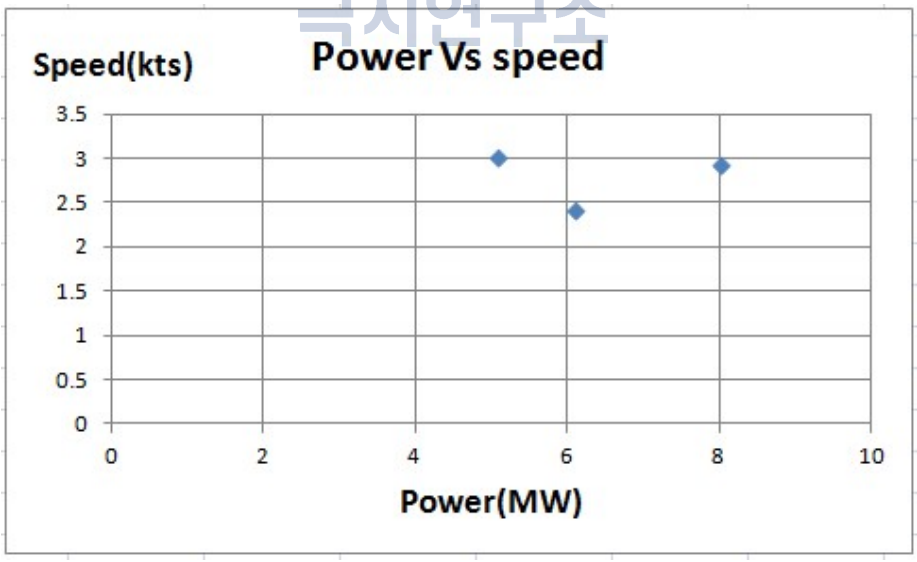

Figure 8.10: Physical-mechanical properties of sea ice floe for icebreaking test #1

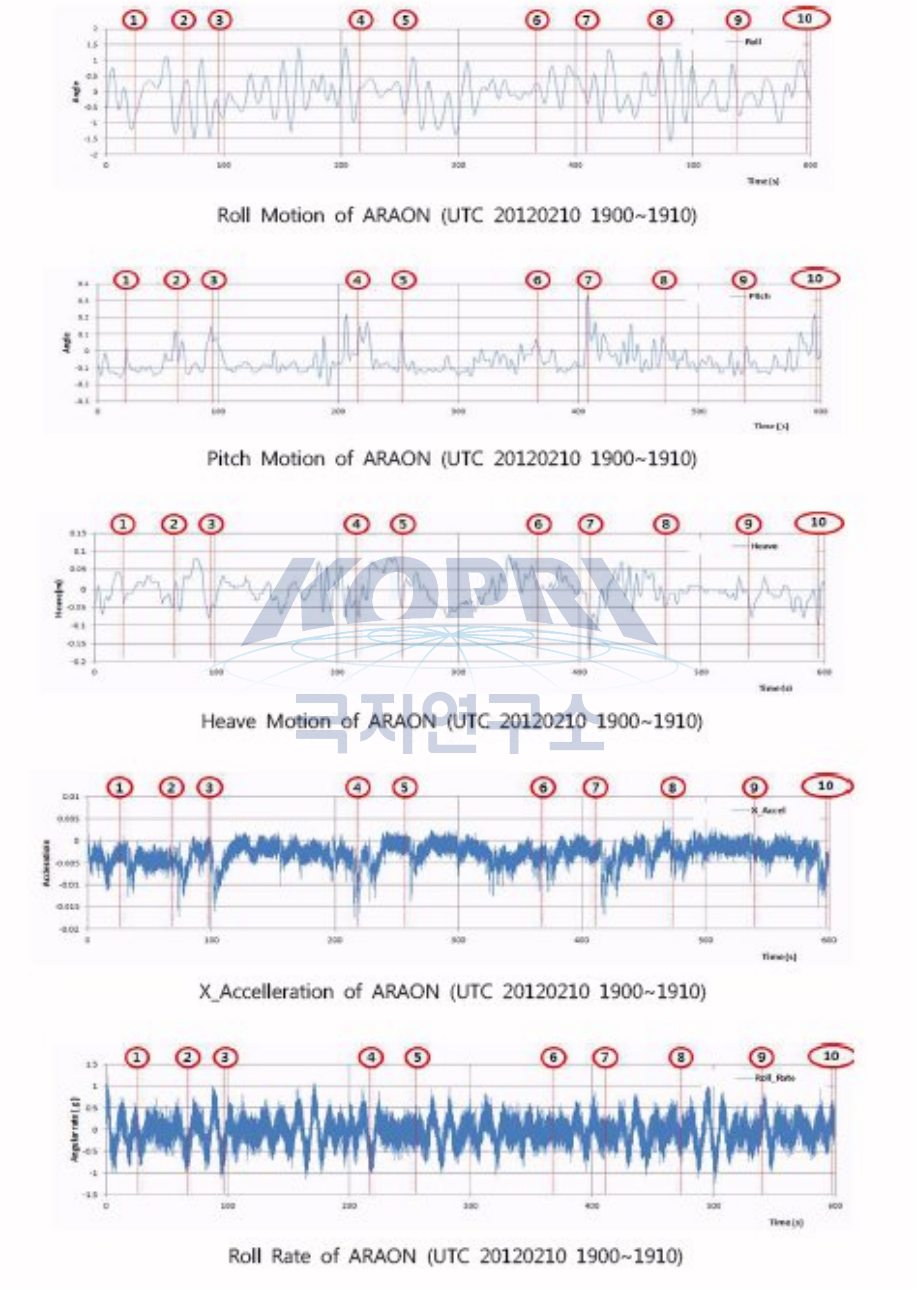

Figure 8.11: Estimated power-speed relationship for icebreaking test #1

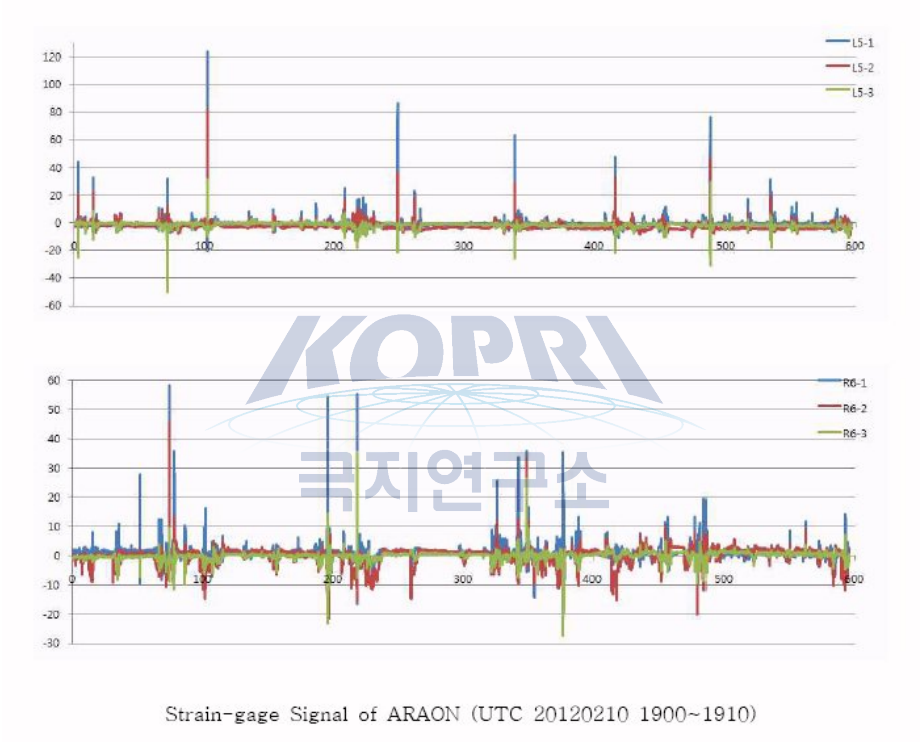

Figure 8.12: Motion sensor signals recorded from an ice impact event (02/10/2012)

References

Kim, H.S., Lee, C.J. and Choi, K., 2011, The Study on the Ice Sea Trial in Chukchi Sea using Korean Icebreaker ARAON, Proc. of the 30th OMAE Conf., Paper No.49482, Rotterdam, The Netherlands

Likhomanov, V., 2010. Full-Scale Ice Trials of the Korean Research Icebreaker Araon, Arctic and Antarctic Research Institute Russian Antarctic Expedition Report

Timco, G.W and O'Brien, S., 1994, Flexural Strength Equation of Sea Ice, Cold Regions Science and Technology, Vol.22, pp.285-298

Acknowledgement

Research fund provided by the Ministry of Knowledge and Economy, Korea, through the Industrial Strategic Technology Development Program (Grant No. 10033640) is greatly acknowledged.

Appendix A

Participants (*aka 'A-Team'*)

2012 A-Team

No.	Name 성 명		Affiliation 소속	연락처(Tel 전화)/이메일
	한글	영문		
1	이상훈	Lee, SangHoon	KOPRI	011 9082 5349 shlee@kopri.re.kr
2	이태식	Rhee, Tae Siek	KOPRI	010 7582 1103 rhee@kopri.re.kr
3	양은진	Yang, Eun Jin	KOPRI	010 3125 0144 ejyang@kopri.re.kr
4	함도식	Hahm, Doshik	KOPRI	010 9911 2067 hahm@kopri.re.kr
5	하호경	Ha, Ho Kyung	KOPRI	010 4360 4350 ha@kopri.re.kr
6	김태완	Kim, Tae Wan	KOPRI	032-260-6260 twkim@kopri.re.kr
7	나형술	La, Hyoung Sul	KOPRI	010-2501-7187 hsla@kopri.re.kr
8	이두별	Lee, Doo Byoul	KOPRI	010 2559 1208 copepod@kopri.re.kr
9	박지수	Park, Ji Soo	KOPRI	010-5390-1576 jspark@kordi.re.kr
10	전현덕	Jeon, Hyunduck	KOPRI	010 9395 2059 hdj0809@kopri.re.kr
11	박경아	Park, Kyung Ah	KOPRI	010 9428 6468 kyung-ah@kopri.re.kr
12	한정민	Han, Jeong Min	KOPRI	010 3211 9931 goal@kopir.re.kr
13	이승겸	Lee, Seung Kyeom	KOPRI	010 6286 9547 keomnara@kopri.re.kr
14	전미사	Jeon, Mi Sa	KOPRI	032-260-6165 misha@kopri.re.kr
15	이동진	Lee, Dong Jin	KOPRI	010-3806-3197 vittone@naver.com
16	최태진	Choi, Tae Jin	KOPRI	010-2427-5964 ctjin@kopri.re.kr
17	홍상범	Hong, Sang-Bum	KOPRI	032-260-6146 hong909@kopri.re.kr
18	박하동	Park, Hadong	KOPRI	010-9024-1945 hadong@kopri.re.kr
19	김형준	Kim, Hyoungjun	KOPRI	010-8640-5588 jun7100@kopri.re.kr
20	문흥수	Moon, Heung Soo	KOPRI	010-2201-7114 jepy@kopri.re.kr
21	권영신	Kwon, Young-Shin	KOPRI	010 2510 0329 kwonys@kopri.re.kr
22	김보경	Kim, Bo Kyung	KOPRI Pusan National Univ	010-6685-6385 bokyung85@kopri.re.kr (Transit only, 2011.12.15 off board)
23	황선아	Hwang, Suna	Pukyung Univ	010-6797-2430 sim2430@naver.com
24	함석현	Haam, Suk Hyun	Neo SeaTech	011 314 6481 haam@kordi.re.kr
25	홍창수	Hong, Chang Su	KORDI	016 689 0861 cshong@kordi.re.kr
26	정진현	Jeong, Jin Hyun	KORDI	011 9538 2819 pujjh@kordi.re.kr
27	이형빈	Lee, Hyoung-Bin	KORDI	010 6398 3823 hblee00@kordi.re.kr
28	현정호	Hyun, Jung-Ho	HanYang Univ	010-2365-6431 hyunjh@hanyang.ac.kr
29	김성한	Kim, Sung Han	HanYang Univ	010-6218-1778 shkim1778@hanmail.net
30	최아연	Choi, A-Yeon	HanYang Univ	010-3894-4953 znzn1020@hanyang.ac.kr
31	김민경	Kim Min Kyoung	POSTECH	010-4460-4508 jhwang@postech.ac.kr
32	김종걸	Kim, Jong-Geol	ChungBuk Nat'l Univ	010-5462-8760 jjonggul2@gmail.com
33	김진우	Kim, Jin-Woo	Seoul National Univ	010-4917-7982 modone79@gmail.com
34	김승희	Kim, Seung Hee	Seoul National Univ	010-8432-2322 dalcomeboy@snu.ac.kr
35	주희태	Joo, Huitae	Pusan National Univ	010-2968-9029 koggil87@gmail.com
36	김미선	Kim, Mi Seon	ChungNam Nat'l Univ	010-9700-0614 miseon609@hanmail.net

37	이재만	Lee, JaeMan	KORDI MOERI	010 8824 7145, gmjm333@moeri.re.kr
38	최걸기	Choi, Gul-Gi	KORDI MOERI	010 9434 8484, gulgi@moeri.re.kr
39	최경식	Choi, Kyung-Sik	HaeYang Univ	010 8553 4324 kchoi@hhu.ac.kr
40	하정석	Ha, Jung-Seok	HaeYang Univ	010 5372 9377 js_ha@hhu.ac.kr
41	김현수	Kim, Hyun-Soo	Inha Tech Univ	010-9931-5355 hyunsookim@inhatc.ac.kr
42		Abrahamsen, Povl	UK BAS	British Antarctic Survey iSTAR program epab@bas.ac.uk
43		Stranne, Christian	Sweden Gothenburg Univ	Department of Earth Sciences christian.stranne@gvc.gu.se
44		Bailluel, Benjamin	US Rutgers Univ	US Rutgers University benjamin@marine.rutgers.edu

Appendix B

Araon cruise track superimposed on the sea-ice map of the Amundsen Sea

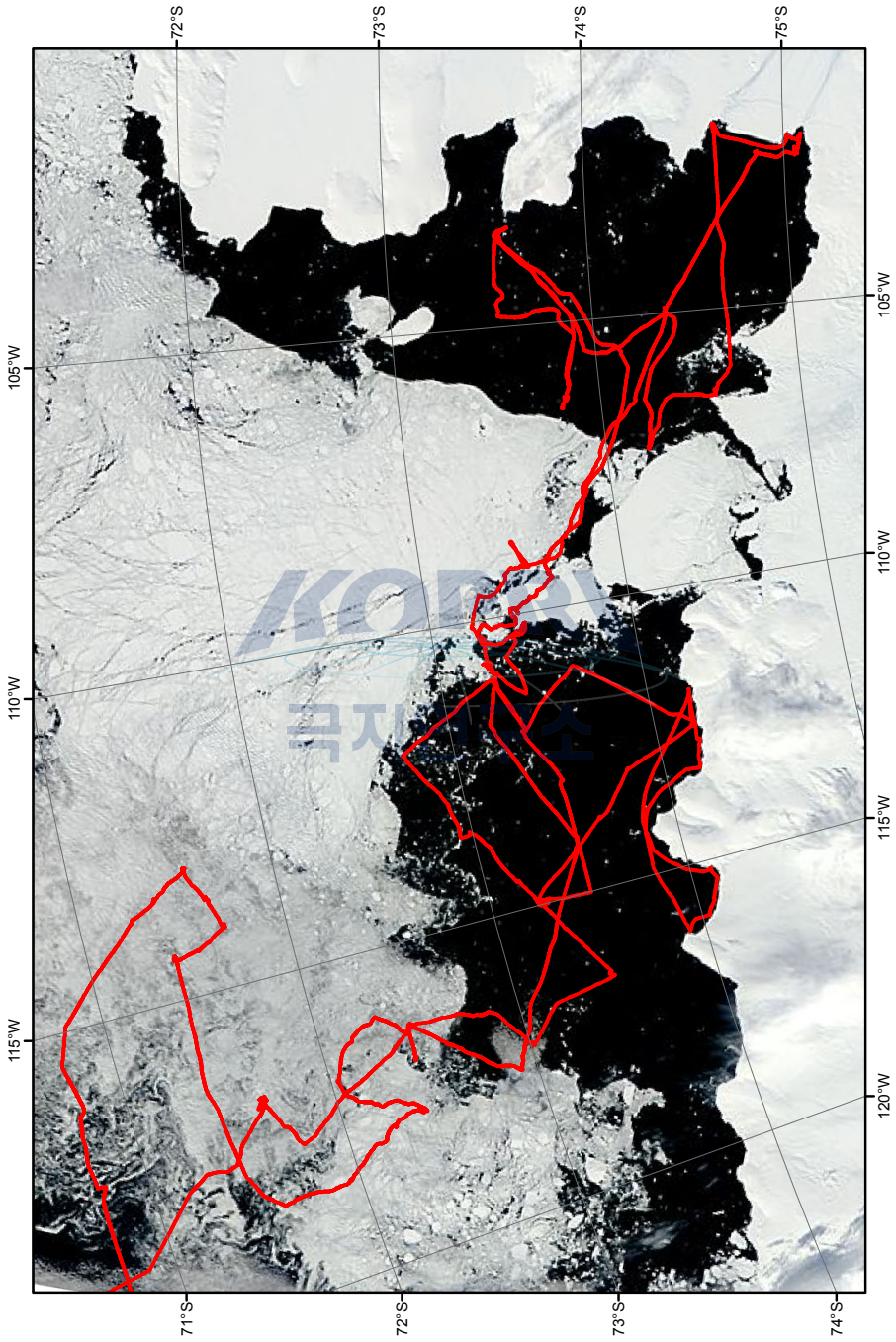
72°S
73°S
74°S
75°S
105°W
110°W
115°W
71°S
72°S
73°S
74°S
105°W
110°W
115°W
120°W